Unione Europea
Fondo Sociale Europeo

Ministero dell'Università e della
Ricerca Scientifica e Tecnologica

Università degli studi di Palermo

Tesi cofinanziata dal Fondo Sociale Europeo

PROGRAMMA OPERATIVO MULTIREGIONALE 1994/99
n. 940023I1

"Ricerca, Sviluppo Tecnologico ed Alta Formazione"
Misura 1.1. sottomisura Dottorati di Ricerca

TYPICAL HYBLEAN LANDSCAPE

GEOCHEMICAL PROCESSES GOVERNING THE CHEMISTRY OF GROUNDWATER HOSTED WITHIN THE HYBLEAN AQUIFERS

(South-Eastern Sicily, Italy)

PhD thesis by:
Fausto Grassa

Tutor:
Prof. Mariano Valenza

DOTTORATO DI RICERCA IN GEOCHIMICA XIII CICLO (Nov.1998 / Ott.2001)

Dipartimento di Chimica e Fisica della Terra
Ed Applicazioni alle Georisorse ed ai Rischi Naturali (C.F.T.A.)

Table of Contents

Abstract

A raingauge network made of six stations was installed in the Hyblean region. Stations were located at different altitudes (from 5 m to 986 m a.s.l.) and along two directions (E-W and SW-NE). Rainwater samples were monthly collected for stable isotope measurements. Spatial distribution of rainwater isotope composition has confirmed the wet air masses move from South-East/South-West toward North. Water balance has highlighted that the annual volume of infiltrating waters is in the range of 1-1.5 $*10^5$ m^3 Km^{-2}.

82 well waters and 12 spring waters located within the Hyblean Plateau (South-Estern Sicily), were also collected from 1999 to 2001 during several surveys for chemical (major, minor and trace elements) analyses. Water chemistry allowed to identify two main aquifers: the first aquifer hosted within sedimentary rocks is characterized by earth-alkaline bicarbonate waters, while the second aquifer, located within the volcanic deposits (mainly towards North- North-East) is characterized by groundwaters evolving from earth-alkaline bicarbonate water-type towards a Na-HCO_3-type.

A slightly anomaly in water temperature (24-28°C) have been identified along the northern margin, while the lower Eh values have been recorded along the M.Lauro-Scicli and the Hyblean Malta Escarpment fault systems. Isotope composition of groundwaters has suggested the occurrence of evaporative processes during soil infiltration having a $\delta D/\delta^{18}O$ slope close to 4.5.

Chemical and isotope composition of dissolved gases ($\delta^{13}C_{TDIC}$, $\delta^{13}C_{CH4}$, $^3He/^4He$) have revealed, as expected, that deeply-derived gases rise along the main tectonic discontinuities. Chemical and isotope analyses of dissolved carbon have revealed the existence of two sampling sites (NA and FE samples) attesting the interaction between groundwaters and a consistent amount of deep inorganic carbon dioxide.

He isotope ratios (from $0.81R_a$ to $6.19\ R_a$) have revealed the occurrence of mixing process, in different proportions, between crustal and mantle components.

On the base of the obtained results, a clear picture of the groundwaters circulation within the Hyblean aquifers has been drawn. In framework of projecting of a geochemical network for the continuous monitoring of the local seismic activity the most suitable geochemical parameters and the sites of great interest have been identified.

1.INTRODUCTION

The Hyblean Mountains, located in the SouthEastern part of the Sicily Island are an area hydrogeologically and tectonically of great interest. They consist mainly of a carbonate plateau of Meso-Cenozoic age alternated with several volcanic horizons that occurred intermittently from the Late Triassic through the early Pleistocene. Because of their huge extension and high permeability values, carbonate platform rocks and volcanic deposits are among the most important regional aquifers.

Furthermore, SouthEastern Sicily, among the Italian regions, has the highest seismic hazard, being located in the junction between the African and Eurasian plates. As a result of these convergent movements, in the past (1169 and 1693), several seismic events (magnitude > XI° MCS) occurred destroying several towns.

Also in the last decades (1980 and 1990), some earthquakes with magnitude of about 3.8 and 5.4 respectively occurred.

In last decades, several authors (Rikitake, 1976, Wakita, 1977, 1982; Valenza and Nuccio, 1993; Favara et al., 2001 and reference therein) have reported hydrological and geochemical variations in groundwaters located in seismically active areas prior to, simultaneously and after the occurrence of intense earthquakes. However in this context, a univocal scenario cannot be drawn. In fact, some physico-chemical parameters that can be considered as geochemical precursors of earthquakes in one region do not change significantly in another one. Furthermore geochemical variations can persist with time or they can be as a transient, disappearing at the end of the mainshock.

For these reasons, the correct geochemical approach aimed to use of some geochemical changes for earthquake prediction implies a detailed knowledge about:

- Geological setting and the structural model;
- Nature of fluids;
- Hydrogeological model of fluid circulation;
- Relationships between shallow and deep fluids;
- Background of geochemical parameters during aseismic periods.

In this study, in order to elaborate a geochemical model for the Hyblean area, several investigations have been performed aimed to:

- Isotope characterization of rainwater by means of a rain-gauge network, installed in the area of the Hyblean Plateau. The stations have been located at different altitude (from 5 m to 986 m a.s.l.) and following two main traverses (NNE-SSW and E-W).

- Chemical (major, minor and trace elements) and isotope (δD and $\delta^{18}O$) characterization of local aquifers (94 discharges).
- Chemical and isotope composition of dissolved gases ($\delta^{13}C_{TDIC}$, $\delta^{13}C_{CH4}$, $^{3}He/^{4}He$);
- Definition of the geochemical background for each parameter, through the monthly samplings of the most representative sites (17 wells and 4 springs).

On the base of the results obtained from this preliminary study, a clear picture of the Hyblean aquifers has been drawn. In particular, the relationships between local meteoric recharge and groundwaters hosted within Hyblean aquifers have been identified. Moreover, rock-leaching processes during groundwater flow path and the presence of input of deep-gases have been also highlighted.

Furthermore, for a future geochemical surveillance of local seismic activity the most suitable parameters and sampling sites have been discerned.

2.GEOLOGICAL AND HYDROGEOLOGICAL FRAMEWORK

The Hyblean Mountains, geodynamically speaking, are part of an important geological structure located in the South-Eastern Sicily comprehending the Hyblean-Malta Platform. It belongs to the same tectonic units constituting the Calabrian Arc and the North Eastern part of the Sicily (Ghisetti and Vezzani, 1980). Furthermore, it represents the junction area between the Apennine-Maghrebian chain, located along E-W direction in the northern portion of the island and the northernmost part of the African plate (Fig. 1).

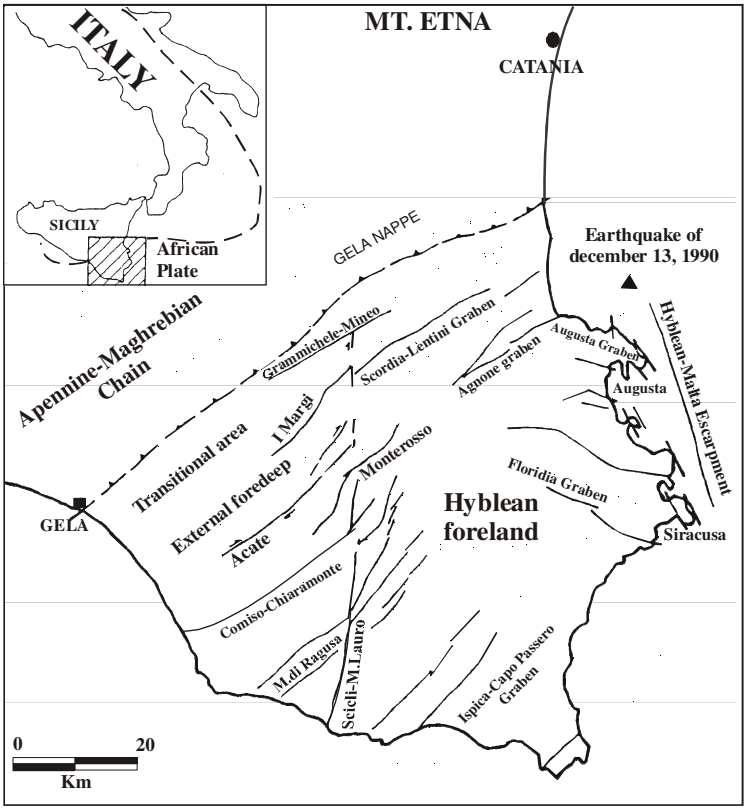

Figure 1: *Schematic map of the South-Eastern Sicily (from Bianchi et al., 1987, modified). In the figure, main tectonic structures are also reported.*

It is surrounded by three active tectonic structures which control the main tectonic systems within Hyblean Plateau: the thrust belt of Gela Nappe on north-west flank, the transcurrent faults system developed along a NNE-SSW direction on south-west boundary and on the East side the Malta Escarpment, extending for more than 300 km eastward, within Ionian Sea (Adam et al., 2000).

The latter structure has been transformed from a Mesozoic passive margin between African and Eurasian plate, into a mega-hinge faults system, and it is thought to be responsible for

neotectonic movements recorded in the eastern part of the Hyblean foreland (Grasso, 1993).

Bianchi et al. (1987) identified in the studied area, four different units representing the actual setting as result of tectonic movements occurred from Miocene-Pliocene to present days (Fig. 1). From North toward South, we can encounter the marginal part of the chain, the thrust zone of Gela-Catania foredeep (Inner foredeep), a transitional area (External foredeep), located mainly on the Western boundary, and finally the Hyblean foreland. The latter appears as a "horst" along a NE-SW direction (Ghisetti and Vezzani, 1981) that is dislocated by several fault systems. Main tectonic structures are: a NNE-SSW transcurrent fault (Scicli-M. Lauro) crossing almost all the Hyblean mountains from the south coast to the northern edge; a huge system oriented along a NE-SW direction parallel to the Hyblean-Malta Escarpment and its conjoined strike-slip faults group dislocating the studied area in several "horst" and "graben" structures.

The most ancient tectonic discontinuities, deriving mainly from distensive movements, have been identified to be active along NW-SE alignments (Trias) while fault systems along NE-SW and NNE-SSW underwent from Miocene to Pliocene both distensive and lateral movements (Patanè and Imposa, 1987) as a consequence of the opening of the Magnaghi-Vavilov basin in the Central Tyrrheninan sea (Mantovani et al., 1996). In some fault systems located within Noto-Augusta area the fault plane have been afterwards reactivated by a compressive action. The proposed rheological model for Hyblean plateau (Patanè and Imposa, 1987) suggests within the studied area that both right and left lateral shears could coexist. The same authors indicate the Hyblean plateau as a land comprises between two relaxation barriers (as defined by Husseini et al., 1975), the Hyblean-Malta escarpment and the Scicli-M.Lauro fault, along which the energy accumulated with tectonic load can be easily released.

The Hyblean plateau is mainly made of a thick carbonate succession deposited mainly in platform facies, Meso-Cenozoic in age, with substantial intercalations of volcanic deposits occurred during several episodes since Cretaceous time (Fig. 2) (Bianchi et al., 1987; Lentini et al., 1987).

The oldest carbonate rocks are Triassic in age but they are only known through several drills for hydrocarbons exploration and seismic investigations. The outcropping stratigraphic sequence starts with Early Cretaceous clays and marl-limestone belonging to the Hybla formation. During Tertiary, carbonate succession can be divided in two different depositional environments: eastern part consists of massif carbonates deposited in reef-

lagoon facies, while western one is characterized by limestones formed in a neritic to pelagic environment. More ancient -not outcropping- geologic formations overlie an heterogeneous basement characterized by basic lithotype evolving northward to granitic or metamorphic type, recognized at the depth of 6.8 Km. They comprise dolostones, limestones, marls in alternated sequences sometime interrupted by clay levels and frequent volcanic deposits.

Figure 2: *Geological sketch map of Hyblean plateau (from Lentini et al., 1984, modified)*

Volcanism occurred intermittently from Late Triassic through early Pleistocene, in an environment characterized by dramatic sea-level fluctuations and intense tectonic activity. Eruption and deposition therefore occurred both under water and above the sea level, leading to the formation of distinctly different facies, and characterized by a span range in rock chemistry and mineralogy. During Trias-Cretaceous, Hyblean lavas are Na-alkaline in chemistry (De Rosa et al., 1992), while most common volcanic rocks belonging to Miocene and Pliocene-Pleistocene eruptive activity, range from low K-tholeiites to basanites and nephelinites (Beccaluva et al., 1998). The more recent volcanic activity in this area has to be related to intra-plate magmatism induced by a regional lithospheric wrench fault system having transtensive movements. Lavas flowed from more than 200 small eruptive centres, aligned along a NE direction. Previous investigations (Romano and Villari, 1973; Battaglia et al., 1976; De Rosa et al., 1992; Beccaluva et al., 1998) on petrologic, petrogenetic, geochemistry (REE and trace elements distribution) and mineralogy of Hyblean volcanic products have suggested that they have been generated during different degrees of partial melting (from 30% to 3% relative to tholeiites and nefelinites respectively) of an enriched upper mantle (a OIB mantle source). Changing of initial high pressure conditions and low degree of partial melting as a consequence of variations in tectonic regime, should be responsible for the occurrence of slightly differentiated volcanic rocks, such as tholeiites (De Rosa et al., 1992).

From a seismogeological point of view, eastern Sicily is ascribed to the most active areas because of the occurrence of several earthquakes, in 1693 (M= XI° MCS scale) and more recently (January, 23, 1980 and December, 13, 1990) even thought with minor intensity (M=5.4).

Seismic investigations carried out on the focal mechanisms of the 1990 earthquake and on the active faulting involving eastern Sicily (Monaco and Tortorici, 2000) have highlighted that the seismogenetic structure responsible for the past earthquakes (1693 as well as 1990) are to be found in the western margin of the Malta escarpment. The epicentre of the mainshocks recorded during the 1980 earthquake was localized onshore, in the central part of the Hyblean foreland and could be related to the Scicli-M-Lauro transcurrent fault (Patanè and Imposa, 1987).

From a hydrogeological point of view, the Hyblean Plateau extending for about 4500 Km^2 can be subdivided in five main hydrogeological basins, as described in figure 3.

Despite the great importance of this area for the water resources of Sicily Island, there are only few published papers on the hydrogeological setting of the Hyblean plateau (Aureli, 1993 a-c; Aureli et al., 1993; Dall'Aglio et al., 1995; Grasso et al., 2000).

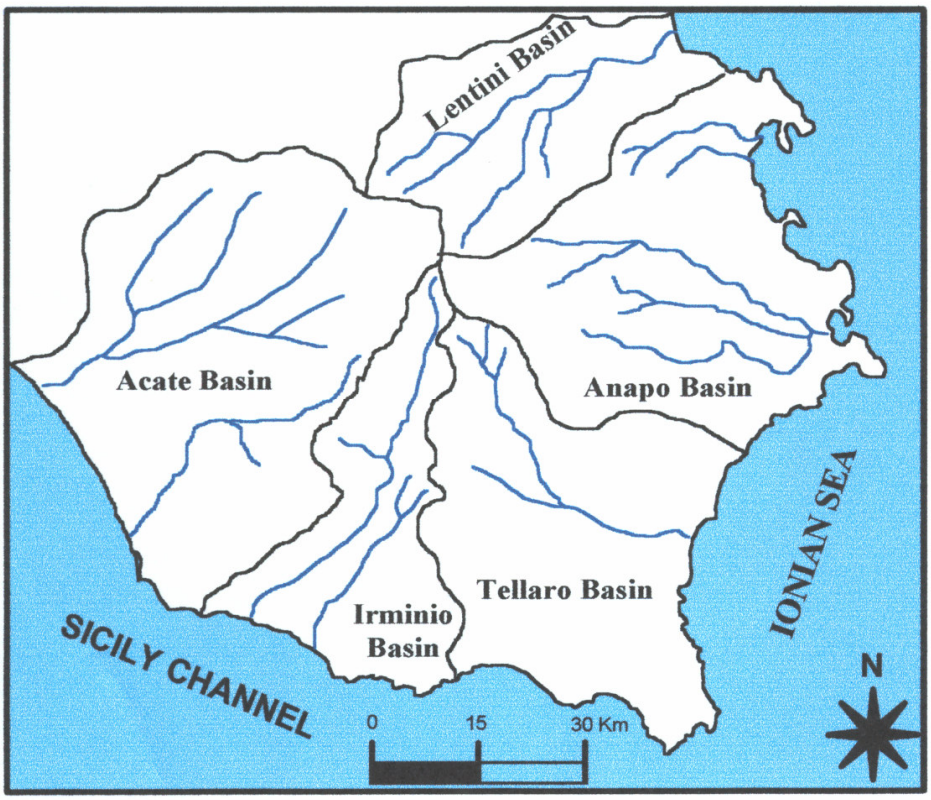

Figure 3: *Hydrogeological setting of the Hyblean region. Five main hydrogeological basins have been identified. Black line = watershed; Blue lines = water course.*

Groundwater circulation occurs in the following hydrogeological structures:

- three sedimentary aquifers (SE aquifers):

- Carbonate succession, Oligo-Miocene in age, that occupies the central area from west to east, covering about 2300 Km^2. It comprises the Ragusa Formation and the underlying Amerillo Formation. Their total thickness until the impermeable substrate made of marls and clays (Early Cretaceous) can be evaluated to be close to 1000 meters and over (Carbonate aquifer);
- Pleistocene Calcarenites host the main aquifer of the western area, having a quite variable thickness due to a progressive increasing in depth of the impermeable layers (Calcarenite aquifer)
- Aquifers hosted within biocalcarenites, alluvial and evaporite deposits, (Late Miocene to Quaternary) play only a secondary role. They occupy only marginal areas or they are

located within the main fluvial incisions. Furthermore they constitute only very small aquifers that are often polluted by sea-water intrusions (Marginal aquifers).

- Volcanic deposits (VO aquifer) extend for more than 1000 Kmq in the north-north eastern portion of the study area. The thickness of these deposits is quite variable reaching in some sections more than 500 meters. As described in the geological setting, limestone and marl-limestone belonging to the previous aquifer are also interbedded to this unit;

Hydrodynamic parameters reveal for volcanic aquifer permeability and transmissivity values in the range of 10^{-5} m/s and 10^{-3} m^2/sec respectively. Calcarenites and Miocene carbonate aquifers show higher but variable values depending for the latter, on the degree of fracturing and the intensity of the karst dissolution processes. In a previous study Ruggieri (1997) affirms that in the Irminio river basin, karst structures favoured the capture of stream flow and have driven the groundwaters flow path in carbonate aquifers.

Carbonate rocks and volcanic deposits having high permeability values, coupled with their huge extension constitute therefore the most important aquifers in the Hyblean Mountains..

In the central-western part a shallow carbonate aquifer is separated at depth of 100-150 meters by a horizon of marls variable in thickness which allows the occurrence of a deeper carbonate confined aquifer. The hydraulic continuity is however ensured in correspondence of the main tectonic discontinuities. A similar structure is also recognized in the western sector. Here, an aquifer hosted within calcarenites is overlapped an impermeable marl formation (Tellaro Fm.) constituting the roof of the deeper aquifer lying in the Miocene limestone. Isophreatic contour lines indicate that shallow and deep groundwaters flow direction is preferentially centrifuge, departing from higher topographically areas (M.Lauro) toward the marginal ones. Decreasing in vertical and lateral permeability due respectively to the closing of fractures and contact with marls allow most relevant natural water discharges along the whole edge of the Hyblean plateau (Ruggieri, 1990).

3.CLIMATIC FEATURES

Temperature and rainfall long-term observation data (Servizio Idrografico del Genio Civile, Hydrographic Service of Civil Engineers 1966-1990), allow to subdivide the Hyblean region in two main areas.

The first one is the most elevated part of the study area (max altitude 986 m a.s.l.) characterized by low mean annual temperature (13-15°C) relatively abundant rainfall (650-850 mm/year) and some snow events.

The second one is less elevated section of the study area showing relatively high annual average temperature (16-19°C), low rainfall (less than 400 mm/year) (Figures 4 and 5).

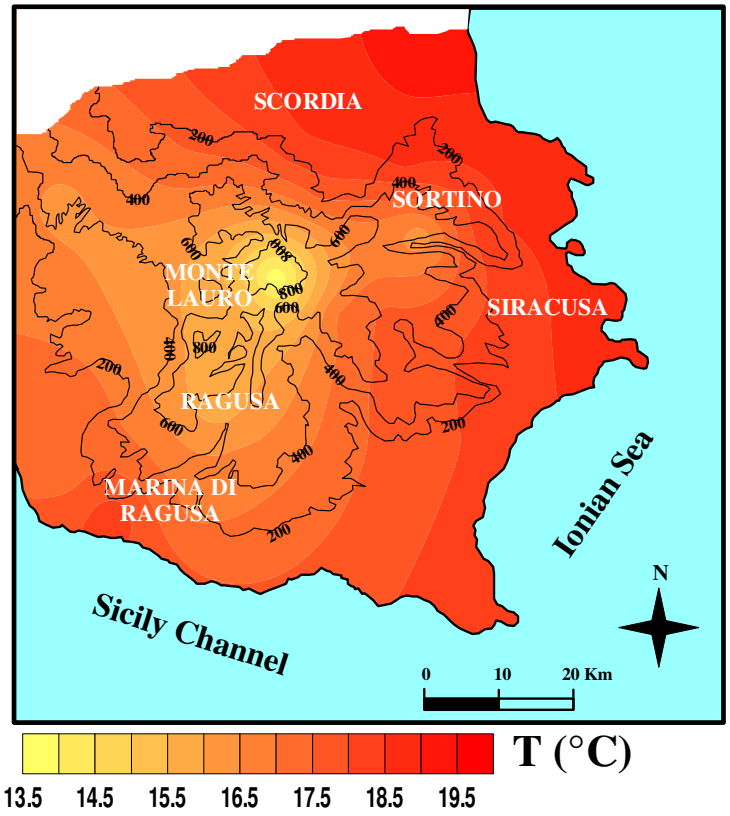

Figure 4: *Distribution map of air temperature (expressed in °C) at Hyblean Mountains. Data from Servizio Idrografico del Genio Civile (1966-1990).*

Sicily Island is located between the tropical climatic area and the European continental one. Throughout the different seasons, the boundary between these two zones is shifted due to the alternating expansion of these climatic belts. This process results in wide ranges of both air temperature and amount of rainfall, the main changes being between the rainy and the dry season

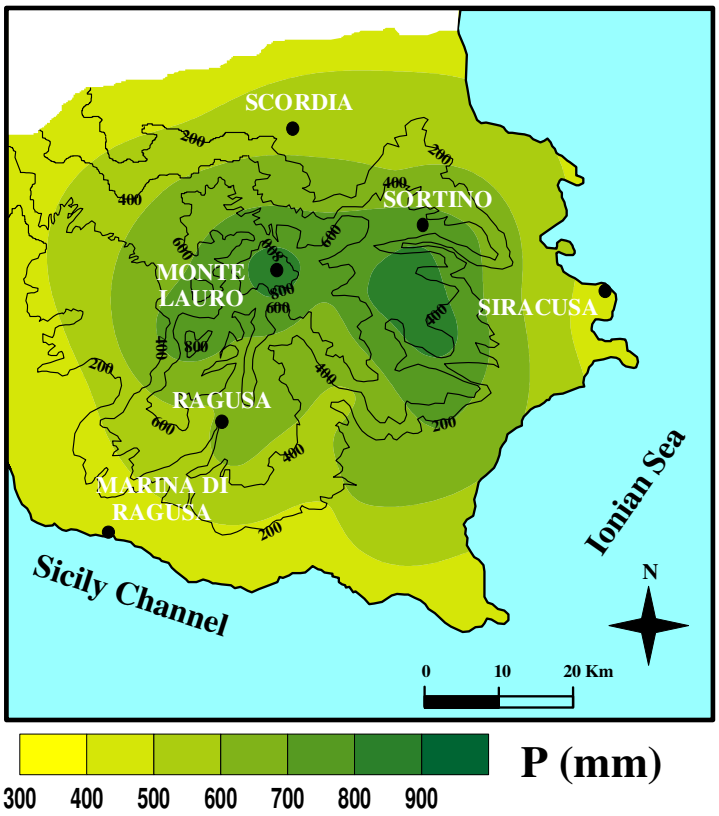

Figure 5: *Distribution map of precipiatation (expressed in mm/year) at Hyblean Mountains. Data from Servizio Idrografico del Genio Civile (1966-1990).*

Climatic diagrams, considering the mean monthly temperature and rainfall values relatively to two representative locations (Siracusa: 15 m a.s.l. and Monterosso: 691 m a.s.l.), are displayed in figures 6a and 6b.

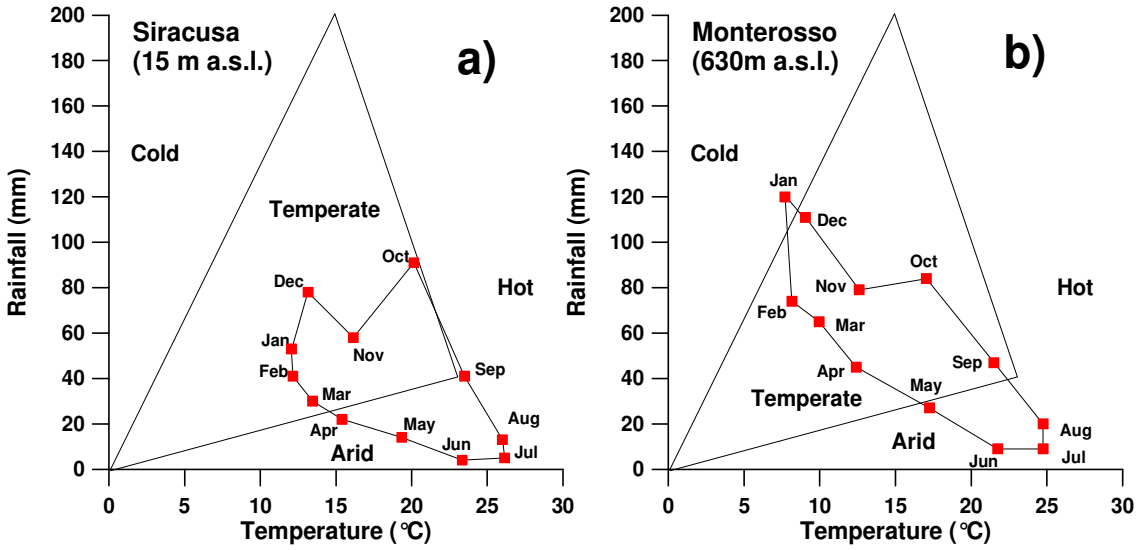

Figure 6 (a,b): *Peguy diagrams for Siracusa (a) and Monterosso (b) stations. Data from Servizio Idrografico del Genio Civile (1966-1990).*

It is easy to note, as the climate conditions are quite different between high- and low-altitude stations, mainly during cold months. This aspect plays an important role on the evapotranspiration process and on the control of the amount and the isotopic composition of infiltrating waters. High mean temperature values coupled with low amount of rainfall are the main reasons causing intense desertification processes in the topographically low areas of the Hyblean region. In this framework, the knowledge of the main factors controlling the isotopic composition of both the precipitation and the infiltrating water is very important in determining the relationships with local groundwaters.

4.WATER BUDGET

In order to estimate the amount of water involved in the annual water cycle in the Hyblean region a simplified water balance has been performed.

The equation used for the water balance:

$$P = E + R + I \qquad \text{(Eq. 1)}$$

where *P* is the amount of rainfall, *E* the amount of water lost for evapotranspiration, *R* surface runoff and *I* effective infiltration.

Areas assigned to each station have been obtained by subdividing the surface following the method proposed by Thiessen (1911).

For each basin, the direct surface rainfall (*P*) was computed by the sum of average annual rainfall value (*Pi*) of each raingauge station multiplied by its influence area (Ai) as follows:

$$P = \Sigma Pi * Ai \qquad \text{(Eq. 2)}$$

The average rainfall value for each of the five hydrogeological basins described previously is reported in table 1.

Evapotranspiration was estimated as a monthly potential evapotranspiration applying the formula proposed by Thorntwaite (1948), Hargreaves (1994) and Turc (1955). The latter has been modified considering the parameters specifically suitable for Sicilian areas (Santoro, 1970). Average values obtained by these three different calculations allow to define the amount of water that is monthly lost from the soils. Estimated values of monthly potential evapotranspiration are reported in figures 7a and 7b together with the temporal variation of the rainfall at Monterosso (630 m a.s.l.) and at Siracusa (15 m a.s.l.) stations. These stations represent two extreme cases, relative to the high and low portion of the basin, respectively.

By subtracting the monthly potential evapotranspiration from the monthly amount of rainfall, the effective precipitation (Ep=I+R) has been calculated. From the diagrams 7a

and 7b, it clearly appears that groundwaters meteoric recharge takes place only during some months of the cold season. In particular, at the station located at high altitude (Monterosso) it occurs from September-October to March, whereas at the station close to sea level (Siracusa) it occurs mainly from October to February.

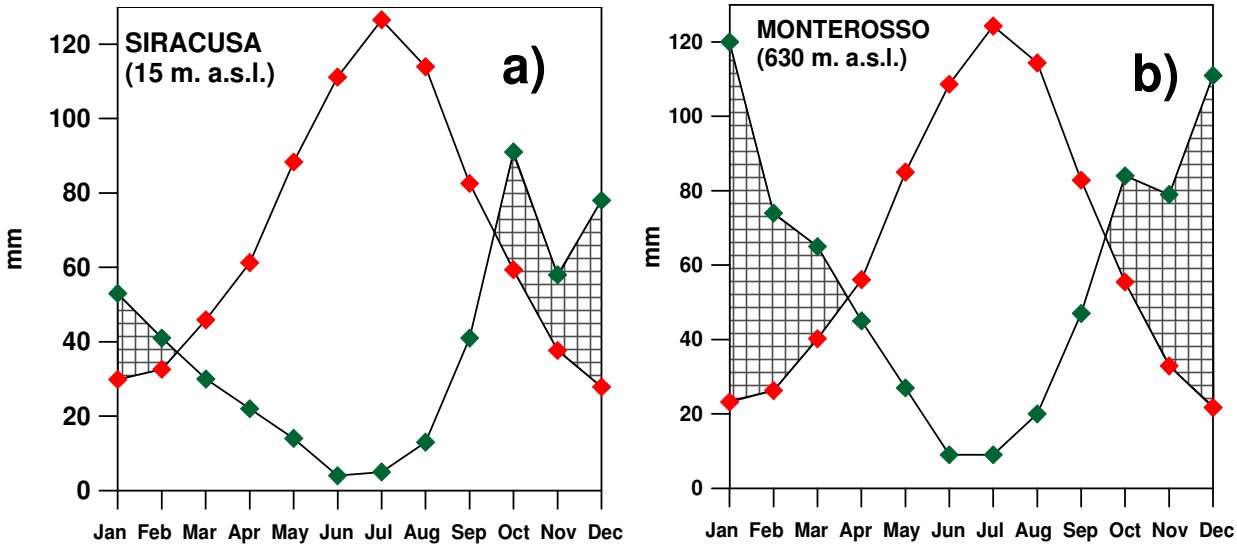

Figure 7 (a,b): *Monthly variations in the rainfall (R= green diamonds) and the average potential evapotranspiration (E_{tr}= red diamonds) at Siracusa (a) and Monterosso (b) stations. Data from Servizio Idrografico del Genio Civile (1966-1990).*

At all the stations, annual evapotranspiration values estimated as the sum of monthly effective evapotranspiration range from about 51% to 65 % of the total amount of the rainfall.

Because of the lack of data on the surface runoff and the complexity of the karst systems characterized by continuous insurgences and resurgences, the potential infiltration coefficient (P.I.C) has been used, in order to estimate the volume of infiltrating waters. It represents the ratio between the amount of infiltrating water (I) and the effective precipitation (Ep):

$$P.I.C.= I/Ep \qquad \text{(Eq. 3)}$$

These calculations do not take into account some factors such as the acclivity, the occurrence and the type of vegetation, the spatial distribution of the surface karst elements, the degree of weathering of the volcanic rocks. However, it is reasonable to think that the use of maximum and minimum PIC values can give an acceptable evaluation of the water volume involved in the infiltrating process.

The outcropping lithology and the used PIC values are reported in table 2.

The calculated volume of infiltrating water ranges between 4.7 and 6.8 10^8 m^3 per year corresponding to a yield of 1.1÷1.6 10^5 m^3 Km^{-2}. The water volume yield from the Hyblean Plateau can be estimated to be close to 15-20 m^3 sec^{-1}.

As can be observed in table 2, more than 90% of the total water volume infiltrates through the carbonate rocks and the volcanic deposits. Due to the extension and the high permeability values of carbonate and volcanic rocks their aquifers constitute the most important hydrogeological units of the Hyblean region.

5.RAINWATER ISOTOPIC COMPOSITION

Several studies on the isotopic composition of global precipitation throughout the world pointed out that the combined analysis of oxygen and hydrogen isotopes of the rainfall are indispensable for the understanding of the processes leading to their formation. Furthermore, rainwater isotope composition allows to better define some local climate conditions and to characterize the local meteoric recharge.

A wide range of temporal and spatial variations is displayed by the rainwater isotope values (Tab. 3). The most negative δD and $\delta^{18}O$ values have been measured during the cold-rainy season (-11.8 and –72, for $\delta^{18}O$ and δD respectively in Jan-00 at ML), while the most positive values (0.4 and –7, for $\delta^{18}O$ and δD respectively in Apr-99 at SR) have been recorded during the warm season. As an example, the temporal variations of rainwater isotope composition (SO station) are reported in figure 8.

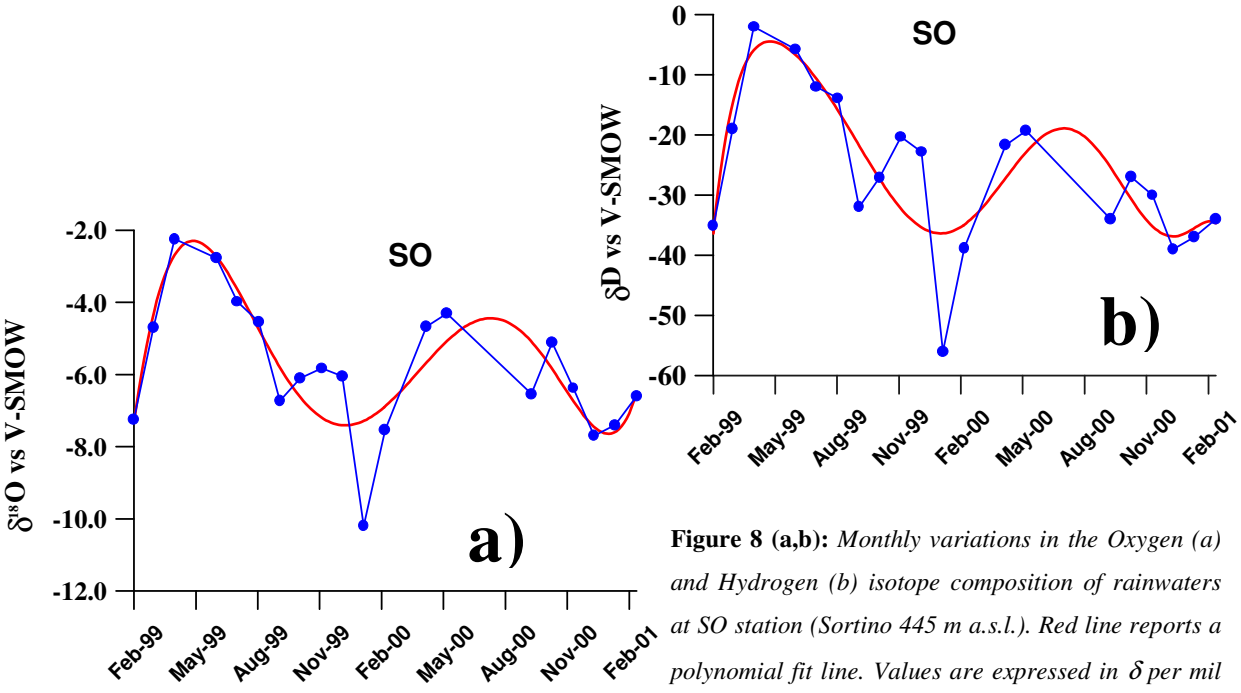

Figure 8 (a,b): *Monthly variations in the Oxygen (a) and Hydrogen (b) isotope composition of rainwaters at SO station (Sortino 445 m a.s.l.). Red line reports a polynomial fit line. Values are expressed in δ per mil vs V-SMOW*

This trend is quite similar to that relative to the other stations in the same area.

At each station a very good linear relationship ($0.86<r<0.95$) exists between $\delta^{18}O$ and δD (Fig. 9 a-f). The slopes of the least-squares fitting lines range from 5.96 (SR) to 6.87 (ML).

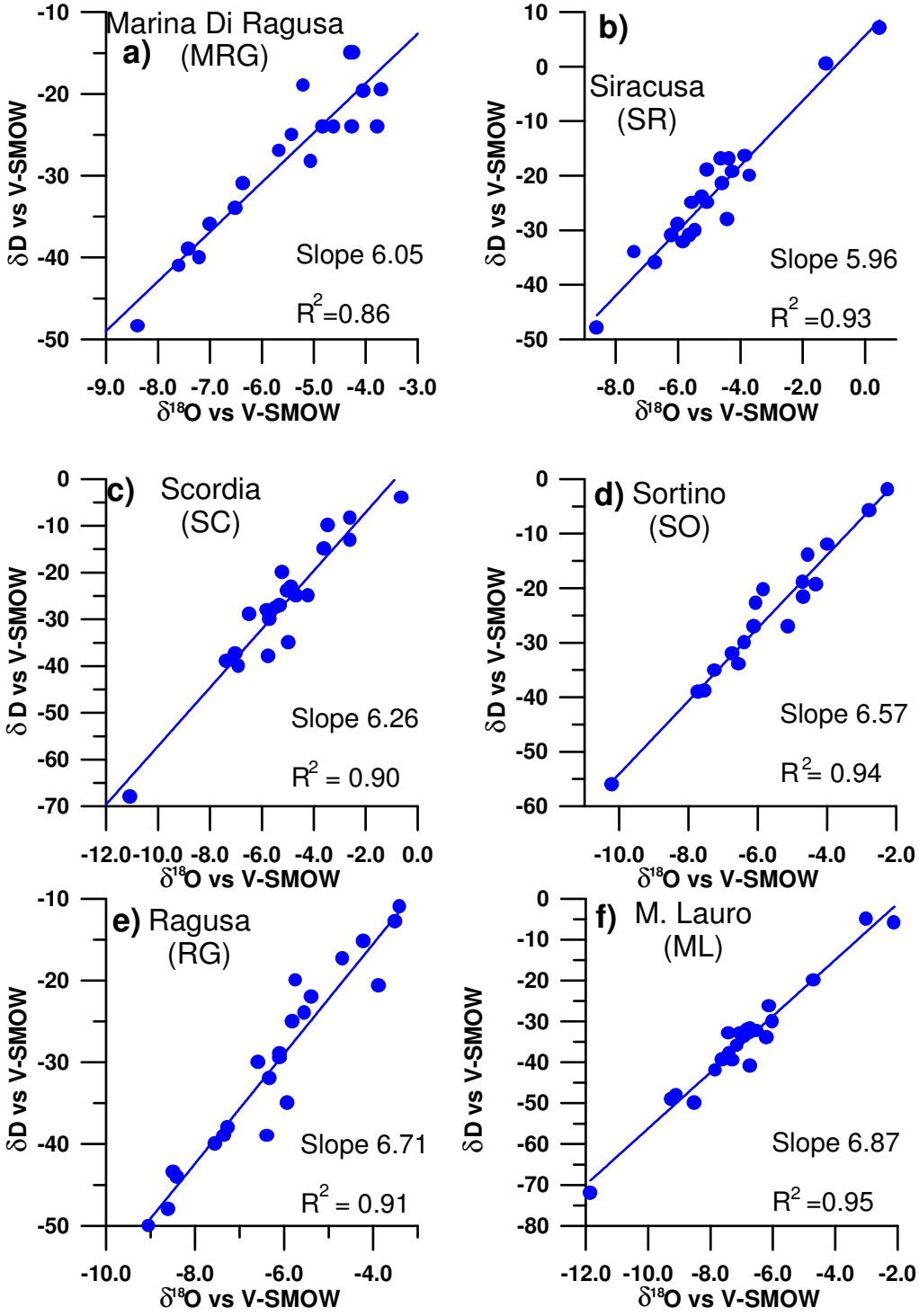

Figure 9 (a-f): *δD-$\delta^{18}O$ relationships for each station. Marina di Ragusa (MRG, a), Siracusa (SR, b), Scordia (SC, c), Sortino (SO, d), Ragusa (RG, e) and M. Lauro (ML, f).*

In a $\delta D/\delta^{18}O$ diagram (Fig. 10) almost all the rainwater samples fall between the meteoric water line (M.W.L. Craig, 1961) and the Mediterranean meteoric water line (M.M.W.L. Gat and Carmi, 1970).

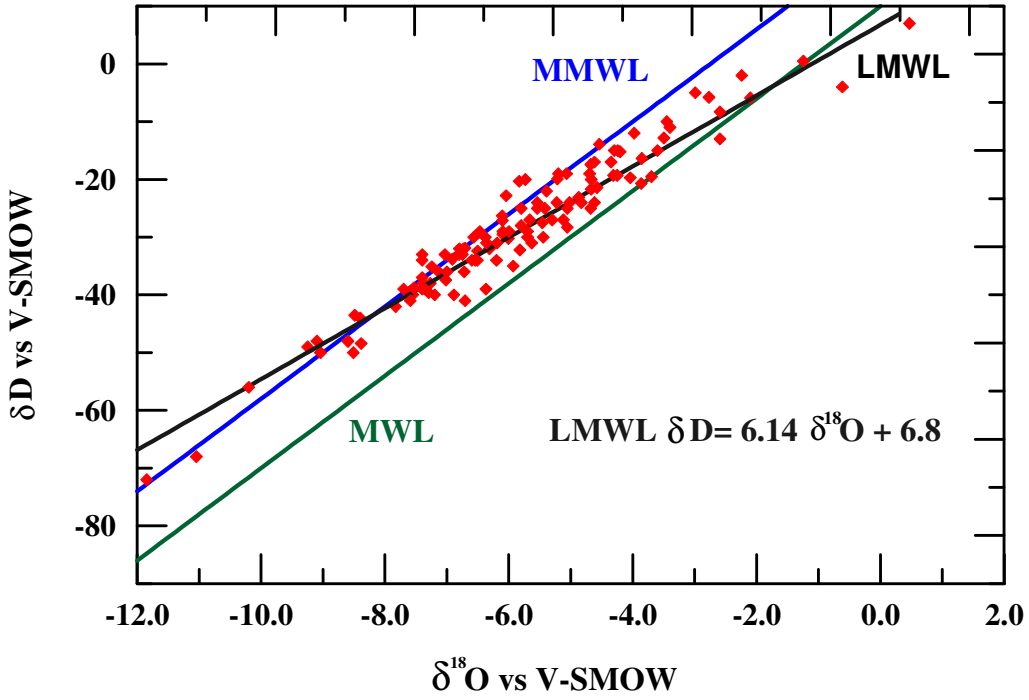

Figure 10: *δD-$\delta^{18}O$ relationship in rainwater collected at all the stations. In the same figure the Mediterranean Meteoric Water Line (MMWL, Gat and Carmi, 1970 blue line), the world Meteoric Water Line (MWL, Craig 1961 green line) and the Local Metoric Water Line (LMWL, black line) are also reported.*

The least-squares regression line for these data, representing the local meteoric water line, is:

$$\delta D = 6.14\ (\pm 0.18)\ \delta^{18}O + 6.8\ (\pm 1.08) \qquad \text{(Eq. 4)} \qquad (n=131,\ R^2=0.90)$$

The value of the slope of the $\delta D/\delta^{18}O$ line is a parameter indicative of the processes affecting the rainfall events. Values close to 8 suggest that precipitations occur under near isotopic equilibrium conditions, while lower values indicate that equilibrium fractionation is not the only process occurring in the atmosphere during the droplet condensation, evaporative processes taking place during the falling of the drops (Gonfiantini, 1986). If evaporation occurs at 20°C the $\delta D/\delta^{18}O$ ratio should be close to 4 (Jouzel, 1986).

In the Hyblean region, the discrepancy between "*global*" and "*local*" rainwater isotope composition, is a consequence of non-equilibrium processes, being probably related either to the monthly amount of rainfall, to the altitude and to the relative humidity of the atmosphere.

In fact, the slope of the best fitting line relative to rainfalls higher than 65 mm/month (R^2=0.97) is 7.45, while a slope of 5.97 (R^2=0.88) has been found interpolating values relative to rainfall lower than 65 mm/month (Fig. 11). Generally, this arrangement coincides with the rainfall occurred during cold and warm months respectively.

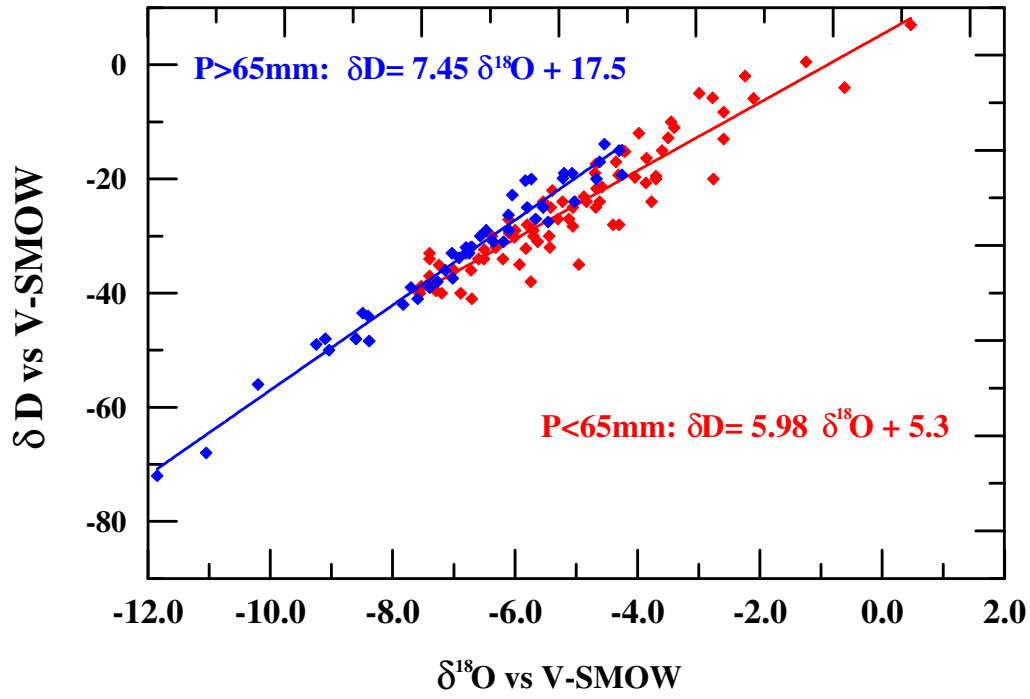

Figure 11: *δD-δ^{18}O relationship in rainwater collected at all the stations. Samples are arranged in two groups as a function of the amount of monthly rainfall.*

Furthermore, evaporative process become less intense while air masses move from the coast to high altitudes. In fact, for all the stations, a clear, but non linear correlation between elevation and slope of the δD/δ^{18}O relationship can be observed (Fig. 12). The slope value increases progressively from the coast to the high-elevation stations.

In order to determine the main factors that affect the rainfall isotopic composition occurred in the Hyblean region, a correlation matrix has been performed. It includes the weighted mean isotopic composition (both δD and δ^{18}O), annual average temperature, amount of rainfall, and altitude.

Weighted mean $\delta^{18}O_{wm}$ and δD_{wm} have been related to temperature (T), altitude (Q) and amount of rainfall (P). The obtained linear equation is the following:

$$\delta^{18}O_{wm} = -4.47 - 0.096T - 0.003\,Q + 0.0009\,P \qquad \text{(Eq. 6)} \qquad R^2=0.94$$

where coefficients are calculated from a multiple regression.

Temperature is naturally the most relevant independent variable with respect to rainfall and altitude, followed by altitude and amount of rainfall.

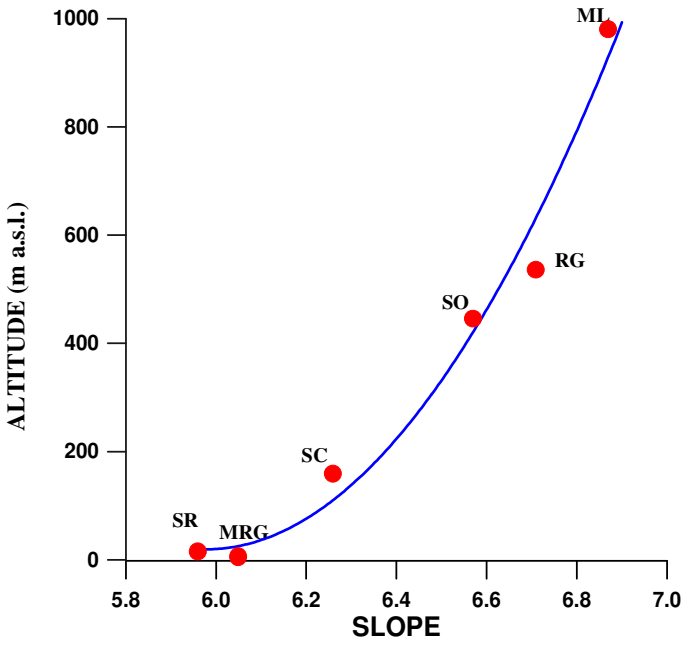

Figure12: *Slope-altitude relationship at Hyblean raingauge stations*

By applying the equation 6, a map showing the 18-Oxygen spatial variation has been realized, including within our raingauge network, also those belonging to the network of Hydrographic Service of Civil Engineers (Fig. 13).

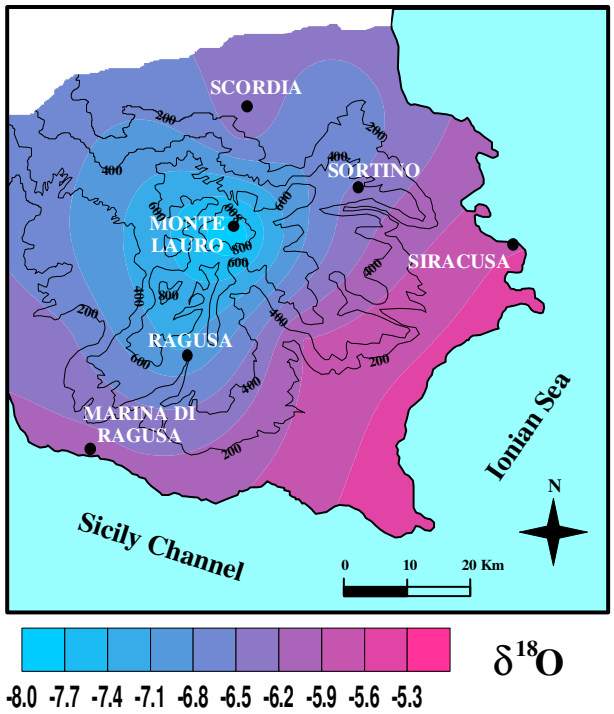

Figure 13: *Distribution map of the oxygen isotope composition in rainwater. Collected data have been integrated with those collected from the Civil Engineers network. Isotope values have been calculated from the multiple linear regression (see text).*

A very good linear relationship between altitude and weighted mean δD and $\delta^{18}O$ values has allowed to estimate the vertical isotope gradients. These parameters quantify the entity of the changes in the isotopic composition due to the altitude effect (Figs. 14a-14b).

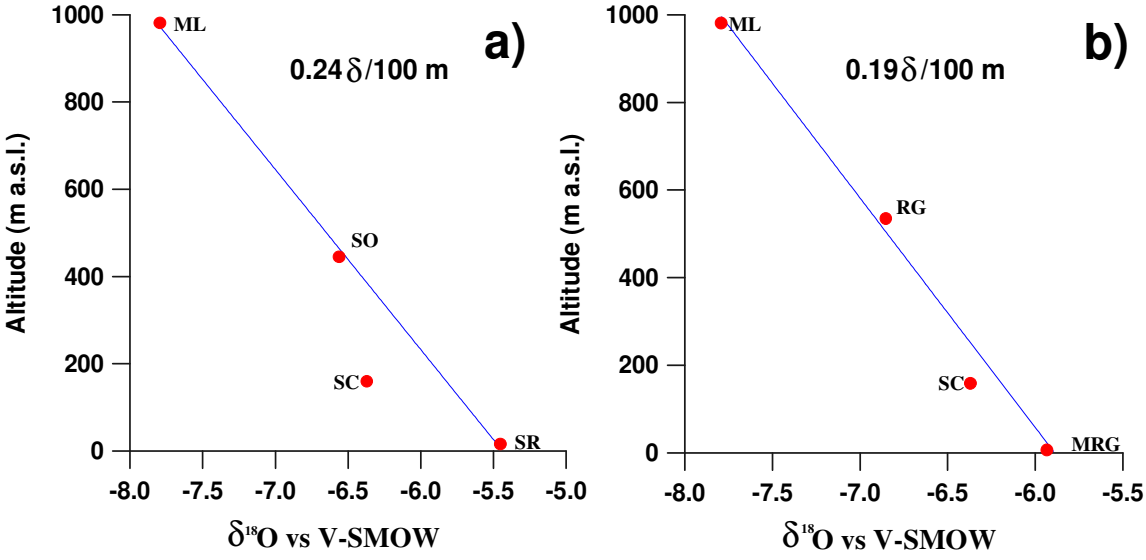

Figure 14 (a,b): *Vertical ^{18}O gradients for eastern (a) and southern (b) flanks*

Raingauges located on the eastern side (ML, SO and SR) indicate a values close to 0.24 $\delta^{18}O$/100 m and 1.6δD/100 m whereas 0.19 $\delta^{18}O$/100 m and 1.2δD/100 m where found for the stations located on the south flank (ML, RG and MRG), from M. Lauro towards M. di Ragusa. These values are consistent with those found by several authors in other Sicilian areas (Hauser et al., 1980, Favara et al., 1998). The small difference between the two flanks could be related to the morphology of the sides. In fact, the geometry of the topographic surface of the southern flank is mild and the slope quite constant, while the eastern one is characterized by several discontinuities.

SC station is located on the northern side of the Hyblean Mountains. As can be seen from figures 14a and 14b, the mean weighted δD and $\delta^{18}O$ values relative to SC station are slightly more negative with respect to those expected from the best fitting line for both South and East boundary. The depletion in heavy isotopic species in the rainwaters at SC rain-gauge, located about 100 Km inland from the south coast, seems to reflect the combined influence of both the "*continental effect*" and of the presence of a topographic barrier, represented by M. Lauro along the prevalent air mass movements.

These insights allow to model the spatial distribution of the isotopic composition of rainwater and to define the main courses of atmospheric perturbations. The proposed model confirmed that wet air masses provenience is mainly from Southwest and/or from East. Afterwards as a consequence of progressive partial condensation processes during

their movement Northward, air masses will be depleted in heavy isotopes. This is also consistent with the spatial distribution of chloride contents in rainwater. Figures 15a and 15b, represents the spatial pattern of chloride contents in the raingauges at December 1999 and February 2000 respectively. Chloride content, entirely derived from marine aerosol, has been assumed as a tracer of air masses movement from the coast to inland. It clearly appears that higher chloride concentrations have been observed at SR and MRG station and lower chloride concentrations have been observed at SC station.

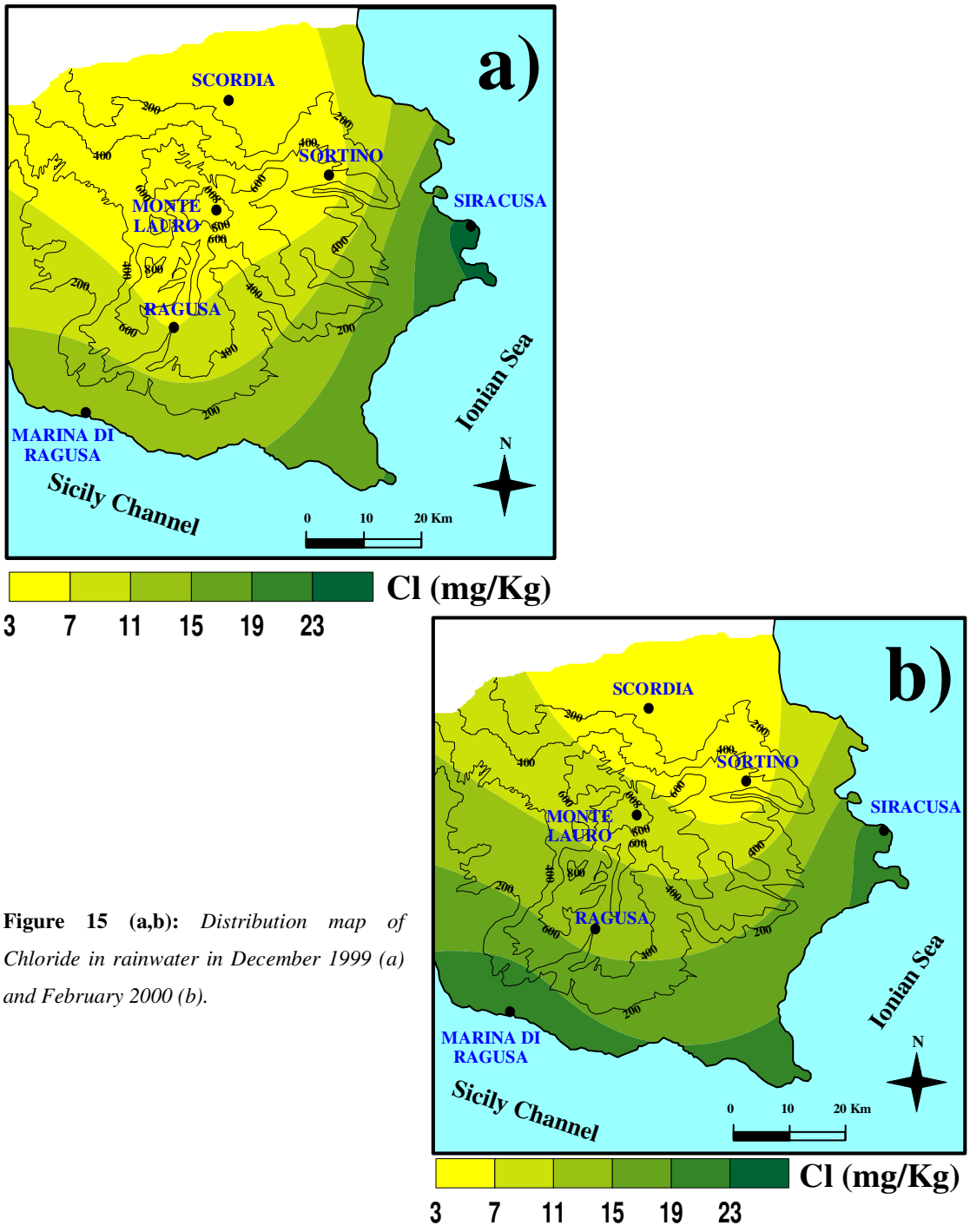

Figure 15 (a,b): *Distribution map of Chloride in rainwater in December 1999 (a) and February 2000 (b).*

6. GROUNDWATER ISOTOPE COMPOSITION AND RELATIONSHIP WITH METEORIC RECHARGE

Between 1999 and 2000, groundwaters were collected from springs and wells widespread within the Hyblean Plateau. The stable isotope compositions, reported in Table 4, are in the range -38 to –11 δ per mil vs V-SMOW for Hydrogen and–6.7 to –2.6 δ per mil vs V-SMOW for Oxygen.

Among Hyblean groundwaters, SU spring is the most enriched in heavy isotopes. Chloride and bromide contents suggest that this sample receives a non-negligible and variable with time contribution of seawater in the range 20-35%.

The frequency distribution of $\delta^{18}O$ values is shown in Figure 16. Average of $\delta^{18}O$ and δD are -6.0 per mil and –31 per mil respectively.

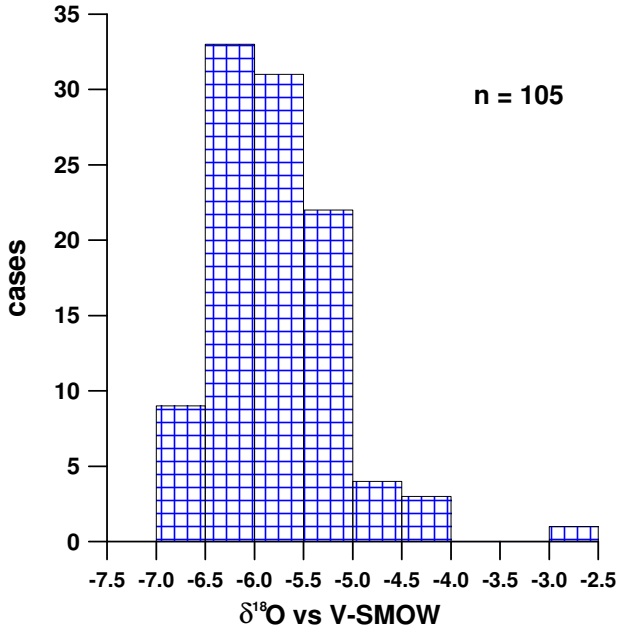

Figure 16: *Frequency distribution of Hyblean groundwater oxygen isotope composition.*

Figure 17, reporting the spatial distribution of 18-Oxygen values in groundwaters, obviously shows that the isotopically lightest groundwater samples (δD= -38 and $\delta^{18}O$ =-6.7) occur in the topographically most elevated sections of the Hyblean Mountains. Furthermore it is possible to observe a relative uniformity in isotope composition in almost all the Hyblean aquifers whose values range from –6.4 to –5.8 δ per mil vs V-SMOW. Similar spatial distribution is also apparent for deuterium, with values ranging between –33 and – 28 δ per mil vs V-SMOW.

This feature suggests the existence of a rather homogeneous groundwater system, flowing within the sedimentary and volcanic hydrogeologic units. Along the coastal zone (Capo Passero and Augusta), more positive values have been measured due to isotopically enriched meteoric recharge.

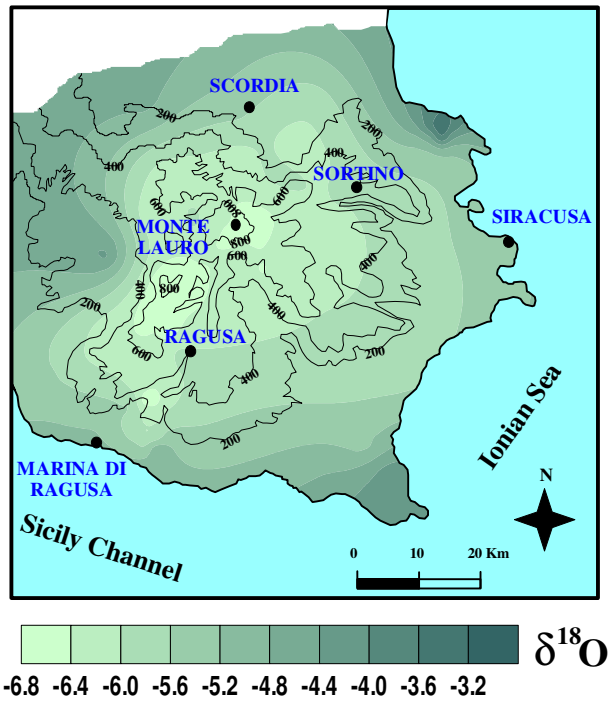

Figure 17: Distribution map of the Hyblean groundwater oxygen isotope composition

For what concerns the temporal variations in the stable isotope composition of groundwater, on the bases of the difference between the heaviest and the lightest isotopic values ($\Delta\delta^{18}O = \delta^{18}O_{max} - \delta^{18}O_{min}$) recorded throughout the seasons, two different temporal trends can be easily discerned.

- Waters showing an almost constant isotopic composition throughout the whole hydrological year ($\Delta\delta^{18}O$ =0.3÷0.4 δ per mil) such as BA ($\delta^{18}O$ = -5.1÷ -5.5) and GU ($\delta^{18}O$ = -4.7÷ -5.0) wells (Fig. 18a);
- Water showing a wider range in the δ-values ($\Delta\delta^{18}O$ 0.7÷1 δ per mil) and displaying more negative values at the end of the rainy months such as GE spring and P9 well (Fig. 18b).

This demonstrates that the first group belongs to groundwater fed by extensive aquifers, characterized by large recharge areas and long residence time, thus having very small seasonal variations in the isotopic composition.

The second group refers to shallower groundwaters, characterized by short hydrogeological circuits, relatively short residence time and consequently, reduced

possibility of homogeneization of seasonal contributions. However, the isotopic changes are smaller than those observed in the local meteoric recharge.

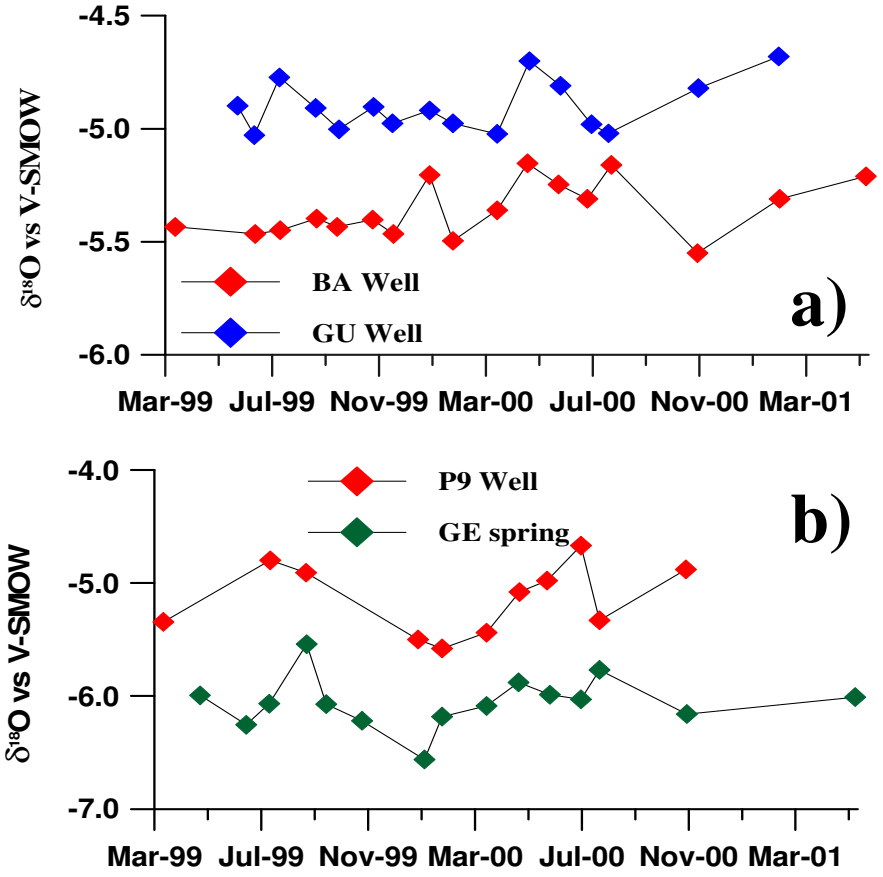

Figure 18 (a.b): *Temporal variation in Oxygen isotope composition in discharges fed by huge (BA and GU wells, a), and small (P9 and GE, b) aquifers respectively.*

However, some samples (such as CM, and SO in figure 19) hydrogeologically belonging to the first group display quite constant values except during the rainy period at the end of 1999 when most positive isotope values were measured.

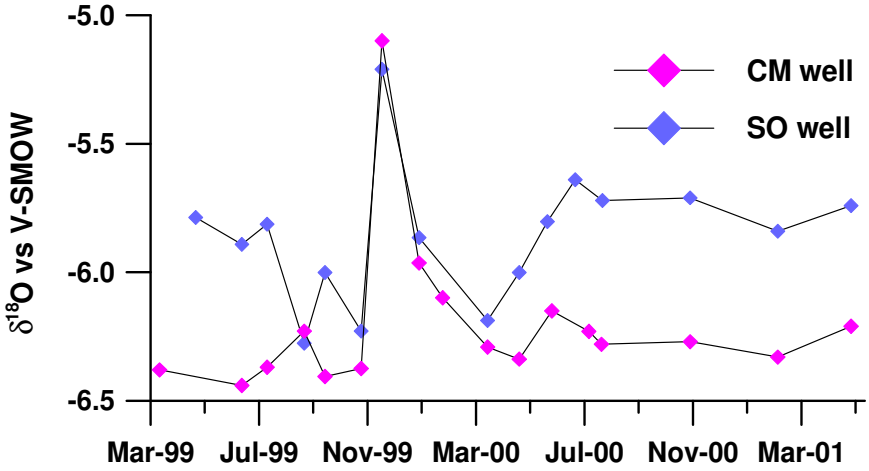

Figure 19: *Temporal variation in oxygen isotope composition at CM and SO wells.*

This peak seems to be linked to peculiar recharging events, charaterized by high amount of rainfall occurred in only five days (Nov. 99). The change in the isotopic composition appears as the result of a mixing between the background values of the well and the local shallow aquifer (like P 9 or GU wells) as a consequence of an increasing in the hydraulic gradient. It seems reasonable the occurrence of a mixing processes between these two overlapped aquifers through the structure of the well. The isotopic variations are also well-correlated to changes in the chemical composition, recorded in the same period.

In order to compare the stable isotope compositions of precipitation to those of groundwater it is pf importance to evaluate the average isotopic composition of infiltrating water. This value has been calculated by subtracting the aliquot relative to evapotranspiration from the weighted isotopic values calculated for each station as previously described. In this preliminary evaluation, we have supposed that evapotranspiration causes only a mass loss and no isotope fractionation processes occur. The obtained values for infiltrating waters are more negative with respect to the precipitation up to 0.7 δ per mil for 18-oxygen and 3.5 δ per mil for deuterium. This isotope effect is due to the fact that infiltration takes place during the wet season, when the precipitations are more depleted in heavy isotopes, whereas during warm months the Hyblean aquifers do not receive any substantial meteoric contribution.

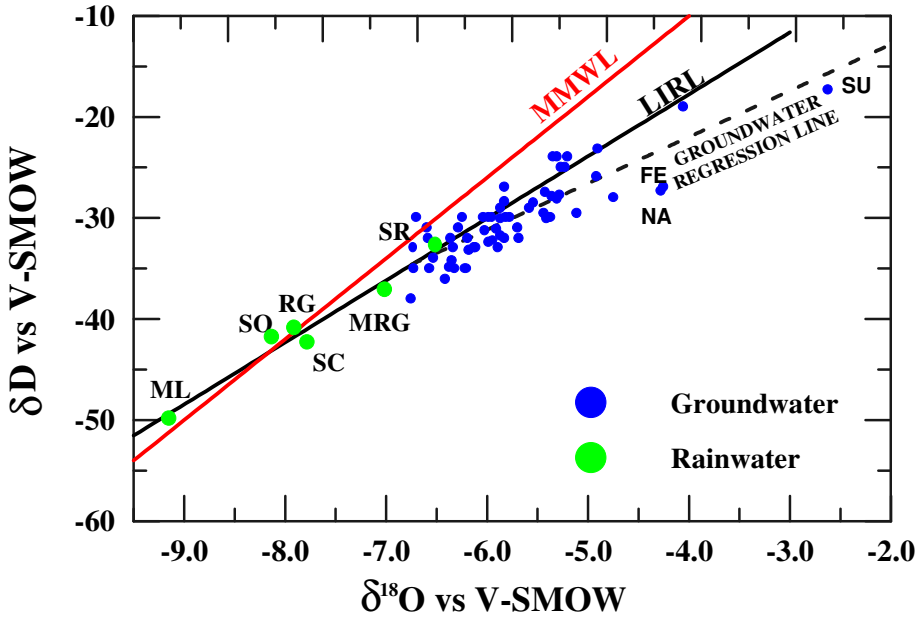

Figure 20: δD-δ^{18}O relationship in groundwater collected from Hyblean aquifers. In the same plot, Mediterranean meteoric line (MMWL, red line) and local infiltrating rainwater line (LIRL, black line) are also shown.

The representative points of the infiltrating waters calculated for each rain-gauge station fall in proximity of the MMWL, except for coastal stations MRG and SR (Fig. 20).The best-fit line for the infiltrating water is:

$$\delta D = 6.15\ \delta^{18}O + 6.9 \qquad \text{(Eq. 7)} \qquad (R^2 = 0.97)$$

which represents the Local Infiltrating Rainwater Line (LIRL).The average isotopic composition of groundwater samples collected from Hyblean aquifers, plotted in a $\delta D/\delta^{18}O$ diagram (fig.20), lies generally to the right of the MMWL. The best linear fitting of deuterium 18-oxygen relationship is:

$$\delta D = 4.56\ \delta^{18}O - 3.79 \qquad \text{(Eq. 8)} \qquad (R^2 = 0.65)$$

The slope of this best fitting-line is lower than that of the infiltrating waters, thus suggesting that groundwater during or after infiltration, undergoes some secondary process under non-equilibrium conditions.

The distribution of the points reported in figure 20 suggests the absence of groundwaters having isotopic composition in the range defined by ML and MRG stations. Almost all groundwater samples show isotopic values enriched in heavy isotope with respect to the infiltrating waters

The difference between the relative isotopic composition of infiltrating water and groundwaters suggests at least of two hypotheses:

- the presence of occasionally anomalous meteoric events that shift the isotopic composition of infiltrating waters toward more negative values;

and/or

- the occurrence of secondary processes, causing an enrichment in heavy isotope in groundwater (evaporative processes or mixing with isotope-enriched waters)

As regard the first hypothesis, it needs to note that isotope data relative to the month of January, 2000 at almost all the stations, show extremely lower δ-values with respect both to the isotopic composition of the cold season and to January 2001 (Fig.8). These differences range generally from 1 and 3.6 δ per mil for 18-oxygen and from 6 to 29 δ per mil for deuterium. Furthermore, weighted isotopic values for infiltration waters will be appreciably influenced being January one of the rainiest months.

In order to reduce the effect of anomalous isotopic rainfall events, the δ-values of January 2000 have been substituted with those relative to January 2001. After this correction, the weighted mean values for infiltration waters at all stations, are shifted towards more positive values. Heavy isotop enrichments have been estimate in the range of 0.5 to 1 δ per mil for 18-oxygen and from 5 to 8 δ per mil for deuterium, respectively (Fig. 21).

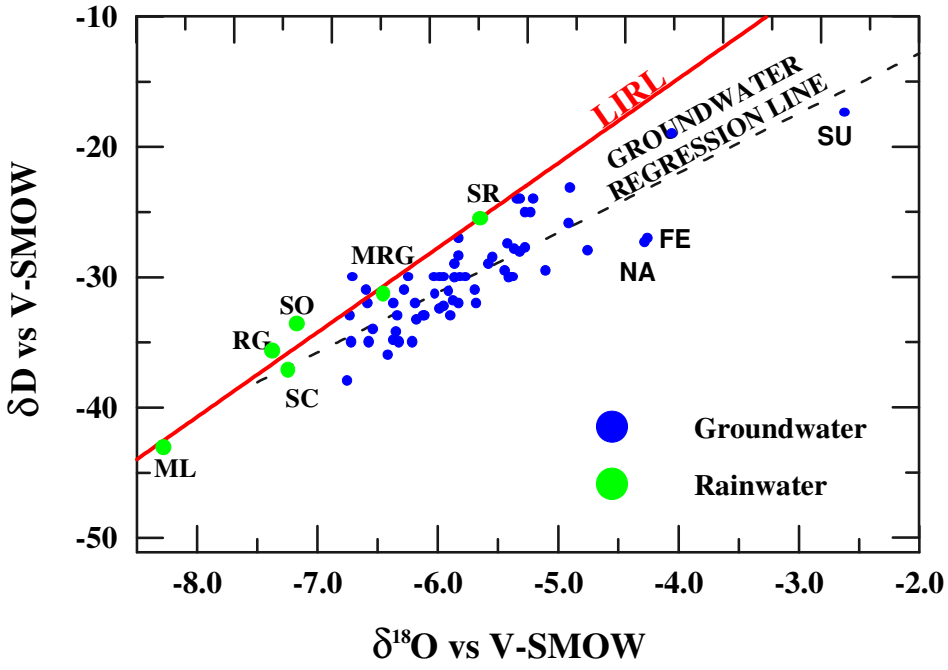

Figure 21: $\delta D/\delta^{18}O$ relationships in groundwaters collected from Hyblean aquifers. Local infiltrating rainwaters have been corrected substituting the values relative to January 2000 with those of January 2001. For further details see text.

However, the $\delta D/\delta^{18}O$ relationship ($\delta D = 6.49\ \delta^{18}O + 11.2$ ($R^2 = 0.97$)) doesn't not change significantly.

For what concerns the second hypothesis, it is relevant to highlight that the slope of the best fit line for Hyblean groundwater (4.56) is lower than that relative to the infiltrating waters (6.49). This fact suggests that Hyblean groundwaters, during infiltration in the unsaturated soil zone, undergo fractionation processes. These non-equilibrium processes commonly occur worldwide in areas characterized by arid or semi-arid climate (Zimmerman et al., 1967; Leontiadis et al., 1996).

Another explanation could be found in a possible relevant role played by evaporated surface-waters such as rivers or marsh, during groundwater recharge.

Groundwater stable isotope composition of deuterium and 18-oxygen is usually used for the understanding of the mechanisms of the meteoric recharge and to characterize the hydrogeological circuits feeding the aquifers. However, in the case of the Hyblean aquifers, the occurrence of evaporation processes in the soil during infiltration makes difficult the interpretation of stable isotope as natural tracers in identifying the recharge areas and in modeling of hydrogeological circuits.

7. GEOCHEMISTRY OF MAJOR ELEMENTS

Field determinations and laboratory analytical results for water samples collected within the Hyblean Plateau are showed in table 5.

It is possible to observe a large variability both in the measured physico-chemical parameters (e.g. Temperature, Conductivity, pH, Eh) and in the content of major elements, thus suggesting the existence of several geochemical processes governing the chemistry of the studied groundwaters.

The mean water temperatures is 19.2 °C. Lower temperature values were generally measured at higher altitudes, while a slightly thermal anomaly has been identified along the Northern boundary, where the highest measured water temperature was 28.4°C (Figure 22).

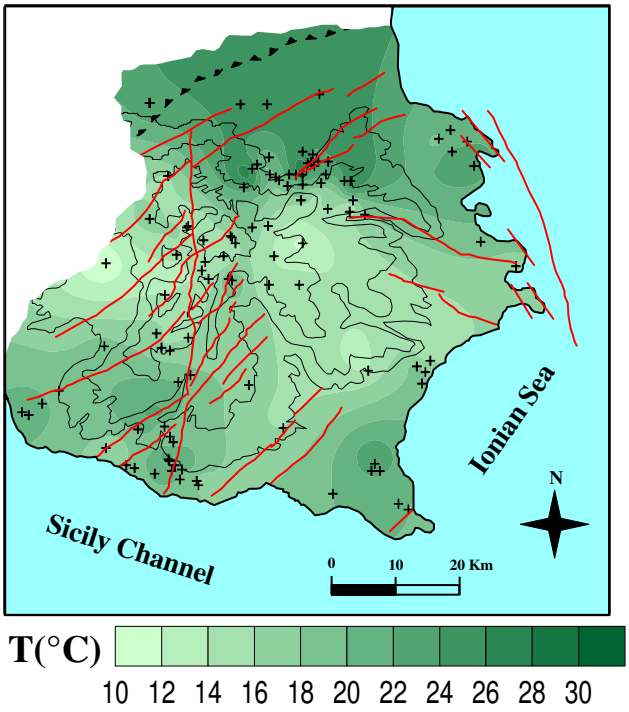

Figure 22: *Distribution map of temperature in Hyblean groundwater.*

The conductivity values of waters range from 208 up to 16230 µS/cm, with a mean value of about 1000 µS/cm. The central part of the Hyblean Plateau exhibits the lower conductivity values, while higher values are located along the perimeter of the studied area (Fig. 23). The latter waters have higher conductivity values due to:

- Variable seawater contamination (SU, AR, PR and GN samples);
- Interaction with evaporite rocks mainly made of sulphate-bearing minerals (PB, BL).
- High deep-CO_2 input (NA and FE) and consequently a more intense rock leaching.

The pH values range from 6.04 to 9.25. The highest values have been recorded in the

northern border (BO, SS, PA and PR samples), while the lower value has been measured in the "Mofeta dei Palici" area (NA sample), where a high deep CO_2 input to the water table is present (Fig. 24). The recorded Eh values range from –345 mV to 402 mV. The lowest Eh values have been measured close to the main tectonic structures (M. Lauro-Scicli; Hyblean Malta escarpment, Fig. 25).

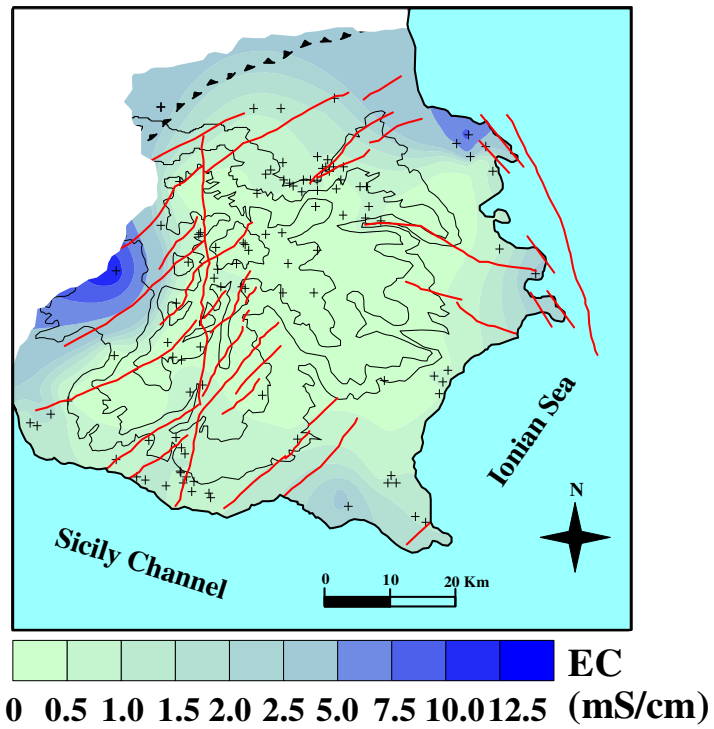

Figure 23: *Distribution map of electrical conductivity in Hyblean groundwater*

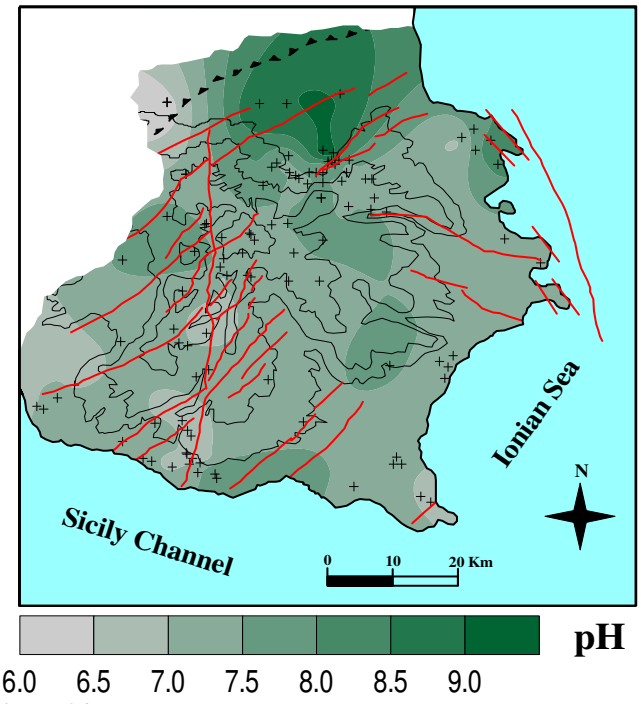

Figure 24: *Distribution map of pH values in Hyblean groundwater.*

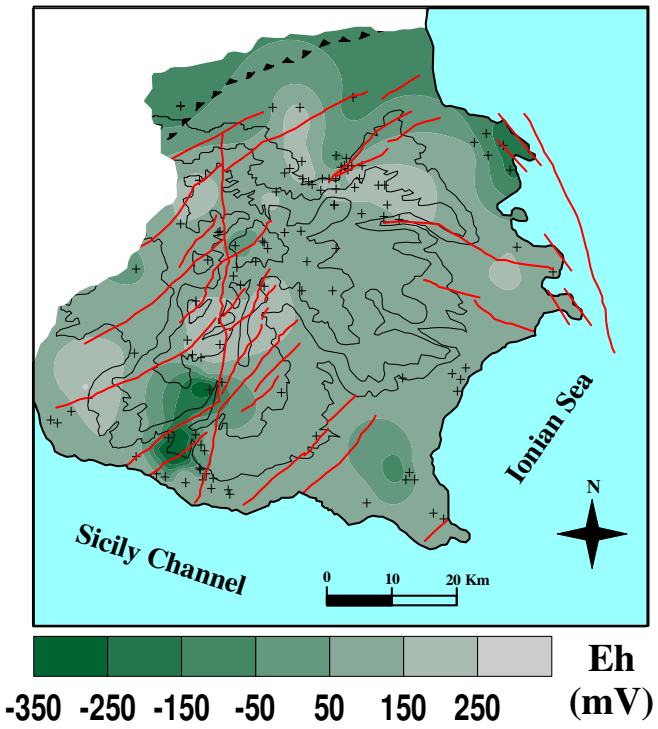

Figure 25: *Distribution map of Eh values in Hyblean groundwater.*

In agreement with the hydrogeological setting and on the base of the location of sampling points, groundwaters have been arranged in three groups hosted in fractured carbonate (squares) weathered basaltic rocks (circles) and porous marginal deposits (triangles) respectively.

The chemical classification of the sampled waters has been realized through two Langelier diagrams (figures 26 and 34). In the first reports overall samples hosted within the sedimentary aquifers (SE aquifer), mainly carbonate are reported, while groundwaters flowing through volcanic rocks (VO aquifer) are shown in the second one.

7.1 SEDIMENTARY AQUIFER

Water samples belonging to the first group (SE aquifer) fall mainly in the field relative to the alkaline-earth bicarbonate water-type (Group A) (Fig. 26). Other samples lie within the chloride-sulphate alkaline-earth field (Groups B and C) and finally within the chloride-sulphate alkaline field (D).

Groups B,C and D can be identified respectively as follows:

- SO_4-water type (Group B, violet triangles). Their mineralization process is linked to dissolution of evaporite rocks made mainly of sulphate-bearing minerals such as gypsum. These sediments outcrop only in a restricted area located along the south-western margin.
- Nitrate-rich waters (group C, black triangles). Their unusual composition can be related

to high nitrate concentrations being in some cases the most abundant anion. This suggests that anthropic pollution mainly derived from agricultural practices affect in a relevant way the chemistry of this group.

- Sodium-Clhoride waters (Group D) (green triangles). In these groundwaters, mainly located along the eastern and southern coast, Na and Cl are the dominant elements, having a Na/Cl ratio close to the seawaters. This suggests their chemistry is mainly controlled by sea water contribution (up to 30%, SU sample). Only one sample (FE) located on the western side and far from the coast, differs from the other ones. In fact, this sample has high bicarbonate content (1200-1300 mg/l) and a Na/Cl ratio slightly higher with respect to seawater. This sample could be contaminated by an input of brackish water.

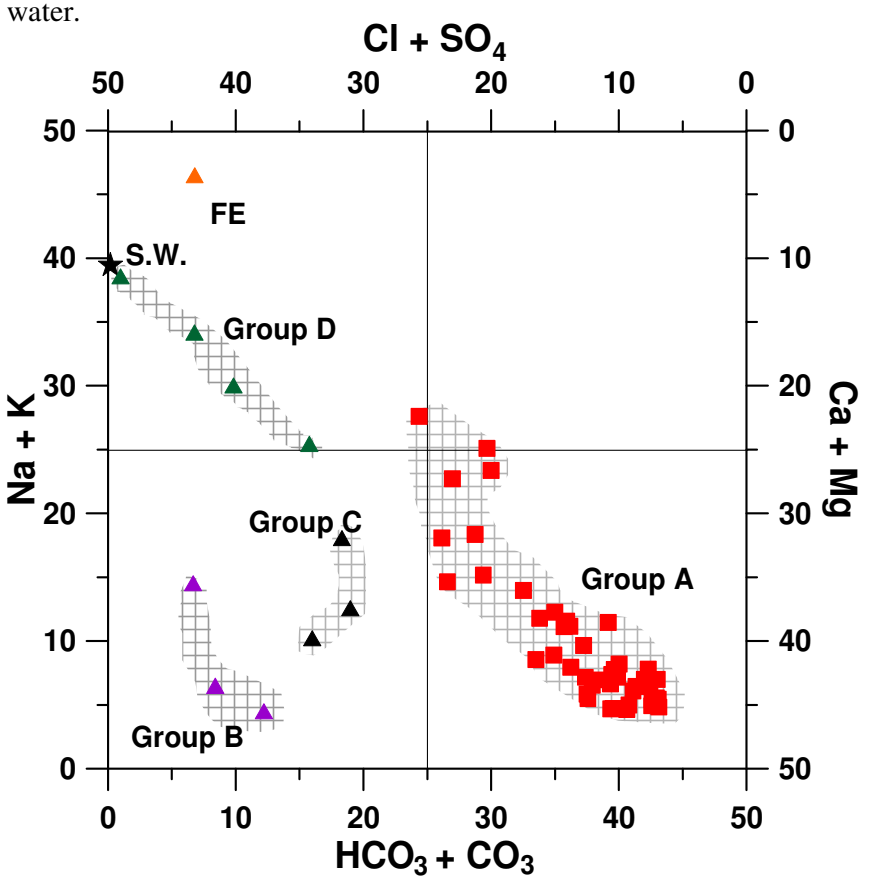

Figure 26: *Langelier classification diagram. In this plot groundwaters flowing within sedimentary aquifers (SE aquifers) are reported.*

Within the group A groundwaters two end-members have been distinguished. The first term (A1) is characterized by low Mg and high Ca content. The second end-member (A2) shows higher Mg content up to reach a Ca/Mg ratio close to 1 (fig. 27). In the Ca/HCO_3 diagram (Fig. 28), groundwaters having low Mg content are arranged along a line representing the stoichiometric dissolution ratio of calcite, while the waters belonging to

the Mg-rich group diverge from this trend, exhibiting a deficit in Ca content.

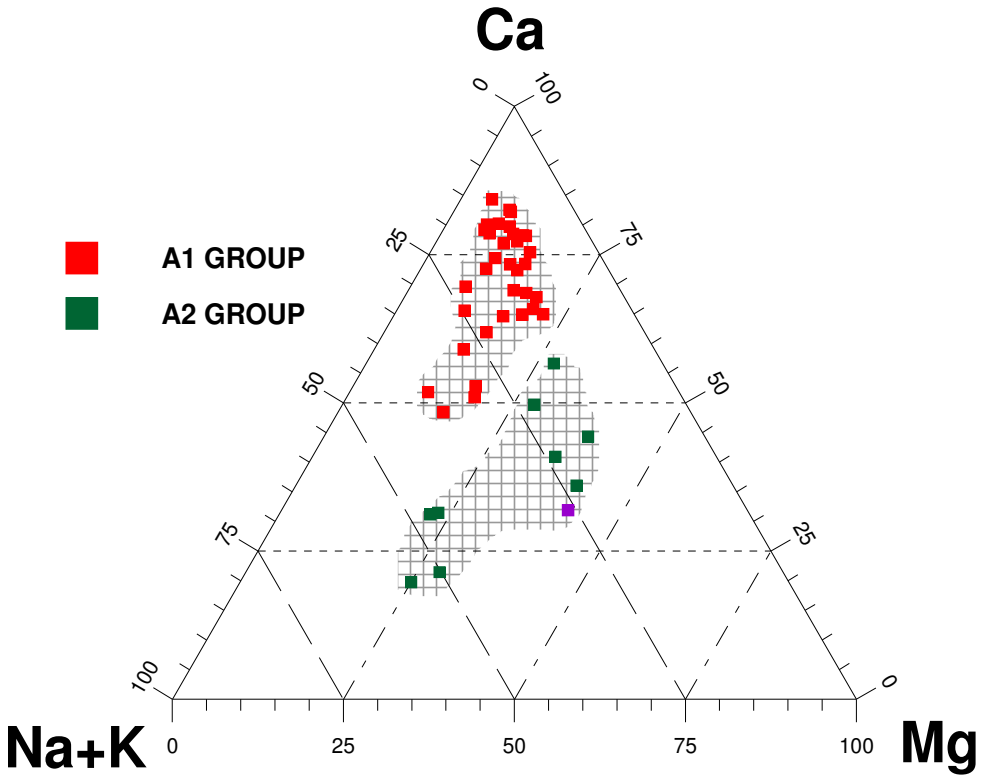

Figure 27: *Na+K/Ca/Mg triangular diagram. Representative point of SE sample interacting with Cretaceous volcanic deposits is also reported (violet square).*

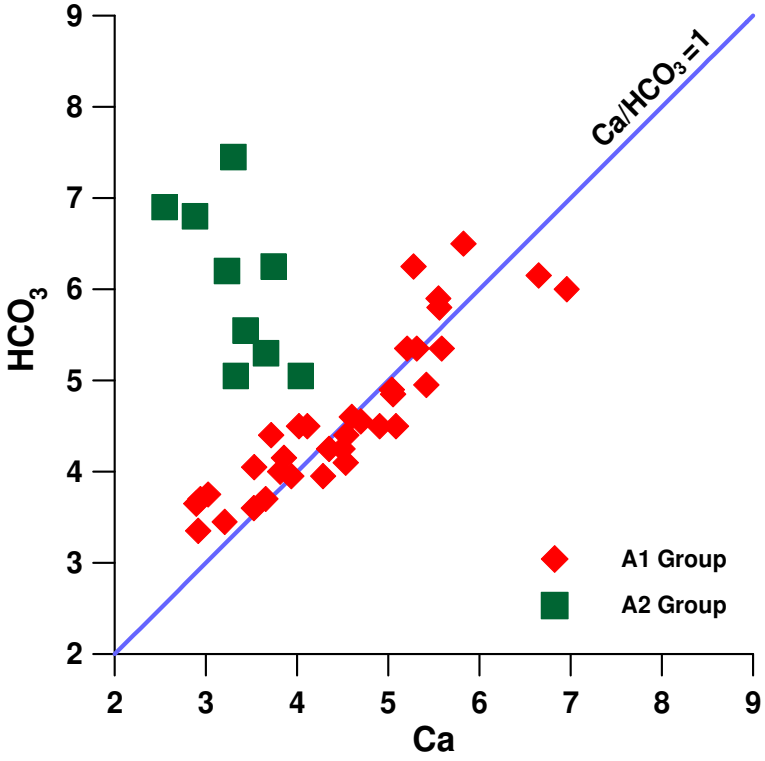

Figure 28: *Ca vs HCO_3 diagram. Blue line identifies the stoichiometric ratio of calcite dissolution*

On the base of magnesium content and the water temperature (fig. 29) a further division between these two end-members has been operated.

High-Mg contents correspond to a higher temperature, even if some exceptions have been recognized. Average groundwater temperatures of the Mg-low aquifer is about 16°C, very close to the average temperature of the infiltrating waters. While mean water temperature of the samples belonging to the A2 aquifer is about 22°C.

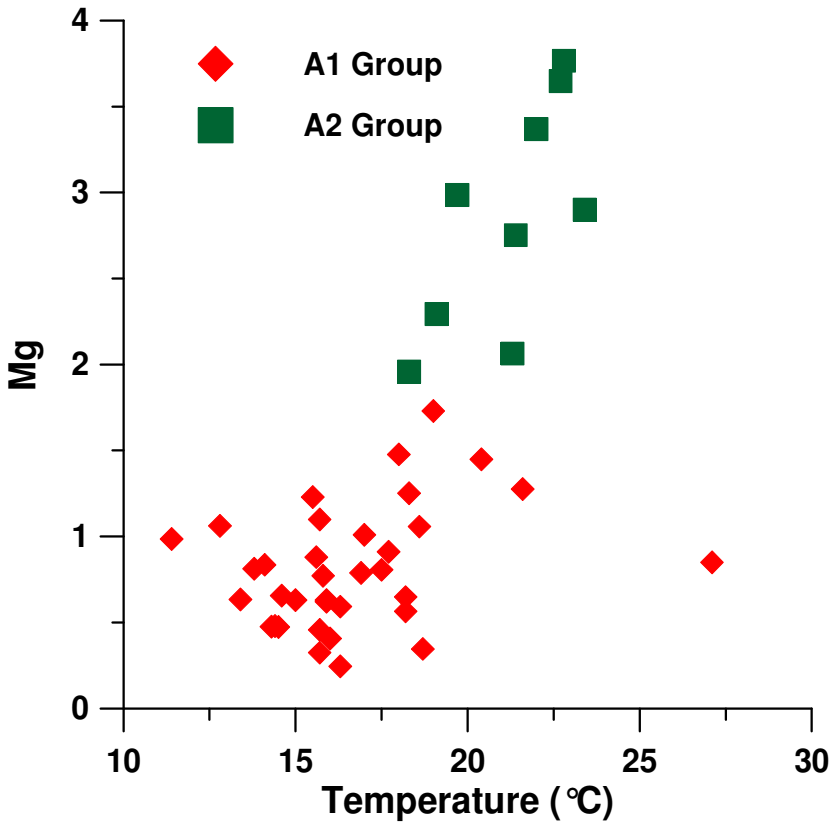

Figure 29: *Magnesium-water temperature diagram.*

According to the hydrogeological setting, these insights confirm the existence of two overlapped hydrogeological structures. The shallow aquifer, hosted within the Irminio member of the Ragusa Formation, extends at depth no greater than 100-150 m. It is separated through a marls layer from a deeper aquifer, mainly hosted within the underlying Leonardo Member (Ragusa Formation) and the Amerillo formation.

$MgCO_3$ content of carbonate rocks outcropping in the studied area is in the range 0.21÷3.8% (Tab.6). According to this composition the examined rocks fall within the range accepted for Low-Mg calcite (Milliman, 1974; Brand, 1981). Such low-Mg content in these carbonate rocks cannot explain the presence of Mg-rich groundwaters. On the other hand, in the investigated area, dolostones and dolomite-rich limestones (Trias-Lias in age) have been found only at great depths (1500-2000 m, b.s.l., Carbone et al., 1987).

Therefore, it appears more likely that high-Mg contents of the deeper aquifer (A2) could be related to interaction between groundwaters and Mg-silicates of volcanic rocks. In fact, alternating basic volcanic horizons, mainly Cretaceous in age, have been found inside the sedimentary sequences within both Amerillo Formation (Upper Cretaceous-Eocene) and the other underlying geologic complexes (Longaretti and Rocchi, 1990). The occurrence of water rock interaction processes with volcanic rocks seems to be confirmed by similar chemical features exhibited by SE sample (violet square in Fig. 27). This well water is located in the south western corner of the Hyblean plateau, where Cretaceous alkaline volcanic rocks are present, both as limited outcropping and at shallow depth (thickness 400-600 m).

Both A1 and A2 groundwater subgroups evolve towards more alkali-rich end-members (Fig.27). At the same time, a chloride and sulphate enrichment have been also identified (Fig. 30).

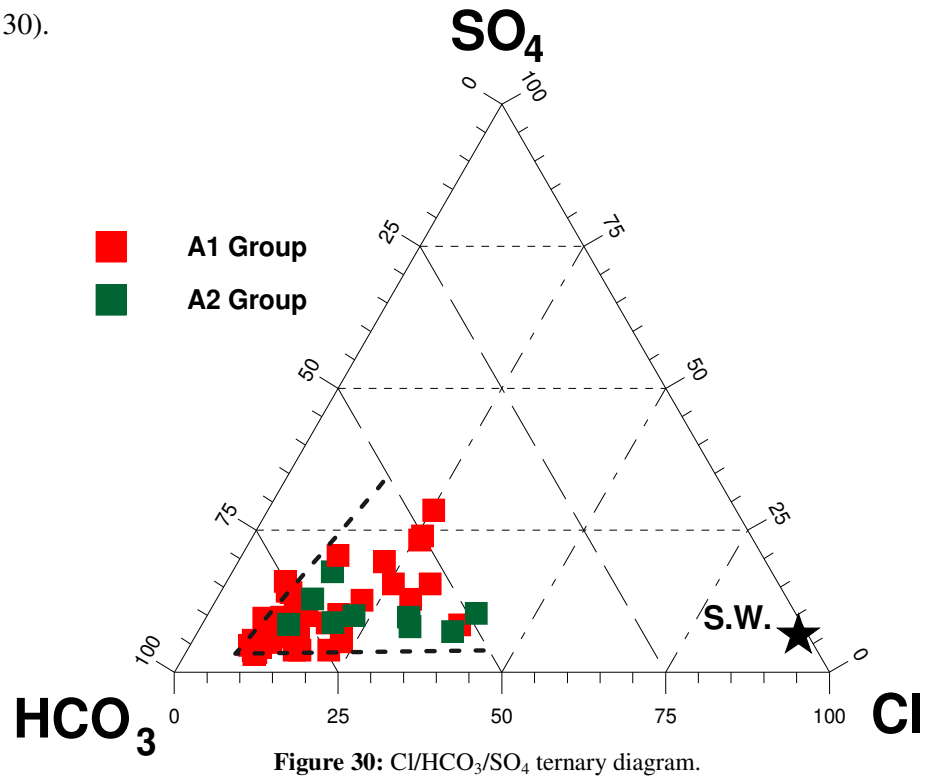

Figure 30: $Cl/HCO_3/SO_4$ ternary diagram.

For the most evolved terms the Na/Cl ratio (Fig. 31) is appreciable higher than seawater thus suggesting a contribution in alkali content from volcanic rocks. However an input of deep Na- and Cl-rich brines generally associated with hydrocarbon reservoirs cannot be ruled out

The Mg/Na plot (Fig. 32) referred to the A1 and A2 groundwater groups allows to define better the geochemical processes governing the chemistry of these groundwaters groups. In this diagram, two different alignments with Mg/Na ratio close to 0.5 and 4 respectively

have been identified. The intersection of these two alignments is representative of the less contaminated A1 aquifer, while MA and CN samples represent two extremes of the deep Mg-rich aquifer (A2). The Mg-content in A2 group seems to be buffered by dolomite saturation (see section 8.2.2).

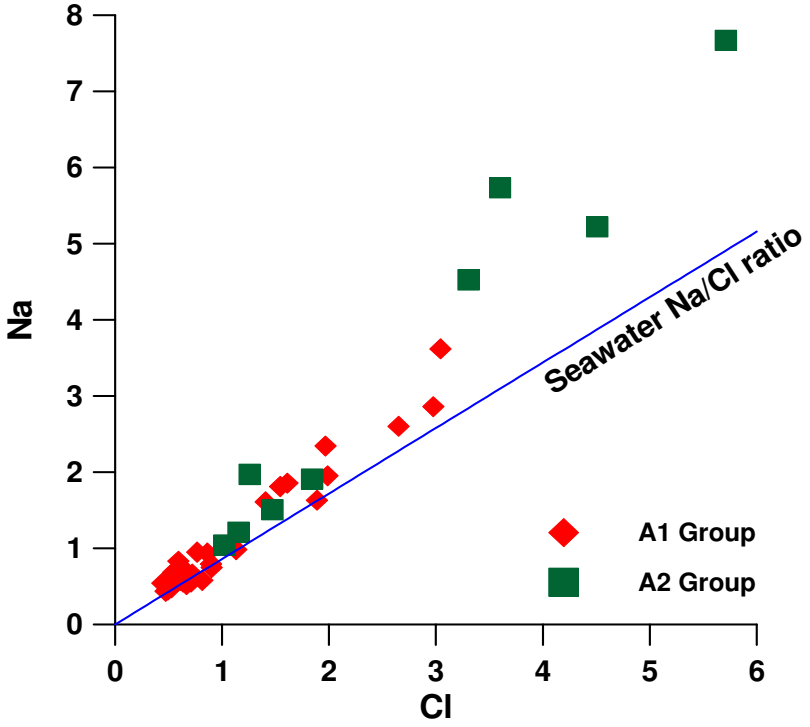

Figure 31: *Na vs Cl plot. Blue line represents Na/Cl ratio in seawater.*

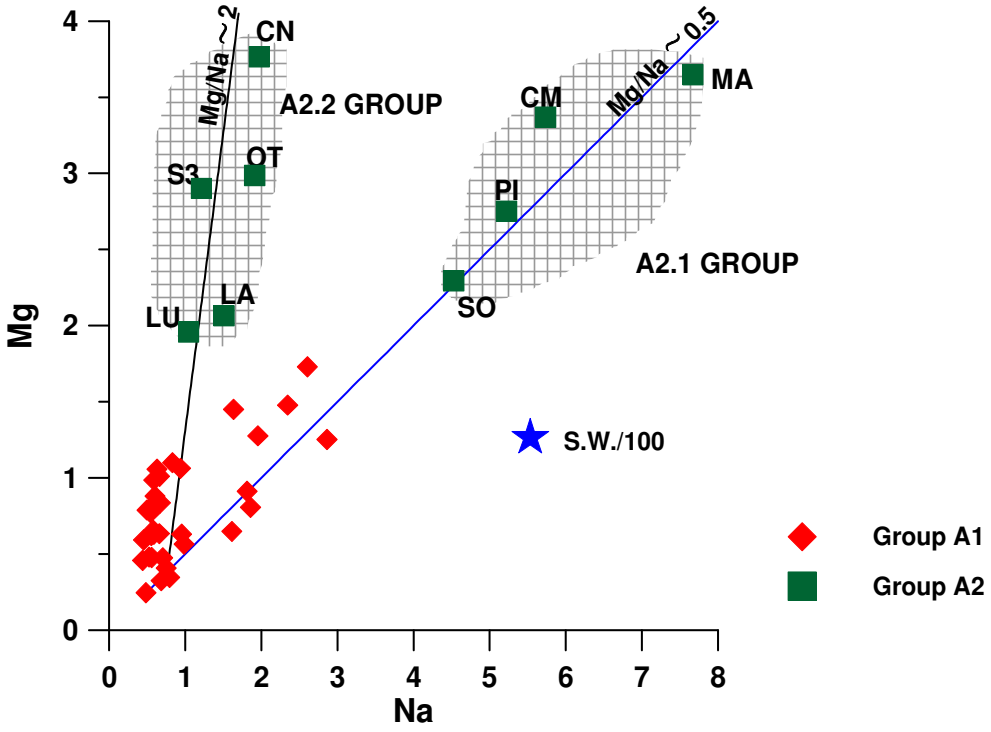

Figure 32: *Magnesium-Sodium diagram.*

Within the A2 aquifer, MA, CM, PI and SO samples have been arranged as A2.1 group; CN, OT, LA, LU, and S3 samples have been arranged as A2.2 group.

All the group A samples, can be described as mixing of A1-A2.1 and A1-A2.2 waters. The occurrence of these intermediate terms, confirms the existence of a hydraulic connection between the shallow aquifer (A1) and the deeper one (A2). Mixing processes between the two deep groundwater groups (A2.1 and A2.2) haven't been identified.

A2.1 group waters are located along the tectonic structure connecting the Scicli-M. Lauro and the M. di Ragusa fault systems. They have high Mg, Na and Cl contents, low Eh values (from –280 mV to –345 mV), intense smell of hydrogen sulphide, higher dissolved methane contents (pCH_4 up to 1.64 atm) and high helium content.

The A2.2 groundwaters are located in the central part of the Scicli-M. Lauro fault, upstream, with respect to A2.1 group. These groundwaters show similar Mg content with respect to A2.1, but they have lower Na and Cl content, intermediate Eh values, only small amounts of dissolved gases (CH_4 and He) and only a light smell of H_2S.

However, higher Na and Cl contents coupled with the strong presence both of reduced (CH_4 and H_2S) and deeply-derived gases (He), indicate that only the groundwaters relative to the A2.2 group, could receive a not-negligible contribution from a pocket of fluids deriving from hydrocarbons reservoirs. Similar characteristics (brackish water, gaseous hydrocarbons and H_2S) have been recorded also during a well perforation not far from the sampling site (AGIP, 1994).

Figure 33 represents a schematic section of groundwater circulation of the carbonate aquifers hosted in the Hyblean Mountains.

7.2 VOLCANIC AQUIFER

In the Langelier classification diagram (Fig 34) blue circles identify groundwater samples hosted within the volcanic aquifer (VO aquifer). Less mature groundwaters belonging to this group fall within the bicarbonate alkaline-earth field not distinguishable from those hosted within sedimentary aquifers. During their flow-path, from the recharge zone to the discharge area, proceeding of water rock interaction processes causes marked changes both in physico-chemical parameters and in the water chemistry. Two evolutive trends, from the bicarbonate alkaline earth end-member towards bicarbonate alkaline field and chloride-sulphate alkaline field respectively, have been identified.

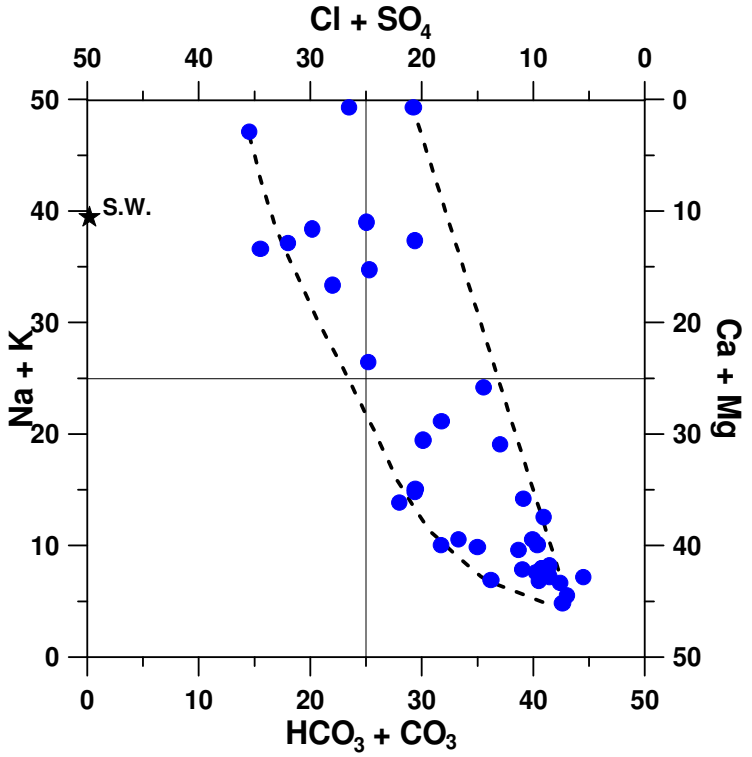

Figure 34: *Langelier classification diagram. In this plot groundwaters flowing within volcanic aquifer (VO aquifers) are reported*

The geochemical evolution of groundwaters hosted within the volcanic deposit aquifer is also clearly represented in the Ca/Mg/Na+K ternary diagram (fig. 35). From this plot, it appears evident that headwaters in which Ca is the dominant cation, during flow-path become progressively enriched in Mg (intermediate stage) and finally Na-rich groundwaters.

Taking into account the geological setting of the studied area, characterized by alternating volcanic and carbonate rocks (Bianchi et al., 1987) it is reasonable to assume that, the origin of alkaline earth elements into groundwaters is both from carbonates and from

basaltic rocks. While alkaline elements will derive mainly from basaltic glass and plagioclase dissolution.

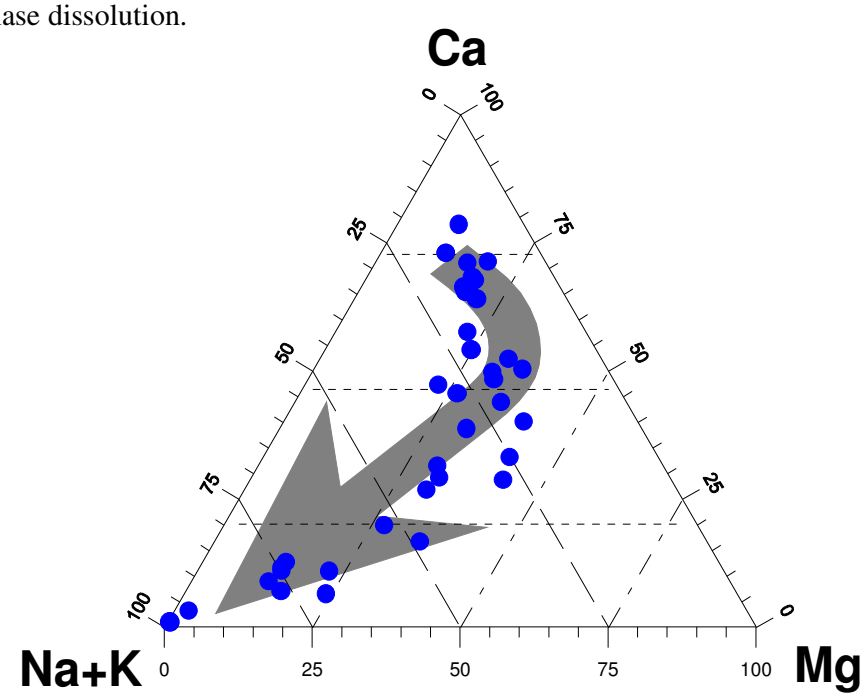

Figure 35: *Cations ternary diagram*

In fact, all the water samples belonging to VO aquifer, have a Na/Cl ratio higher than the seawater Na/Cl ratio (Figure 36) being the increasing in alkali contents related to water-volcanic rocks interaction.

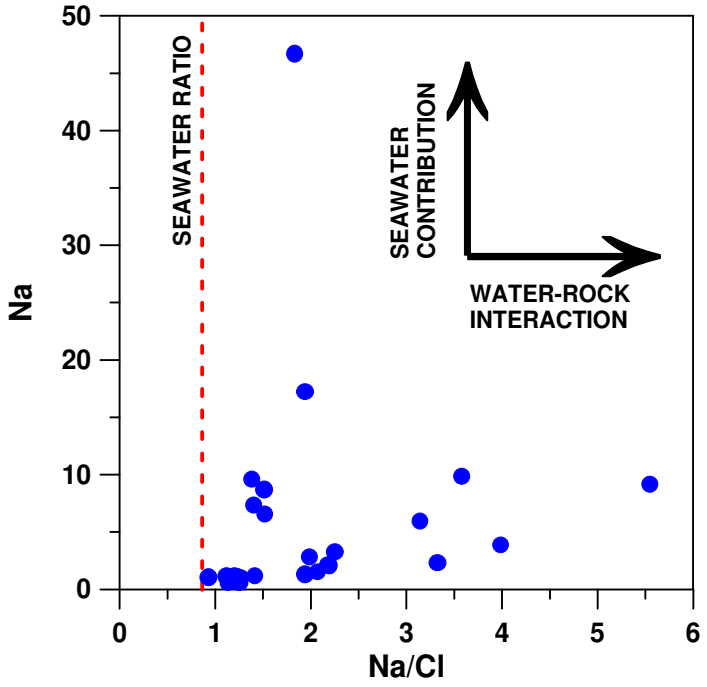

Figure 36: *Na-Na/Cl diagram.*

However, in some samples from VO aquifer having high Na content and relatively low Na/Cl ratio, a mixing with more saline waters could be present. For inland samples this could be attributable to the mixing with deep Cl-rich waters. While for water samples located along the coast the relative chloride enrichment, could be related to a limited seawater contribution, less that 2%.

During the groundwater evolution, as a consequence of a longer residence time, TDS (Total Dissolved Solid) values increase progressively. Furthermore, pristine neutral-slightly alkaline pH values become more alkaline up to reach values as high as 9.25. This is caused by the neutralizing nature of the basalts leaching. In fact, cation releasing into solution, as a consequence of weathering of primary basaltic minerals, is balanced by depletion of protons from the solution.

In figure 37, it is possible to distinguish two different trends. Groundwaters having pH values ranging from 7 to 8, show a fair positive correlation between TDS and Ca+Mg (VO1 group). These samples are located at higher altitudes and they represent the initial stage of the groundwater flow-path.

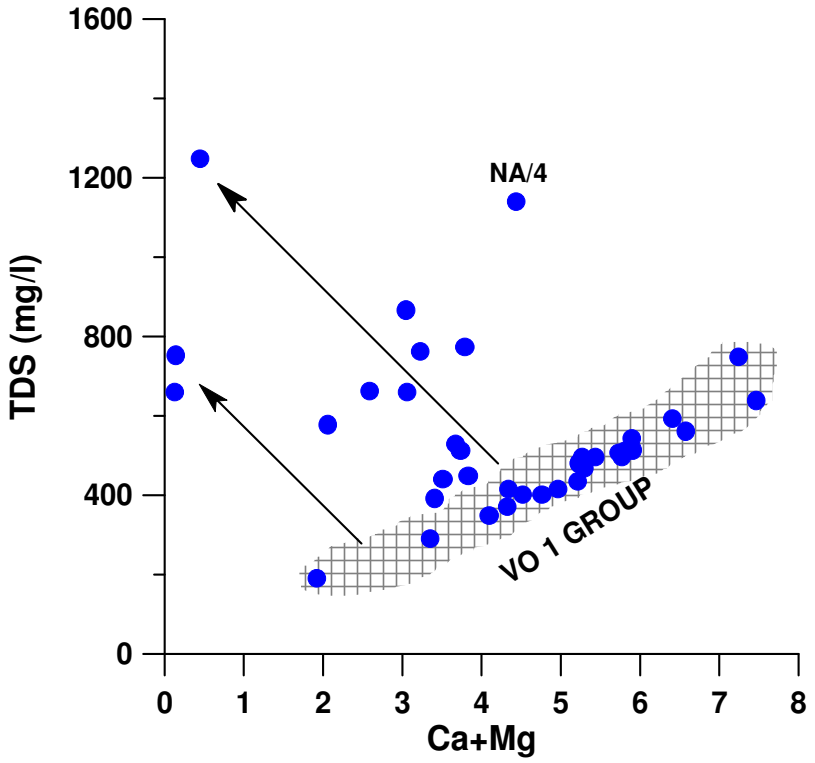

Figure 37: *Ca+Mg vs Total Dissolved Solid (TDS).*

The second alignment is characterized by an inverse relationship between TDS and earth alkaline cations. In this group, the increase of salinity is mainly due to alkaline elements, essentially Na. If we detract at each sample the amount of seawater contribution by

assuming chloride as indicator of marine contamination, we can easily calculate the concentration of residual Na (Na_{res}), related to silicate-water interaction.

In figure 38, where Na_{res} is reported against Ca+Mg, groundwaters belonging to VO2 group show an inverse correlation, thus confirming that the increase of salinity in this group is due to the Na release from weathering of basaltic rocks.

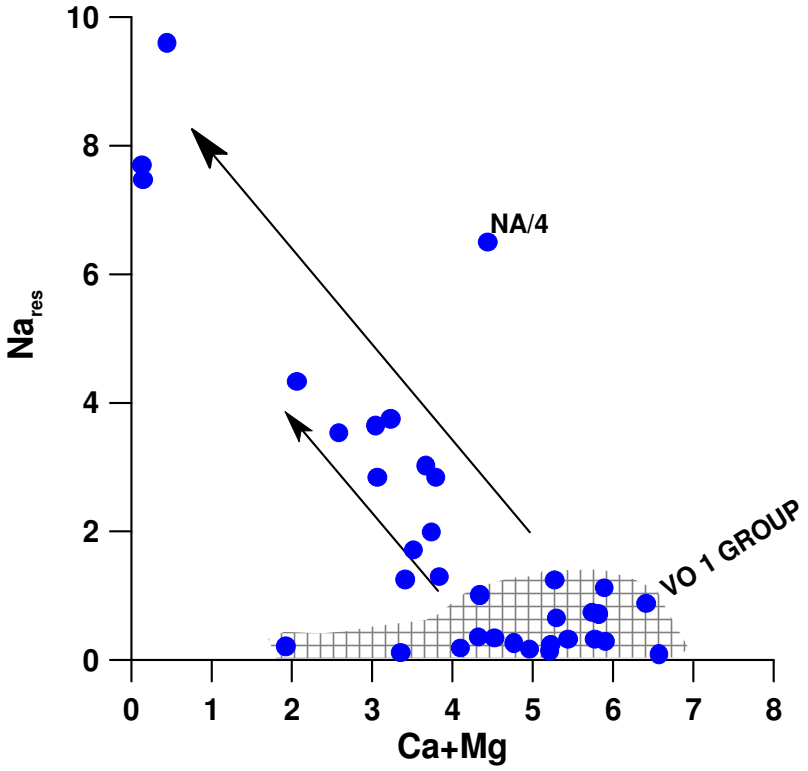

Figure 38: *Ca+Mg vs residual Na (Na_{res}).*

Furthermore, the same figure suggests that together with carbonate dissolution and basalt weathering, secondary geochemical processes should be responsible for the evolution of V2 group groundwaters. In fact, when pH increases and Na-smectites stability field is reached (see paragraph 8.2.1), both the formation of secondary minerals and ion-exchange process involving groundwaters and clay minerals could also contribute to the increase of Na content and decrease of divalent cations is solution.

A possible ion-exchange reaction suggested by Appelo and Postma (1993) could be:

AE^{2+} + 2 Na-Clay <> $2Na^{+}$ + AE-clay

where AE stands for alkaline earth elements.

The geochemical processes able to explain the evolution of VO groundwaters could be therefore summarized as follows:

- In the higher part of the groundwater flow-path, the main contribution to the cation content in solution is given by Ca+Mg (VO1 group).

- In the lower part, the system remains essentially close to CO_2 input and water-rock interaction determines a Na-enrichment and an increase in pH values up to 9.25.

In this context, the formation of Ca- and Mg-bearing secondary minerals (both carbonate and silicate) is enhanced resulting in both Ca and Mg depletion from the solution.

The NA sample needs different considerations. In fact, in this case a strong deep input of CO_2-rich gases, maintains the pH of waters at values as low as 6. As a consequence, the calcite and silicate mineral solubilities are increased, giving to this water higher TDS value.

Within VO aquifer, a sulphurous aquifer has been also identified. It comprises the Brucoli sulphur spring (SU spring) and some deep wells (GI and GU) with similar physico-chemical characteristics (trace of H_2S and negative Eh values; fig.25). Previous studies (Aureli, 1989; Dall'Aglio et al., 1995) have highlighted that both sulphur spring and deep wells are aligned along a NNW-SSE direction, coinciding with the Hyblean-Malta escarpment direction. In these springs, located very close to the epicentre area of the 1990 earthquakes, some geochemical changes accompanying the seismic sequence have been recorded (Dall'Aglio et al., 1995). All these findings seem to indicate that geochemical anomalies observed in groundwaters both during seismic and aseismic periods, and the structural setting in the Hyblean Foreland are intrinsically connected.

8.AQUEOUS SPECIATION AND SATURATION STATE

The PHREEQC computer program (Parkhurst, 1995) has been used to calculate both the activities of aqueous species and the saturation state with respect to pure mineralogical phases. PHREEQC database has been extended with WATEQ4F database, containing the thermodynamic data of some trace metal aqueous complex. In tables 7 and 8 are reported the calculated saturation indexes relative to some pure mineralogical phases.

8.1 AQUEOUS SPECIATION

Aqueous speciation of Hyblean groundwaters has been performed introducing in the PHREEQC computer program (Parkhurst, 1995) field data relative to physico-chemical parameters (Eh, T, and pH) and HPLC, ICP-MS and UV analytical results on major, minor and trace elements.

Redox conditions are expressed in terms of *Eh* or *pe* and these two parameters are related by means of this expression:

$$pe = F\ Eh /\ 2.303\ R\ T$$

where F is the Faraday constant (23.06 kcal/volt gram-equivalent) and T is the temperature in K.

On the base of the input data, PHREEQC code computes the relative abundance of almost all the most common aqueous species.

Taking into account the influence of redox conditions on the elements aqueous speciation, water samples have been divided in two groups: oxidised waters having Eh > 0 and reducing waters with Eh values < 0.In table 9 are summarized the obtained results. In the table 9 only the species having a relative abundance greater than 5% have been reported.

Of course, metals having more than one oxidation state are extremely redox-sensitive, while, elements with different acid-base properties are pH sensitive. The main ligands are carbonate and sometime both sulphate and fluoride.

Alkaline and alkaline earth elements (Ca, Na, Mg, Rb, K, Sr, Ba) are present as free ions, in an inert gas-type electronic configuration both in reduced and in oxidised waters. In some cases Ba, and, to a lesser extent Ca, Mg, Sr, tend to be complexed with sulphate (e.g. $BaSO_4^0$) or with carbonate ligands respectively in waters having pH > 7.5. A similar behaviour is shown by Mn and Zn which displays less abundant forms $MnHCO_3^-$ and

$MnCO_3^0$, as a function of pH values, while Ni is present in great proportions as $NiCO_3^0$ or as $Ni(CO_3)_2^=$ rather than as free ion.

As expected, broad differences in the main stable aqueous species are linked to elements having more than one oxidation state. As and V in reduced environments are more abundant as As(III) and V(III), respectively in form of $H_3AsO_3^0$ and as $V(OH)_3$. While in oxidised waters they are pentavalent and they occur as $H_2VO_4^-$ or $HVO_4^=$ and $H_2AsO_4^-$ or $HAsO_4^=$ respectively on the base of the availability of protons in solution (aH^+).

Despite Cr can occur in three oxidation states (Cr II, Cr III and Cr VI) redox conditions within Hyblean groundwaters are not enough oxidising to stabilise Cr (VI) and not so reducing to form Cr (II) species so that the stable aqueous chromium species are trivalent ($Cr(OH)_3$ and $Cr(OH)_2^+$).

Al is more abundant as $Al(OH)_4^-$, but in reduced environment F^- ligand becomes not negligible (AlF_2^+). Fe is stable in both conditions as Fe^{+2} as well as $FeHCO_3^-$. Si is almost entirely present as $H_4SiO_4^0$.

Aqueous speciation for Uranium indicate as U (VI) the most common form in oxidised environment, is highly mobile because of the carbonate complexation to form uranyl-carbonate ($UO_2(CO_3)^0$ and $UO_2(CO_3)_2^{2-}$). Under reducing conditions, less soluble U (V) or U(IV) become stable. U(OH)5$^-$ is the most dominant U-form in Hyblean groundwaters having negative Eh values.

Assuming that redox equilibria have been fully reached, Eh-pH diagram considering simple systems involving the element itself in aqueous solution and S-complexes can offer a complete picture of the distribution of main dissolved aqueous species. In figure 39 and 40 are reported pH-Eh diagrams for V and As, summarising the result of aqueous speciation for these elements.

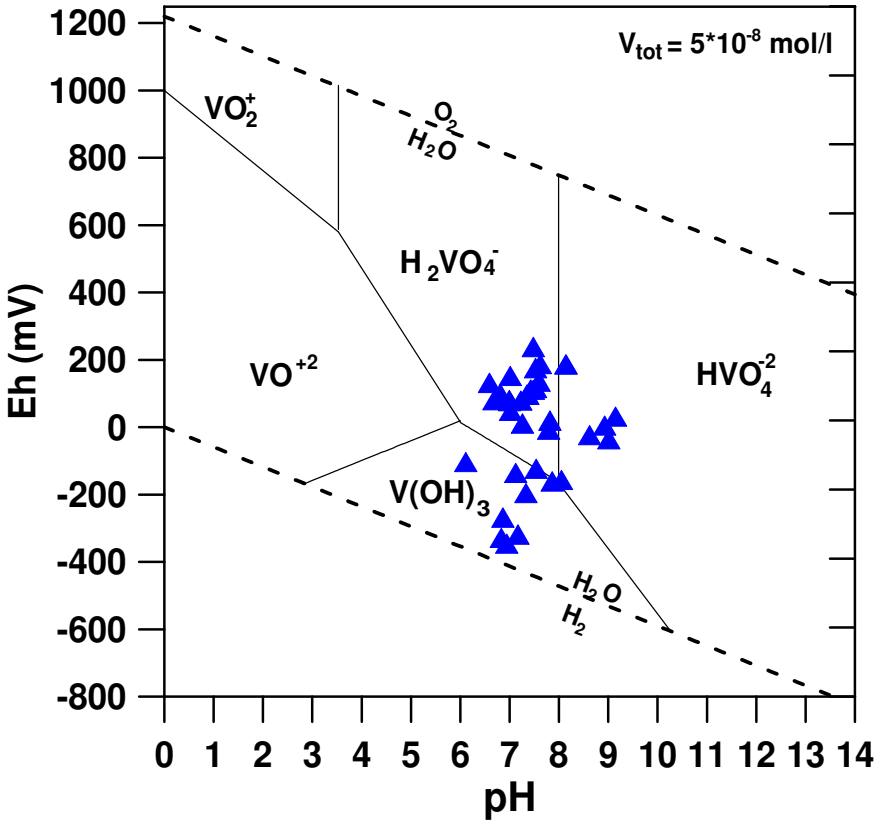

Figure 39: *Eh- pH diagram for vanadium.*

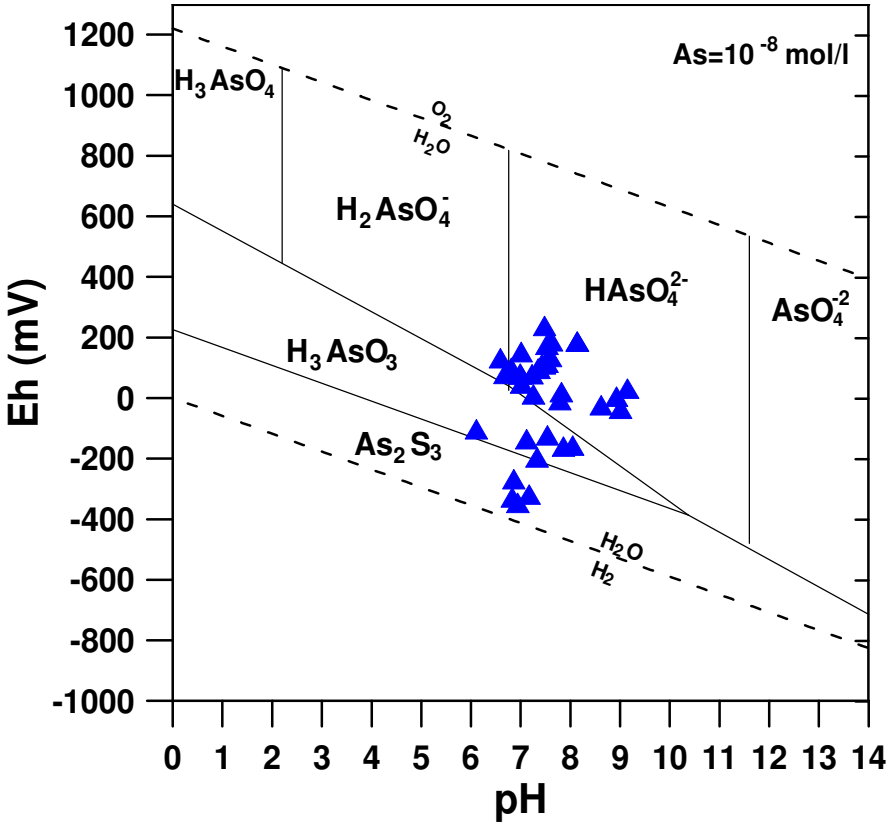

Figure 40*: Eh-pH diagram for arsenic.*

8.2 SATURATION STATE

As previously pointed out, water-rock interaction is the most important processes controlling the chemistry of major elements within the studied groundwaters.

The study of the state of saturation of most common rock-forming primary and secondary minerals is fundamental for the understanding of the relative abundance and mobility of major and trace elements dissolved in the Hyblean groundwaters and to discern the mineralogical phases that control solute contents.

The saturation index with respect to a mineralogical phase is defined as

$$SI = \text{Log } IAP/Ksp \qquad \text{(Eq. 9)}$$

where Ksp is the equilibrium constant of dissolution reaction of the considered mineral and IAP is the corresonding ion activity product.

If IAP > Ksp, the aqueous solution is oversaturated with respect to the considered mineral and its precipitation is possible. If IAP< Ksp, the aqueous solution is undersaturated with respect to the mineral which can be dissolved as long as IAP = Ksp, when the condition of saturation (equilibrium) is attained.

8.2.1 VOLCANIC ACQUIFER (VO aquifer)

Water samples belonging to VO group are saturated with respect to calcite while they range from undersaturated toward a supersaturation state with respect to dolomite (Figure 41).

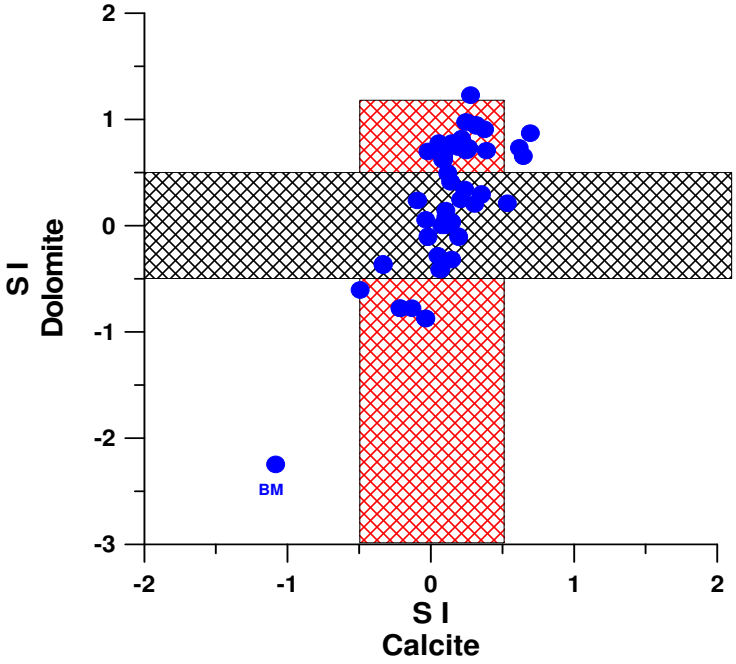

Figure 41: *Saturation indexes of calcite and dolomite in Hyblean groundwaters hosted within the volcanic aquifer.*

Groundwaters circulating in basaltic aquifers are generally undersaturated with respect to calcite (Gislason and Eugster, 1987a; Gislason et al., 1996; Aiuppa et al., 2000). In the study area, basaltic rocks are alternated with carbonate formations, thus suggesting that bivalent cations are released into solution from both silicate and carbonate rocks.

VO groundwaters are supersaturated with respect to quartz, while they are slightly supersaturated with respect to chalcedony and undersaturated with respect to amorphous silica (Figure 42). In this case, according to Gislason and Eugster (1987a), it seems reasonable to assume that silica content in solution derives mainly from basaltic glass.

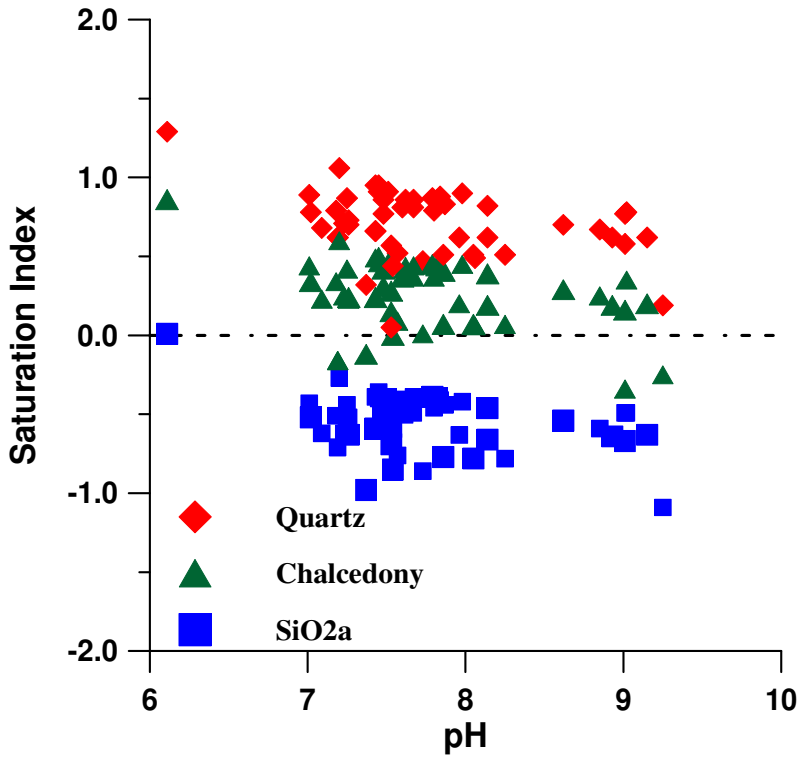

Figure 42: *Saturation indexes of silica minerals in Hyblean groundwaters hosted within the volcanic aquifer.*

Primary minerals forming basaltic rocks are commonly present as solid solution rather than as pure mineralogical phases. Because of saturation state with respect to olivine, clinopyroxene and plagioclase is compositional dependent (Gislason and Arnorsson, 1993), the assessment of the stability of these mineralogical phases in the groundwaters from Hyblean aquifers needs an accurate approach in term of solid solution.

Data on the geochemistry of the Hyblean lavas reveals that Plio-Pleistocene volcanic rocks belongs mainly to basanites up to alkali-basalts and tholeiitic basalts (De Rosa et al., 1992). Most common primary basaltic minerals are present both as phenochrysts and as groundmass (mainly olivine and clinopyroxene). Microprobe analysis has allowed to

define the normative chemical composition of representative minerals. Olivine and plagioclase phenocrysts show a narrow compositional range being forsteritic in the range 83.7-87.4%, and An 59.2% Ab 39.4% Or 1.4% respectively. Clinopyroxene show a wider compositional range as a function of silica content. Within basanites and alkali basalts Ca-pyroxene prevails (Wo=49.1%, En=38%, Fs=12.9%), while tholeiites are characterized by a marked increase in Fe and, to a lesser extent, Mg. In these rocks the composition of the representative pyroxene is of En 44.2%, Wo 31.2% and Fs 24.3% (De Rosa et al., 1992). Unfortunately, no data are available on chemistry of volcanic glasses. As suggested by several authors (Gislason and Eugster, 1987b; Gislason and Arnorsson, 1993), the role played by volcanic glasses dissolution is of great importance in studying basalts weathering, because it is more reactive with respect to most common lava-forming minerals.

The occurrences of silicate minerals as solid solutions imply that the saturation state of primary basaltic minerals needs the calculation of the equilibrium constants of dissolution reactions for each solid solution.

According to Gislason and Arnorsson (1993), the standard state free energy of formation for a binary ideal solid solution can be computed as follows:

$$\Delta G^0_{ss} = X_i \Delta G^0_i + X_j \Delta G^0_J + nRT (X_i \ln X_i + X_j \ln X_j) \qquad \text{(Eq.10)}$$

where the i and j are the two pure end-members, ΔG^0 refers to standard-state Gibbs free energy of dissolution reaction for each pure phase and X represents the molar fraction of i and j component of solid solution, R is the gas constant, T is temperature (°K) and n is the number of exchangeable sites for cell unit.

The dissolution constant for a solid solution can be obtained through the expression:

$$\log K_{ss} = -\Delta G^0_{ss} / RT\ 2.303 \qquad \text{(Eq.11)}$$

SUPCRT92 computer program (Johnson et al., 1992) has been used to calculate the equilibrium constant for pure solid phase.

Dissolution reactions for the most common minerals of Hyblean lavas, as well as ΔG^0_{ss} and $\log K_{ss}$ values, calculated through equations 10 and 11, are reported in table 10. The saturation indexes have been calculated using equation 9.

A comparison among the dissolution constants obtained for olivine, pyroxene and plagioclase solid solutions, reveals, as expected, olivine is the most unstable mineral, followed by clinopyroxene and plagioclase.

From figure 43 it is possible to note that studied groundwaters are in the range of equilibrium state with respect to plagioclase minerals present in the Hyblean lavas. Furthermore, according to Gislason and Arnorsson (1993) saturation index with respect to plagioclase does not show any pH dependence.

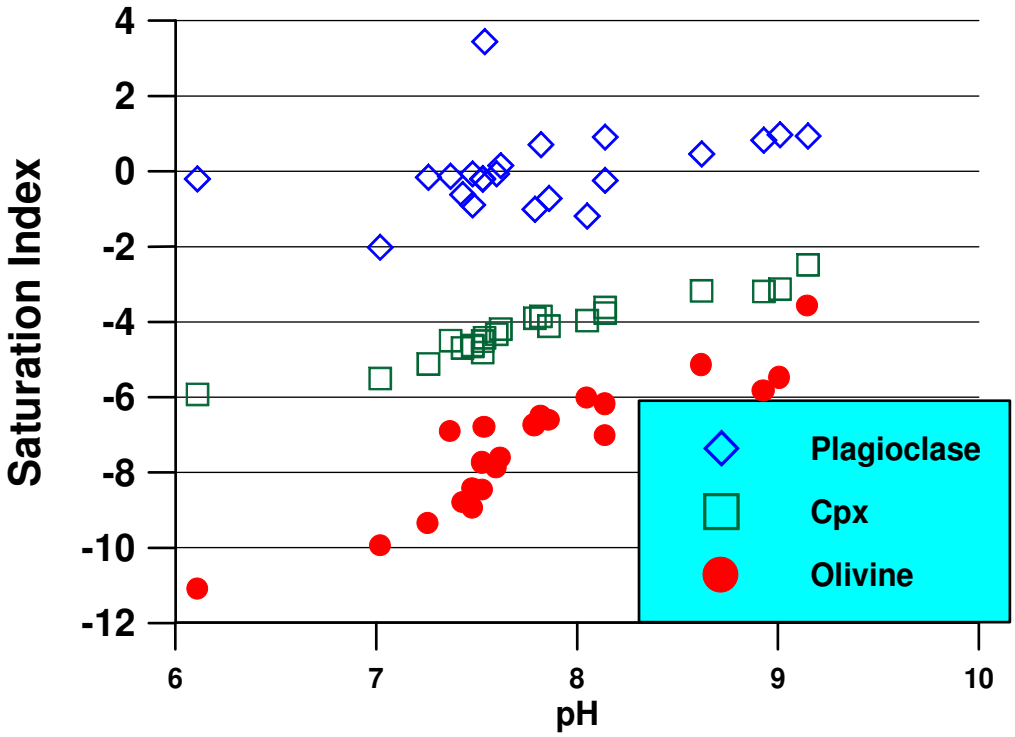

Figure 43: *Saturation indexes of primary basaltic minerals (Olivine, Clinopyroxene and Plagioclase) in Hyblean groundwaters hosted within the volcanic aquifer.*

As regard olivine and pyroxene, figure 43 highlights that saturation indexes range from -11 to -3.5 and from -6 to -2.5, respectively. For ferro-magnesian minerals S.I. is pH dependent having higher values at higher pH values (9-9.25). The positive correlation between SI $_{olivine}$ (R^2=0.83) and Si $_{pyroxene}$ (R^2=0.93) versus pH confirms that basalt weathering neutralizes acid groundwater deriving from infiltrating local rainwater.

On the contrary, NA sample shows very negative saturation index values being very far from the attainment of the chemical equilibrium. This is due to low pH values of this sample (pH ~ 6) imposed by the input of great amount of deep CO_2-rich fluids (CO_2> 3000 cc/litre STP).

Therefore, in absence of any external source of protons, the dissolution of primary basaltic minerals proceeds towards higher pH values and higher cation concentrations in solution (Fe, Mg, and, to a lesser extent, Mn, Ni, Co, V) until the ionic activity product of olivine

and pyroxene dissolution reaction becomes equal to the values of the respective dissolution constants. Within the studied groundwaters, water samples (BO, PA and SS) located along the Northern flank of the Hyblean Plateau reach pH values close to 9.25, thus approaching to the chemical equilibrium with respect to ferro-magnesian basalt-forming minerals.

Although no data are available about secondary minerals assemblage in altered Hyblean lavas, some insights can be deduced both from the mineralogical phase stability diagrams and from PHREEQC aqueous speciation.

In computing saturation state with respect to secondary minerals it was assumed that they occur as pure and well-crystallised phases. This is not true, because in nature, weathering product as well as primary minerals can show various crystallization degrees and variable chemical composition as a consequence of solid solutions formation, affecting the mineral stability. However, the use of both PHREEQC calculations and stability diagrams lead to the same results. Hyblean groundwaters are always supersaturated with respect to most common secondary minerals such as Ca-Montmorillonite, Talc, K-mica, Illite and Kaolinite. At the same way they are always saturated with respect to Al- and Fe- oxide and hydroxide such as Gibbsite ($Al(OH)_3$) Goethite (FeOOH) and Hematite (Fe_2O_3). Mn oxy-hydroxides (Manganite (MnOOH) and Pyrolusite (MnO_2) are unstable (Fig. 44).

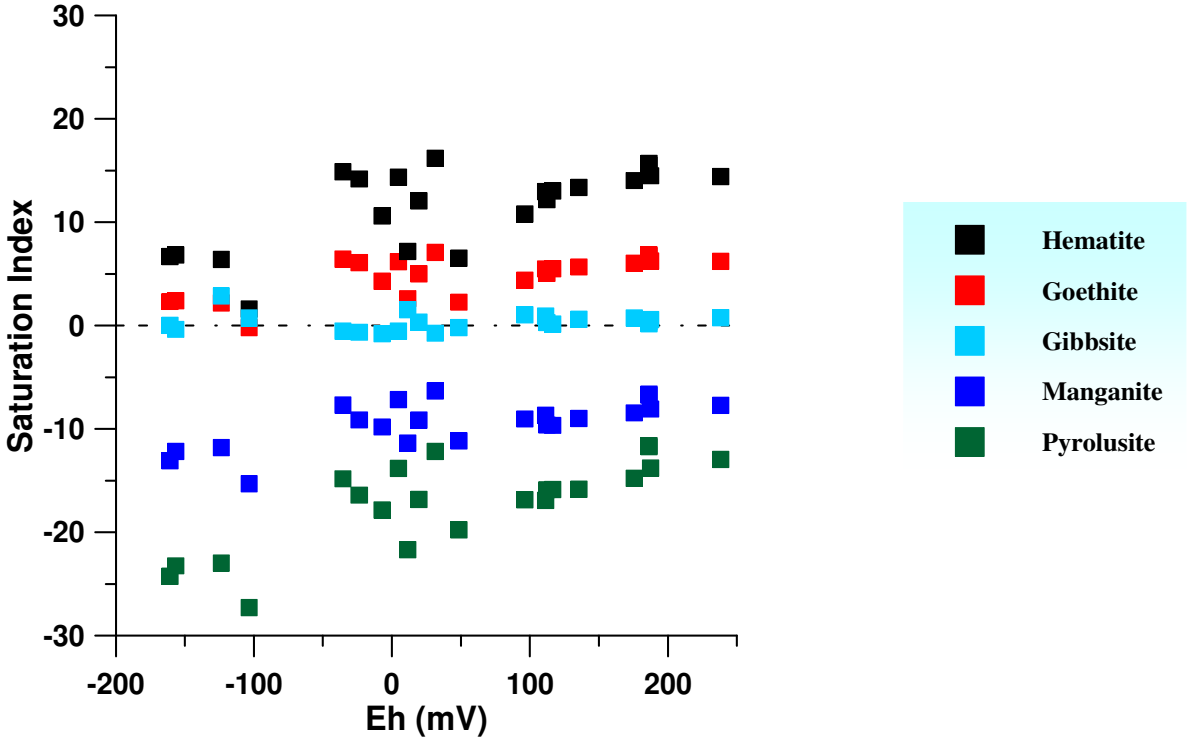

Figure 44: *Saturation indexes of Fe(III)-, Mn- and Al-oxo-hydroxides (Hematite, Goethite, Manganite, Pyrolusite, Gibbsite) in Hyblean groundwaters hosted within the volcanic aquifer*

Activity diagrams for VO groundwaters have been drawn at temperature of 25°C and assuming a log a_{SiO2} equal to -3.3, representing the average silica content dissolved in groundwaters of Hyblean area.

In addition, pure phases instead of solid mixtures are considered in these plots. Despite the assumptions and simplifications introduced to construct activity plots, they represent a useful tool to link the chemical composition of the aqueous solution with that of the mineral phases possibly in equilibrium with it

Both diagrams (figs. 45a and 45b) indicate that in groundwaters from VO aquifer Kaolinite and/or Ca and Mg-Smectite are the characteristic secondary minerals formed by the weathering of basaltic rocks. Moreover, figures 45 a and b show that the most evolved VO groundwaters, with high pH values, fall within the Na-Smectite, and Ca-Zeolites stability field.

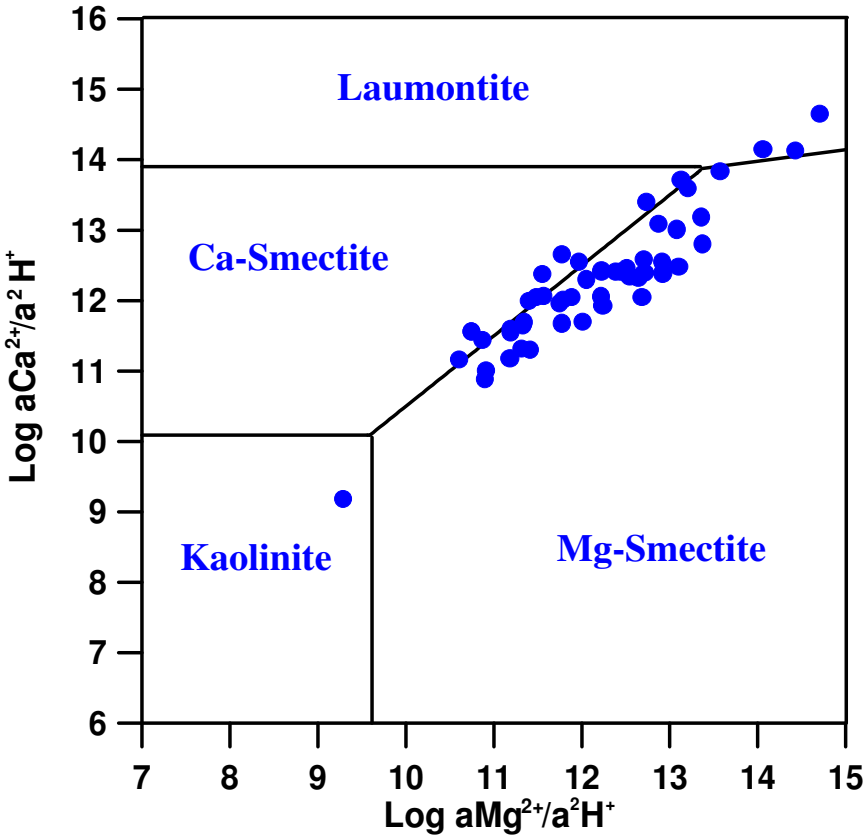

Figure 45 a: *Activity diagrams displaying the stability fields of the most common secondary minerals. Lines have been drawn at T=25°C and log a_{H4SiO4} =-3.3. Thermodynamic data from Helgeson (1969) and Helgeson et al. (1978).*

The achievement of saturation state with respect to Ca- and Mg-bearing minerals, implies that alkaline earth elements in VO groundwaters are partially removed from solution to form both carbonate and Al- and Si-bearing secondary minerals. Together with the

occurrence of ion exchange processes involving alkaline and alkaline earth elements, previously described, they are the most important secondary geochemical processes affecting the chemistry of groundwater hosted in the Hyblean lavas aquifer.

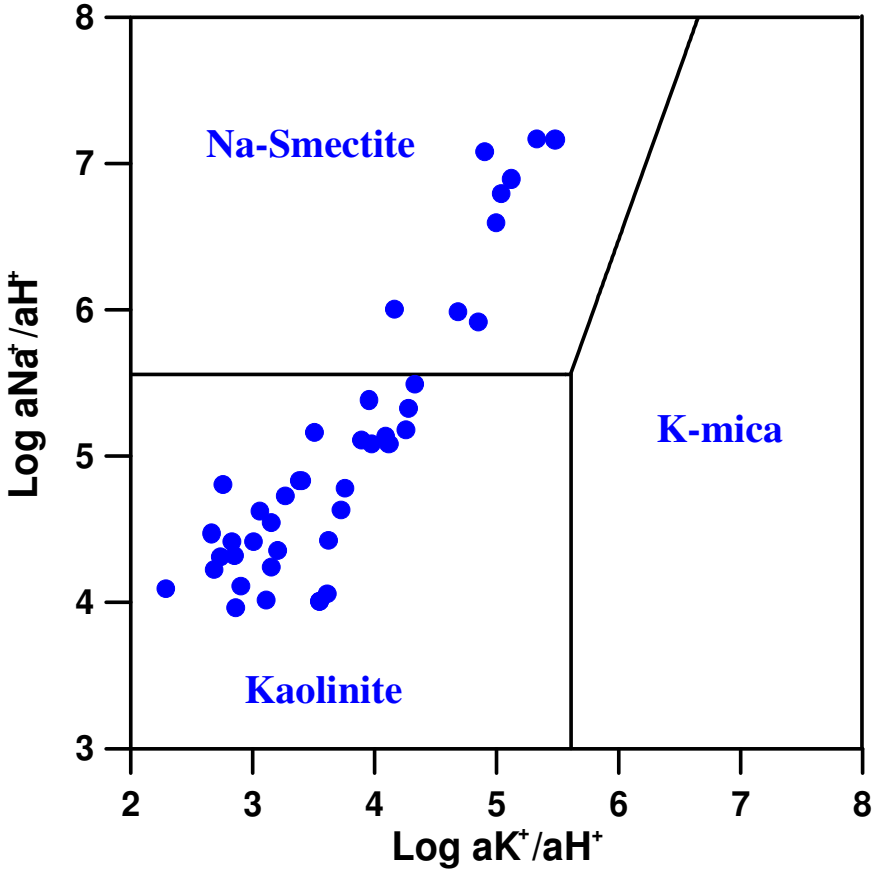

Figure 45 b: *Activity diagrams displaying the stability fields of the most common secondary minerals. Lines have been drawn at T=25°C and log a_{H4SiO4} =-3.3. Thermodynamic data from Helgeson (1969) and Helgeson et al. (1978).*

8.2.2 CARBONATE AQUIFER

Groundwaters hosted in carbonate aquifer are saturated with respect to calcite and from undersaturated to saturated with respect to dolomite (Fig. 46). All the samples are strongly undersaturated with respect to the other carbonate minerals considered (Siderite, Rhodochrosite, Smithsonite, Strontianite and Witherite) (Tab. 7).

These groundwaters have attained the equilibrium with oxidised Fe-bearing minerals such as Goethite and Hematite (Fig. 47), except for some samples, belonging to A2.1 aquifer, (CM, SO, MA and PI samples), where extremely reducing condition prevail. For these groundwaters, saturation state is achieved with respect to some Iron-sulphide minerals (Tab. 7).

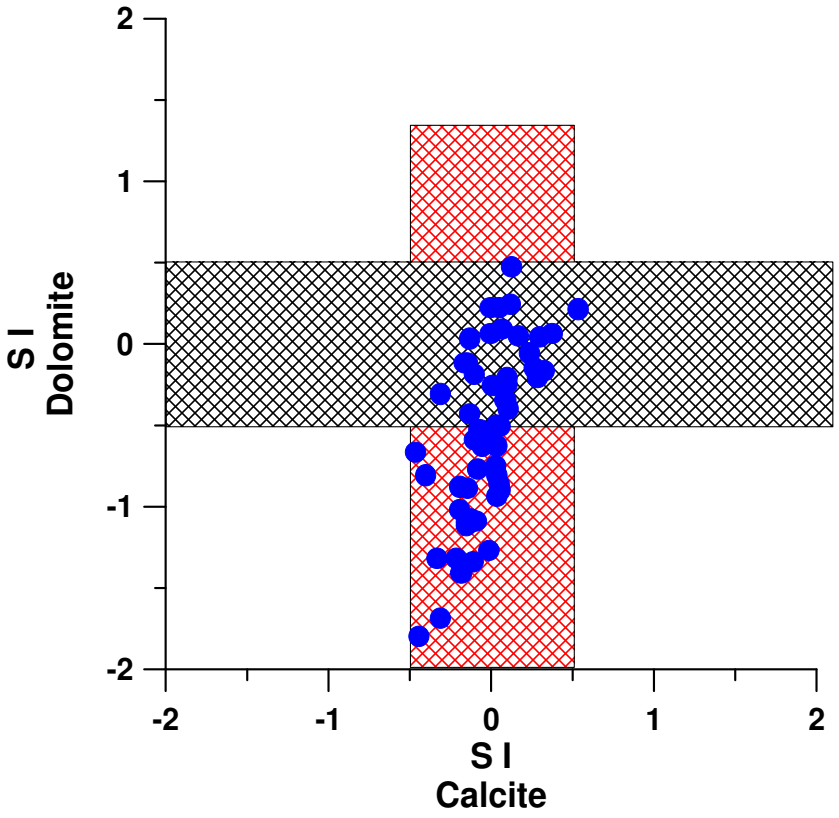

Figure 46: *Saturation indexes of calcite and dolomite in Hyblean groundwaters hosted within the sedimentary aquifer.*

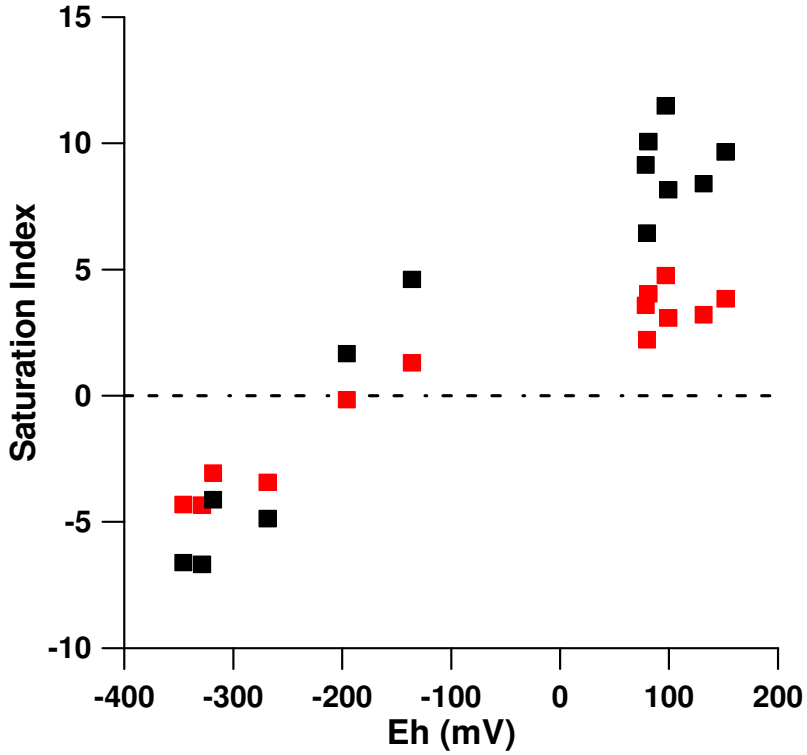

Figure 47: *Saturation indexes of Fe(III)-oxo-hydroxides (Hematite and Goethite) in Hyblean groundwaters hosted within the sedimentary aquifer.*

9.GEOCHEMISTRY OF MINOR AND TRACE ELEMENTS

Average values for analized minor and trace elements (Tab. 11) in Hyblean groundwaters, are arranged in two groups (fig. 48) as a function of the main lithologic characteristics of the aquifers (carbonate and volcanic). It is possible to note that some minor and trace element concentrations are in the same order of magnitude in both types of aquifer. Some elements such as Ba, U and LREE are preferentially enriched in carbonate aquifer, while other metals are more abundant in volcanic aquifer (Fe, Zn, Ni, V, As).

The abundance of trace metals in groundwaters is related to the concentration in the rocks and to prevailing physico-chemical condition in to the aquifer (pH, Eh, presence of complexes).

Trace metal content in groundwaters is also linked to the mineral solubility, due to the mobility control of species, through precipitation and/or dissolution reactions as well as sorption/desorption processes. Formation of secondary minerals such as carbonates and both Fe and Mn oxy-hydroxides will affect the mobility of several metals such as V, Zn, and U, due to their high surface reactivity (Bruno et al. 1998; Xu at el., 1997; Al et al., 2000).

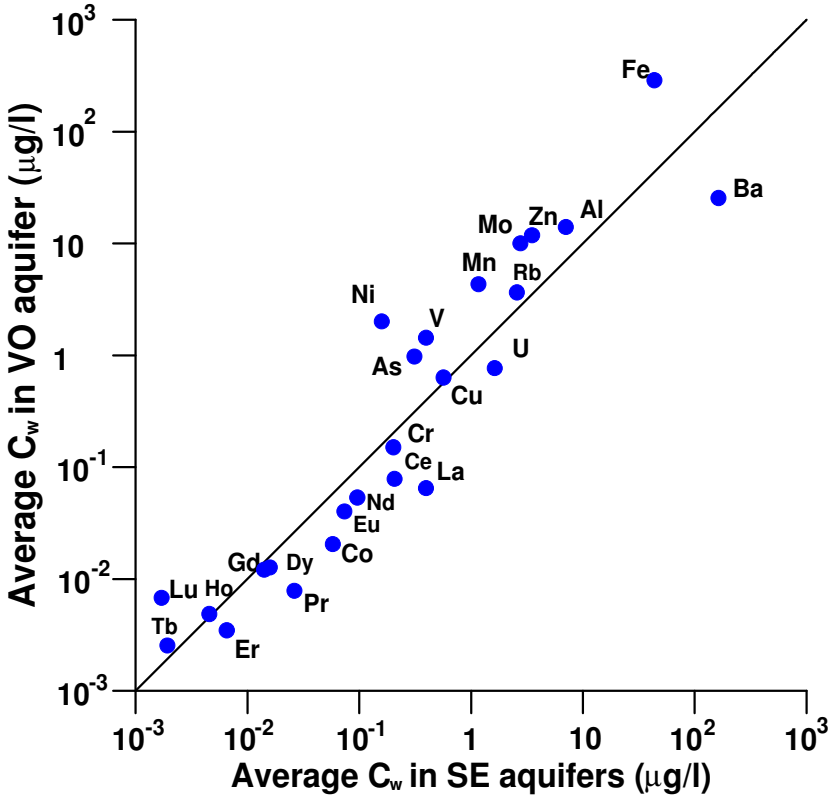

Figure 48: *Comparative plot of minor and trace elements concentration between volcanic and sedimentary aquifers.*

The role played by rock composition is confirmed from the good correlation between average element concentration in groundwater and in host rocks from Hyblean plateau, both for carbonate and for basalt aquifer (Figures 49a and 49b). However, some differences can be observed, being related to the chemical affinity of the elements towards solid phase or solution and to the occurrence of secondary processes affecting groundwaters chemistry.

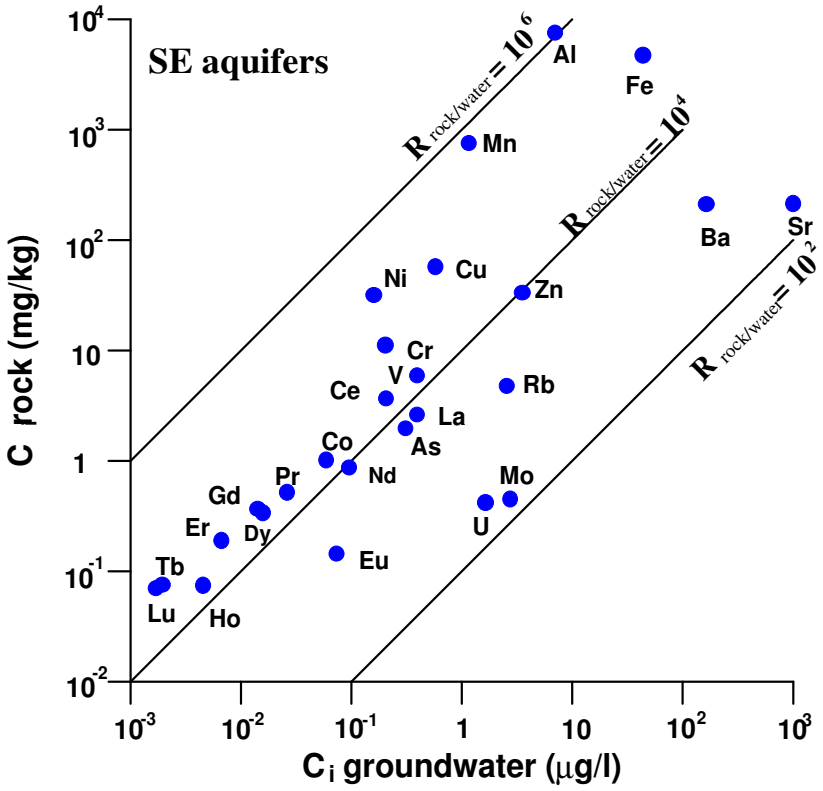

Figure 49a: *Average metal concentrations in sedimentary aquifers versus the average concentrations in carbonates*

This is emphasized mainly from alkaline and earth-alkaline elements (Rb, Ba, Sr), characterized by their marked attitude to remain preferentially into solution. Such a tendency can be also noted for some elements such U and Mo (Oxy-hydroxy anion forming elements) having appreciable mobility mainly in strongly oxidized environments- On the contrary, some elements such as Al and Fe can be considered highly immobile due to their tendency to be stable in solid form both in clay minerals, (Ca-Montmorillonite, Illite, and Kaolinite) and as Goethite, Gibbsite and Magnetite (Tab. 7). Intermediate behavior is shown by transition metals, which partitioning between solid phase and groundwaters is strongly dependent by redox-pH condition and metal complexes formation.

Geochimical mobility of some elements in groundwater will reflect also the occurrence of coprecipitation processes leading to the formation of solid secondary phases generally constituted of solid solutions.

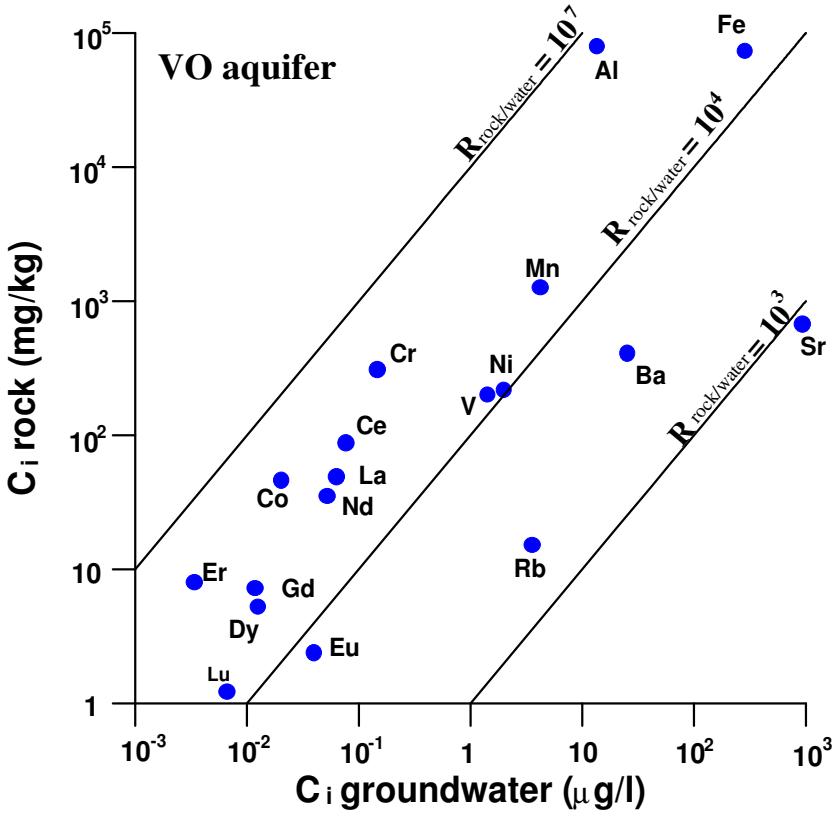

Figure 49b: *Average metal concentrations in volcanic aquifers versus the average concentrations in the corresponding host-rocks. Data for volcanic rocks are from Beccaluva et al (1998)*

In the case of carbonate rocks some trace elements form solid solutions when the ion Ca^{+2} is substituted with another ion such as Mn, Sr, Fe Ba into the lattice of the pure calcite phase. The diadochy of these elements play an important role in modifying the water solubility both of major cation, and of trace element. In particular, when the substitution occurs in relevant amount the solubility of solid solution increases or decreases as a function of relative solubility of the pure phase end-members. Furthermore, the solubility of a constituent is greatly reduced when it represents the minor component of a solid solution phase (Stumm and Morgan, 1996).

A solid solution between a major cation MCO_3 and a trace element TCO_3 can be as follows:

$$M_{(1-x)}T_xCO_3(s) \qquad \text{(Eq. 12)}$$

where M in the case of calcite is assumed to be Calcium, X the molar fraction of sites occupied by the trace element T such as Ba, Mn and Sr in the lattice.

Lattice substitution is ionic radius strongly dependent. When the ionic radius of the substituting ion is lesser than that of Ca (1.00 Å), the solid solution became homogeneous and the ions will be strongly partitioned into a solid phase (rhombohedral carbonates such as calcite). When the ionic radius of the substituting ions is larger than 1.00 Å, a nonlattice substitution becomes the preferential mechanism of substitution (Pingitore 1996) and the element will be enriched into the solution.

Due to their small ion radii, elements such as Cd^{+2}, Zn^{+2}, Cu^{+2}, Mn^{+2}, Co^{+2} and Fe^{+2} will be removed from solution and they will enter into the calcite lattice more easily than Ba, Sr, which will remain in solution (Rimstidt et al., 1998).

The partitioning of a trace element between aqueous solution and metal carbonate phases is generally represented in terms of distribution coefficient (K_d) expressed as follows:

$$K_d = X_{TCO3}/X_{MCO3} * [M^{2+}]/[T^{2+}] \qquad \text{(Eq. 13)}$$

where X is the molar fraction and $[M^{2+}]$ and $[T^{2+}]$ represent the aqueous molal concentration of the major and trace elements respectively. By applying of the equation 13, it is possible to determine concentration in solution of a given trace element when the distribution coefficient, the concentration of major cation and the molar fraction of the given trace element in the carbonate solid solution are known.

Values of distribution coefficient can be calculated on the basis of the ratio between the solubility constants (Ksp) of pure solid phases both major and trace element carbonate.

In fact, solubility constants (Ksp) can be written as follows:

$$K_{spMCO_3} = (a\, M^{2+} * a\, CO_3^{2-})/(X_{MCO3} * X_{MCO3}) \qquad \text{for major cation carbonate} \qquad \text{(Eq. 14)}$$

and

$$K_{spTCO_3} = (a\, T^{2+} * a\, CO_3^{2-})/(X_{TCO3} * X_{TCO3}) \qquad \text{for trace element carbonate} \qquad \text{(Eq. 15)}$$

where X_{MCO3} and X_{TCO3} are the activity coefficients of major cation and trace element carbonate phase, respectively.

At equilibrium conditions, by combining equations 13, 14 and 15, and expliciting the aqueous concentrations in terms of activity, we obtain:

$$K_d = [\gamma M^{2+} * K_{spMCO3} * X_{MCO_3}] / [\gamma T^{2+} * K_{spTCO3} * X_{TCO_3}] \qquad \text{(Eq. 16)}$$

where γM^{2+} and γT^{2+} represent the activity coefficients of the aqueous phases.

We can assume that the ratio between γM^{2+} and γT^{2+} is close to 1. Furthermore, for dilute solid mixtures, the activity coefficient of major cation carbonate is also close to 1. So the equation 16 becomes:

$$K_d = [K_{spMCO3}] / [K_{spTCO3} * X_{TCO_3}] \qquad \text{(Eq. 17)}$$

For ideal substitutions, X_{TCO3} assumes values close to 1. This parameter, generally describes the degree of a non-ideal cation substitution into the lattice.

For some selected water samples hosted within the carbonate aquifer, by applying of the equation 13, Ba, Sr and Mn contents have been estimated assuming coprecipitation of carbonate solid solutions. For these calculations, experimental distribution coefficient (K_d) reported by Rimstidt et al. (1998) have been used.

Because of ionic radius larger than Ca, Ba and Sr cannot easily replace Ca in the lattice of calcite. A miscibility limit for $BaCO_{3(s)}$ and $SrCO_{3(s)}$ in $CaCO_{3(s)}$ (orthorhombic) has been found at a molar fraction of about 0.011 and 0.0035 for Barium and Strontium respectively (Tesoriero and Pankow, 1996). On the contrary, Mn is expected to replace easily Ca in the lattice of rhombohedral carbonate to form Rhodochosite-Calcite solid mixture.

In figure 50 measured Ba contents have been compared with those estimated assuming a Ba partitioning between aqueous solution and carbonate minerals during coprecipitation of a $BaCO_3$-$CaCO_3$ solid solution. Chemical analyses on Hyblean carbonate rocks have revealed an average Ba molar fraction close to $3*10^{-4}$ (Tab. 6b). Furthermore, in the same figure computed Ba content in full equilibrium with pure Ba-bearing mineralogical phases such as Barite ($BaSO_4$) and Witherite ($BaCO_3$) have been also reported. It is evident that equilibrium with Ba-sulphate mineral exerts the control on Ba concentration and therefore its mobility within carbonate aquifer.

PHREEQC calculation, have revealed that groundwaters flowing within volcanic aquifer are strongly undersaturated with respect to barium minerals (Tab. 7). On the other hand, low Ba mobility in basalts weathering is related to the Barium affinity towards solid phase (Aiuppa et al., 2000).

Measured Sr concentrations have been also compared with those calculated assuming the dissolution of Strontianite at equilibrium condition and those computed in equilibrium with a Sr-Ca-CO_3 solid mixture having a Sr molar fraction of 0.00019 (average Sr content in Hyblean carbonate rocks, Table 6b). It is evident (Fig. 51) that the $SrCO_3$-$CaCO_3$ solid mixture seems to exert the control on Sr content in carbonate aquifer.

As regard Mn, chemical analyses have revealed that the average Mn molar fraction in rocks belonging to Hyblean carbonate succession is 0.0015 (Tab.6b). Also in this case, the figure 52 indicates that coprecipitation processes of Mn in carbonate solid solution can control the concentration of manganese in groundwaters hosted within carbonate aquifers. However, the observed differences between measured and estimated Mn contents could be related to the strong influence of precipitation rate on the distribution coefficient (Rimstidt et al., 1998).

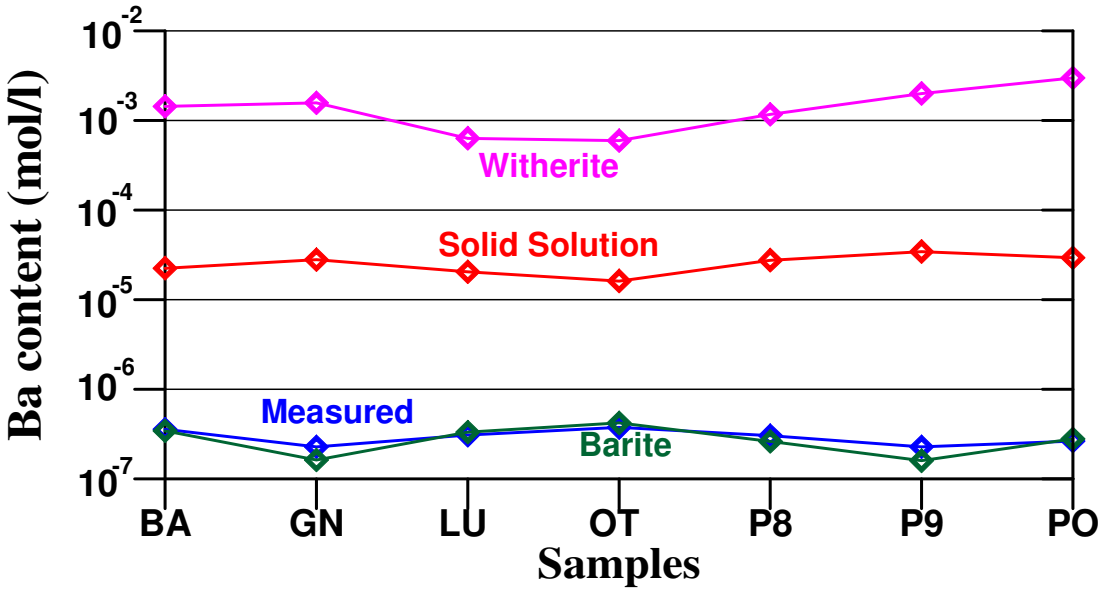

Figure 50: *Barium contents in sedimentary aquifers. Pink line: Ba in equilibrium with pure Witherite. Red line: estimated Ba content from the application of the coprecipitation model with Ba-$CaCO_3$ "solid solution" having a X_{Ba} of 0.0003. Green line: Ba in equilibrium with pure barite. Blue line: Ba measured contents.*

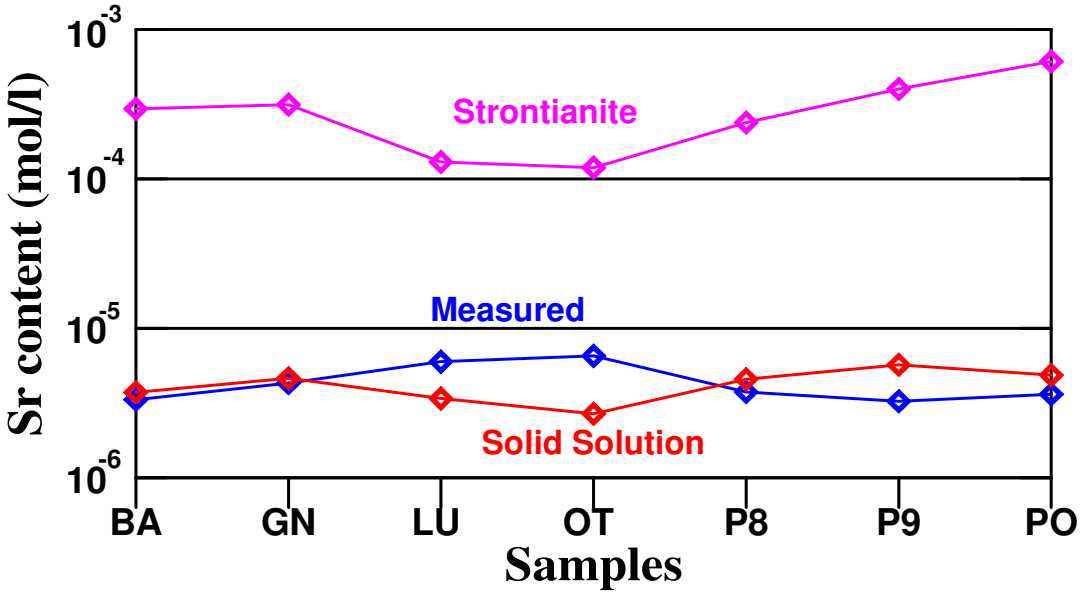

Figure 51: *Strontium contents in sedimentary aquifers. Pink line: Sr in equilibrium with pure Strontianite. Red line: estimated Sr content from the application of the coprecipitation model with Sr-$CaCO_3$ "solid solution" having a X_{Sr} of 0.000193. Blue line: Sr measured contents.*

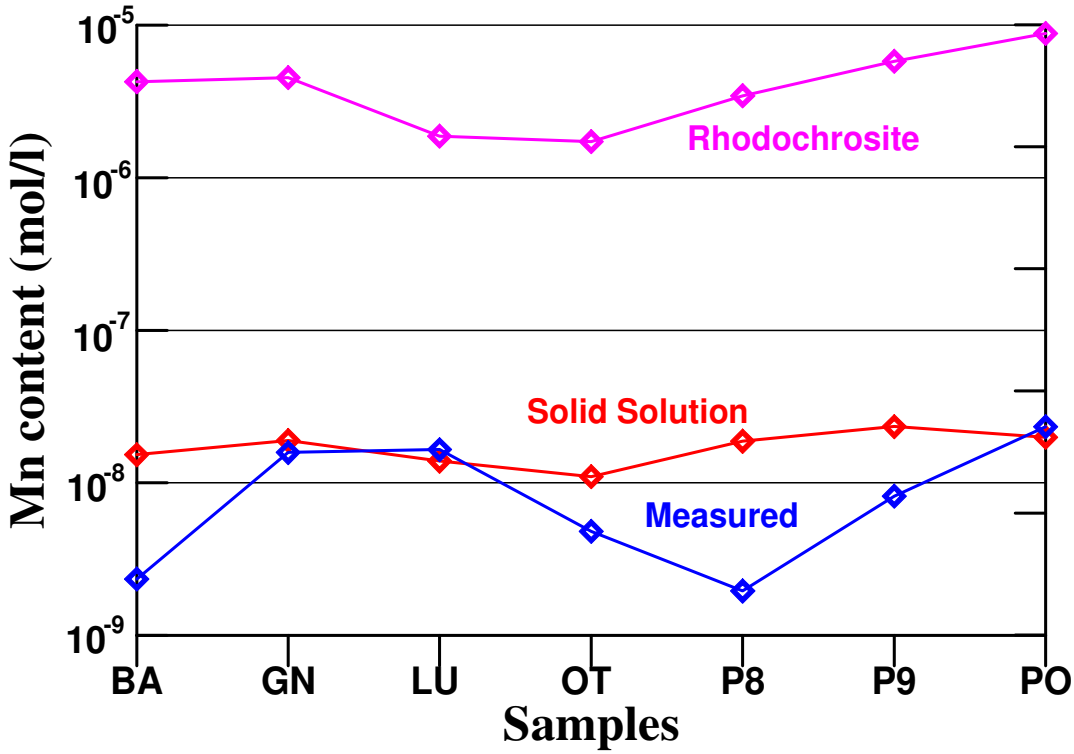

Figure 52: *Manganese contents in sedimentary aquifers. Pink line: Mn in equilibrium with pure Rhodochrosite. Red line: estimated Mn content from the application of the coprecipitation model with Mn-$CaCO_3$ ideal binary "solid solution" having a X_{Mn} of 0.0015. Blue line: Mn measured contents.*

10.GEOCHEMISTRY OF DISSOLVED GASES

Analytical data on the chemical composition of dissolved gases are reported in tables 12. Partial pressure of gases were computed at sampling temperatures based on the K_H reported by Wilhelm et al. (1977).

Air is the main gaseous component interacting with Hyblean groundwaters, except for some CO_2-rich waters located along the Southern coast and in the northern flank, where high pCO_2 (NA sample = 3.37 atm) have been measured. Furthermore, all the groundwaters circulating within the A2.1 deep aquifer (located along the Scicli-M.Lauro fault system) are CH_4-rich waters being methane partial pressure as high as 1.6 atm.

Hydrocarbons released along the Scicli-M.Lauro fault are mainly biogenic in origin ($\delta^{13}C_{CH4}$ ranges between –50 and -75‰ vs PDB, Table 13) and have to be related to the presence of a gas-oil field. At the presence, hydrocarbons are exploited through more than one hundred wells located mainly in the south-central sector of the Hyblean plateau.

He concentrations, above detection limits, have been only found in fourteen groundwater samples. He partial pressure is in the range from $3.6*10^{-6}$ to $2.3*10^{-4}$ atm. Only two of these values are slightly lower than air (He_{asw}= $5.5*10^{-6}$ atm), while all the other samples show He contents up to two orders of magnitude higher.

Figure 53, where pN_2, pO_2 and pCO_2 are reported in a triangular diagram, indicates that all the groundwater samples have N_2/O_2 ratios higher than air.

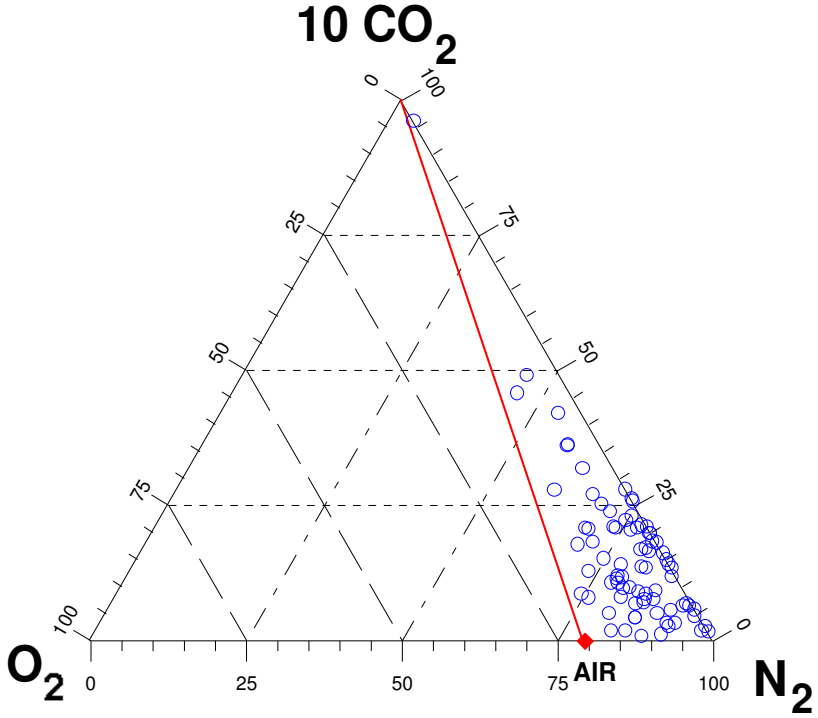

Figure 53: *CO_2-O_2-N_2: triangular plot of dissolved gases. Values reported as partial pressure (see text)*

The relative enrichment in nitrogen content dissolved in Hyblean groundwaters is to be related probably to the oxygen consumption due to the occurrence of oxidation reactions during groundwaters flow path. Such a geochemical process is prevailing in the A2 deep aquifer, where reducing condition are dominant (Eh <- 60 mV). Sometime, in these waters, oxygen content is lower then detection limits ($5*10^{-4}$ atm) and Hydrogen sulphide is also present.

Distribution map of carbon dioxide partial pressure in equilibrium with Hyblean groundwaters (Fig. 54) highlights that all the samples show values ($-3<\log pCO_2<0.5$) higher than atmospheric CO_2 contents ($\log pCO_2 = -3.5$ atm), thus indicating that a CO_2-rich gas phase is dissolved in groundwater. The highest pCO_2 have been observed in Northern area in a well water located very close to the "Mofeta dei Palici" area. The gases discharged from “Mofeta dei Palici” are CO_2-dominant. Recent studies based on Carbon and He isotope composition pointed out a MORB affinity of these gases confirming their mantle origin (unpublished data).

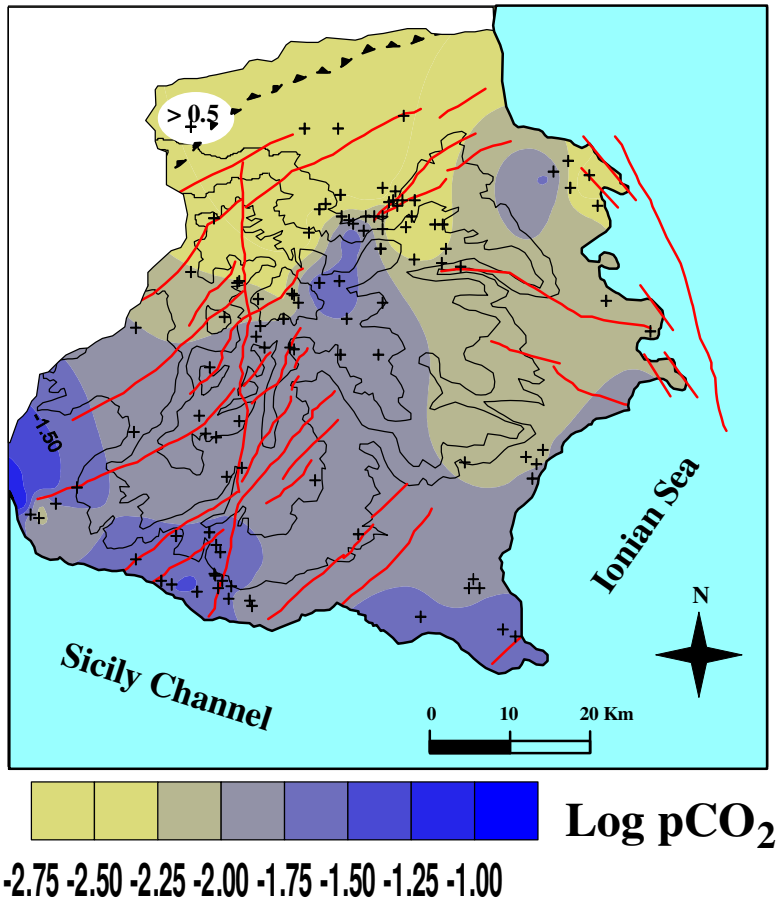

Figure 55: *Distribution map of log pCO_2 in Hyblean groundwaters.*

Data on the isotopic composition of the total dissolved inorganic carbon species ($\delta^{13}C_{TDIC}$) together with the concentration of TDIC for the Hyblean aquifers, are showed in table 14. Wide ranges both in concentration (0.002 to 0.07 molKg^{-1}) and in isotopic values (–21 to –1.1 δ ‰) indicates the presence of more than one carbon source. The main sources of dissolved carbon in Hyblean groundwaters include CO_2 related to volcanic degassing systems, dissolution of carbonate minerals, atmospheric carbon dioxide and biogenic CO_2. Each of these different sources is characterized by a well-constrained isotopic composition. The $\delta^{13}C_{TDIC}$ represents the weighted isotopic composition relatively to each dissolved carbon specie (Wigley et al., 1978), expressed as follows:

$$\delta^{13}C_{TDIC} = \delta^{13}C_{CO_2} X_{CO_2aq} + \delta^{13}C_{HCO_3} X_{HCO_3^-} + \delta^{13}C_{CO_3} X_{CO_3^{2-}} \quad \text{(Eq.18)}$$

where X_{CO_2aq}, X_{HCO_3} and $X_{CO_3^{2-}}$ are the molar fractions of the dissolved carbon species.

Taking into account the fractionation processes between carbon dioxide and the carbon dissolved species ($CO_{2aq,}$ HCO_3^- and CO_3^{2-}) it is possible to calculate the carbon isotopic composition of the CO_2 in equilibrium with groundwater (Favara et al., submitted).

For pH values less than 8.2, $X_{CO_3^{2-}}$ becomes negligible and then equation 18 can be rewritten:

$$\delta^{13}C_{CO2} = \delta^{13}C_{TDIC} - \varepsilon_a * X_{HCO3} - \varepsilon_\beta * X_{CO2} \quad \text{(Eq.19)}$$

For pH values greater than 8.2, XCO_{2aq} becomes negligible and then equation 18 can be rewritten:

$$\delta^{13}C_{CO2} = \delta^{13}C_{TDIC} - \varepsilon_a * X_{HCO3} - \varepsilon_\gamma * X_{CO3} \quad \text{(Eq.20)}$$

$\varepsilon_{a,}$ ε_β and ε_γ are the enrichment factors for $\delta^{13}C_{HCO3}$-$\delta^{13}C_{CO2gas}$ (Mook et al., 1974) $\delta^{13}C_{CO2aq}$ -$\delta^{13}C_{CO2gas}$ and $\delta^{13}C_{CO3}^{2-}$-$\delta^{13}C_{CO2gas}$ (Deines et al., 1974) pairs, respectively.

As pointed out by Wigley et al., (1978) in order to apply equations 19 and 20, it is indispensable the achievement of isotope equilibrium among CO_2-gas, dissolved carbon species and water.

The calculated values assuming the samples have been equilibrated at sampling temperature, range from –27 to –1.4 δ‰ vs PDB. This wide range confirms the presence of carbon dioxide input, coming from different sources.

According to Chiodini et al. (2000), the addition of CO_2 within Hyblean aquifers can be modelled in three simple steps.

In the first step the composition $\delta^{13}C_{TDIC}$ of infiltrating water has been calculated, assuming that isotopic equilibrium between atmospheric carbon dioxide and dissolved carbon species is reached. Some determinations on local rainwater indicate an average pH values close to 6.2 and a total carbon content of about 1.4 10^{-5} mol/l. Thus, infiltrating waters should have a $\delta^{13}C_{TDIC}$ close to –3.8.

During the second step, it has been simulated the process in the unsaturated soils, of addition 0.01 moles of biogenic derived CO_2 per Kg of infiltrating waters. During the CO_2 dissolution, groundwaters are constantly kept in equilibrium with calcite.

PHREEQC computer program (Parkhurst, 1995) has been used to calculate the mass balance and the aqueous speciation. To compute theoretical $\delta^{13}C_{TDIC}$ it needs also to fix both the carbon isotopic composition biogenically derived and that of carbonate minerals. Ten isotopic measurements on carbonate rocks belonging to the Hyblean Plateau (Tab. 15) showed values of $\delta^{13}C_{CaCO3}$ in the range –3.1÷0.8 δ‰ vs V-PDB (mean values –1). Carbon isotopic composition of biogenically derived CO_2 has been assumed to range from –28 to –18 δ‰.

Obtained theoretical curves are reported in figure 55, together with the $\delta^{13}C_{TDIC}$ values measured in the water samples.

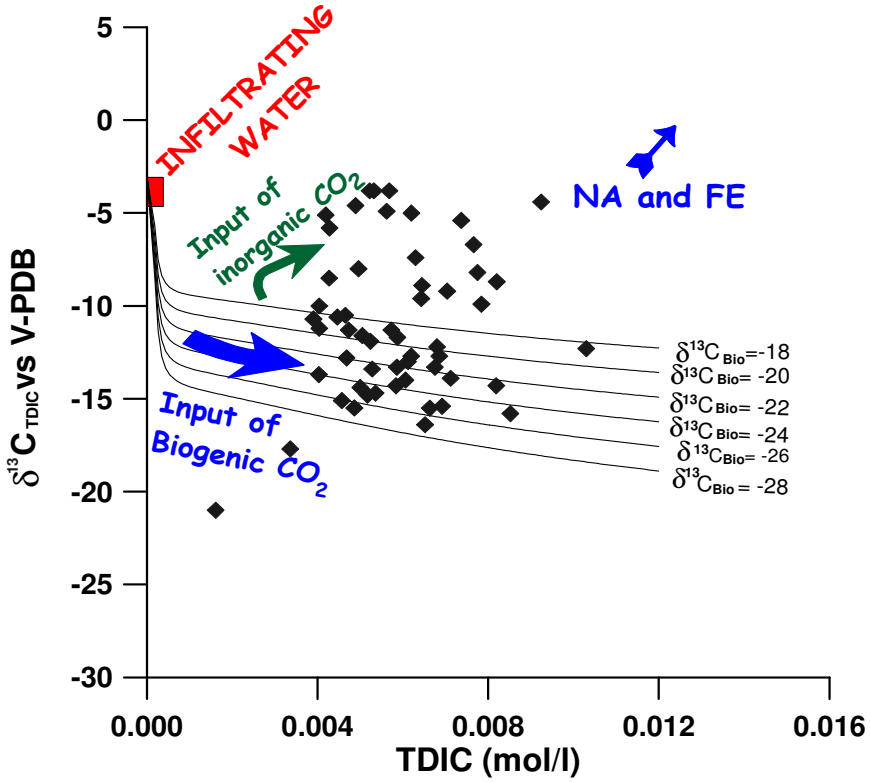

Figure 55: *TDIC vs $\delta^{13}C_{TDIC}$ diagram. Hyblean groundwaters are compared with theoretical curves representing the chemical and the isotope evolution of infiltrating waters (see text).*

It should be noted that some waters fall along the curves representing the addition of biogenic carbon dioxide while other samples lie far from the theoretical values, thus demonstrating also the occurrence of a contribution from other sources of carbon. Only one sample (BM) falls significantly below the theoretical curves being undersaturated with respect to calcite. On the contrary, many samples shift towards more positive $\delta^{13}C$ values identifying a contribute of an isotopically heavy inorganic CO_2.

The third step involves the addition of CO_2 derived from an inorganic deep source. Theoretical curves, simulating this process have been drawn assuming as starting points four infiltrating waters equilibrated with a biogenic CO_2 with $\delta^{13}C$ = -22 δ‰ and containing from 0.002 to 0.005 mol/litre of total dissolved carbon. Also in this case, the equilibrium between solution and calcite has been kept. The isotopic composition of the deep CO_2 source has been assumed equal to that of CO_2 rising at Mofeta dei Palici ($\delta^{13}C_{CO2}$ = –1 ‰ vs PDB). The obtained curves, resulting from this model, fit very well with analytical data for Hyblean groundwater having $\delta^{13}C_{TDIC}$ shifted towards more positive values (Fig. 56).

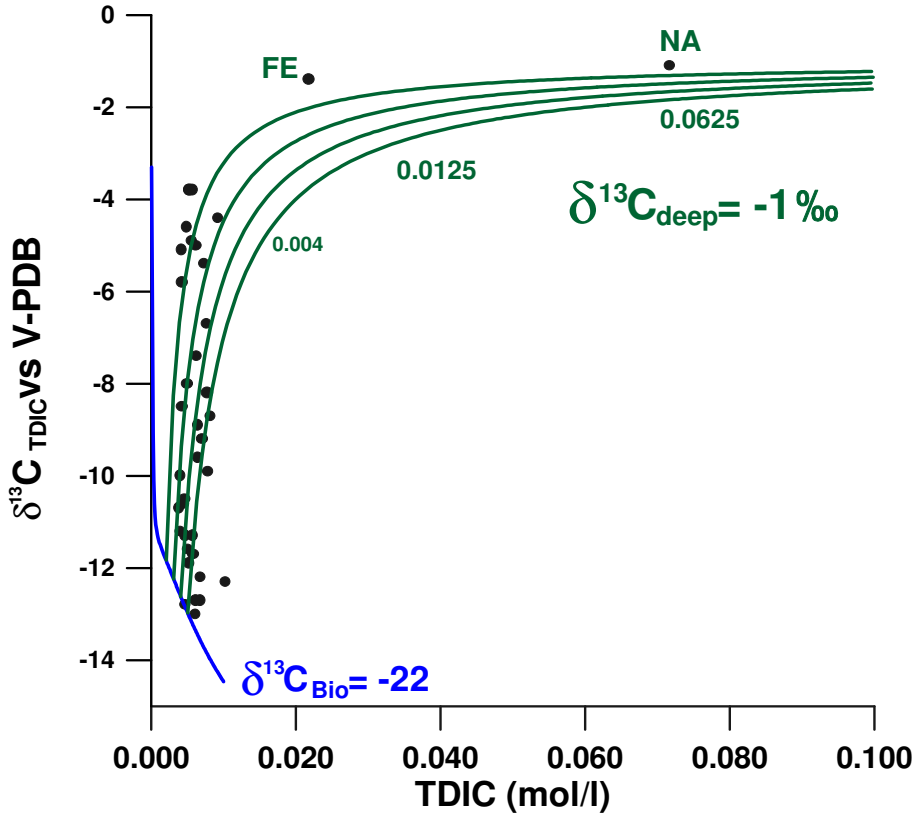

Figure 57: *TDIC vs $\delta^{13}C_{TDIC}$ diagram. Hyblean groundwaters fit theoretical curves drawn assuming that infiltrating waters receive a deeply derived CO_2 input. In this case carbon isotope composition of deep-CO_2 source has been assumed –1 δ‰ vs PDB.*

Representative points of both aquifers (VO and SE) seem to indicate that groundwaters receive less than 0.004 mol/litre deeply derived-CO_2. FE and NA samples depart from the overall picture, indicating they receive greater CO_2 input ranging from 0.012 to 0.057 moles per litre.

The different deep CO_2 inputs into the Hyblean groundwaters could be related to the location of the sampling sites with respect to the tectonic and hydrogeological setting. The sites NA and FE are located within inner marginal flat zones where aquifers show a reduced thickness and smaller water volumes are present. The highest CO_2 input at NA sample is due to its vicinity to Mofeta dei Palici gas emission where high gas fluxes and CO_2 concentrations have been measured. While FE spring shows a lower carbon contribution even probably as a consequence of lower gas fluxes.

High density of tectonic discontinuities along the southern coast (the Scicli and Ispica-Capo Passero grabens and the prolongation towards SW of the Comiso-Chiaramonte fault) allows to obtain relatively high pCO_2 values.

However, distribution map of dissolved pCO_2 doesn't reflect exactly the overall picture of the degassing system at Hyblean Mountains. As previously described in the section 7.2, in areas having lower gas fluxes interacting with groundwaters, water rock interaction processes increase pH and consequently causing a marked lowering in pCO_2 values.

This process is particularly effective at FE sample located on the western margin, where the conspicuous carbon dioxide input are almost entirely converted in HCO_3 ion (1200-1300 mg/l; average Hyblean groundwaters 295 mg/l).

Within the Hyblean aquifers, the presence of several structural discontinuities promotes the migration of deep fluids towards surface. As previously reported, dissolved He has been found only in some groundwaters hosted within aquifers in which active tectonic structures are present (fig.58). In particular, high dissolved He contents have been measured in groundwaters (PI, CM, SO and MA samples) hosted within the deep A aquifer (A2.1 group). Furthermore, relevant amounts of dissolved He have been measured at NA sample (the north-western CO_2-rich area) and at GU and GI samples, (close to Hyblean Malta escarpment).

He isotope ratio dissolved in groundwaters is a well-known geochemical tracer.

Commonly, three main Helium sources (atmosphere, mantle, and crust) can be distinguished, each of them is characterized by a marked difference in $^3He/^4He$ ratio.

Measured $^{3}He/^{4}He$ isotope ratios, normalized to the atmospheric $^{3}He/^{4}He$ ratio ($Ra=1.39*10^{-6}$) range from 0.81 to 6.19 Ra. Wide ranges observed both in He content and in its isotope ratio, indicate that dissolved He in Hyblean groundwaters is a mixing, in different proportions, among the three main He-sources.

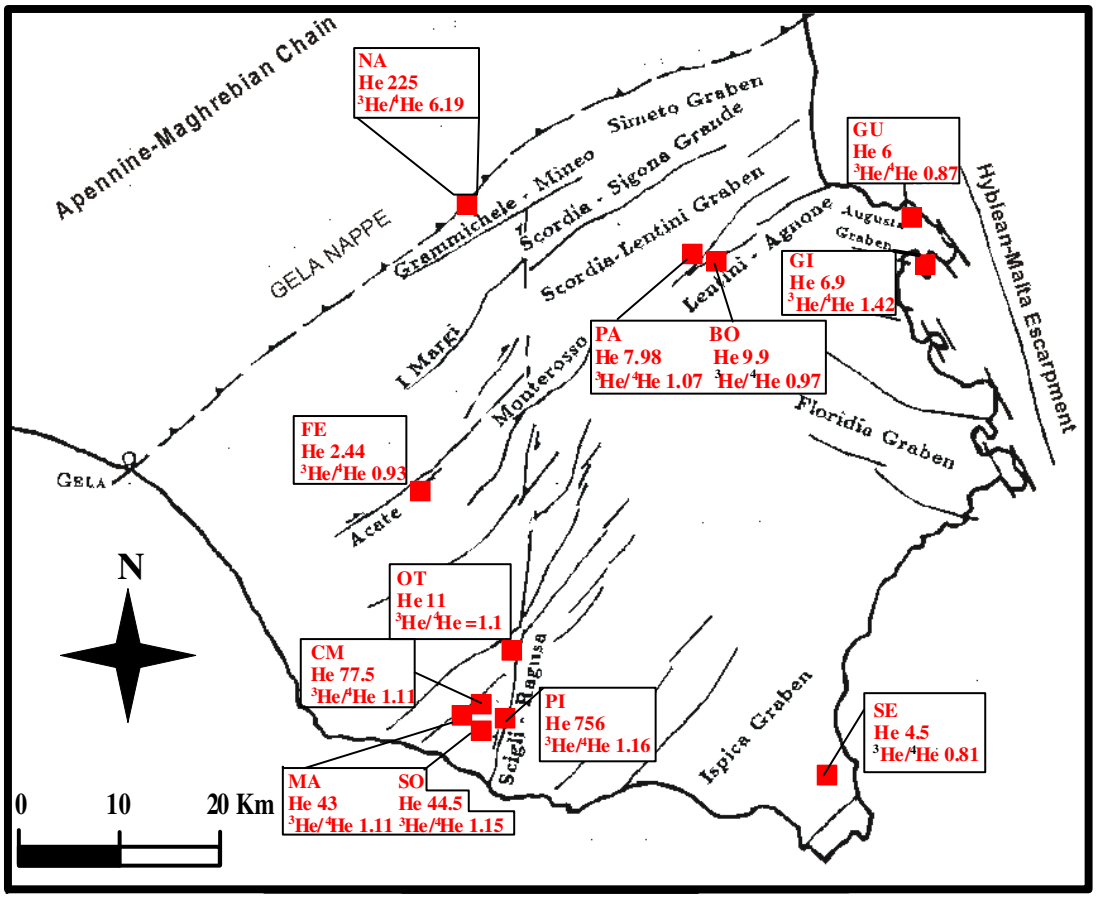

Figure 58: *Location map showing concentration and isotope ratio of dissolved helium. Concentrations are reported in cc STP/l *10^{8}. $^{3}He/4He$ ratio are expressed with respect to the same ratio in air*

In figure 59 are reported the R/Ra ratio versus the $^{4}He/^{20}Ne$. In the same figure, two mixing lines between crustal-atmospheric He and MORB-type-atmospheric He are also reported. Three sample-types have been distinguished:

- a MORB-type helium-enriched (NA sample) plotting near to the air-mantle mixing line;
- a mixed crustal-MORB type, having R/Ra close to 1.1-1.2 (SO, PI, CM and MA samples), but with $^{4}He/^{20}Ne$ ratio greater than 3.1
- air-equilibrated He (other samples) falling very close to the air saturated water point.

According to Sano et al. (1982) $^{4}He/^{20}Ne$ ratio can be used to compute the contribution of each of the three main He sources, basing on the following mass balance equations:

$$(^3He/^4He)s=(^3He/^4He)m * M + (^3He/^4He)c *C + (^3He/^4He)a *A \quad \text{(Eq.21)}$$

and

$$(^4He/^{20}Ne)s= (^4He/^{20}Ne)m\ M + (^4He/^{20}Ne)c* C + (^4He/^{20}Ne)a * A \quad \text{(Eq.22)}$$

where A, M, and C are the He fractions deriving from air (A), mantle (M) and crust (C) respectively.

In table 16 the measured $^4He/^{20}Ne$ ratios and air-normalised $^3He/^4He$ ratios, together with the calculated mixing ratios for each component are reported. The $^4He/^{20}Ne$ ratio fluctuates significantly, ranging from 0.290 to 10.29. This implies that the fraction of air component is quite variable being in some samples more than 45%, but in five samples it doesn't reach 10%.

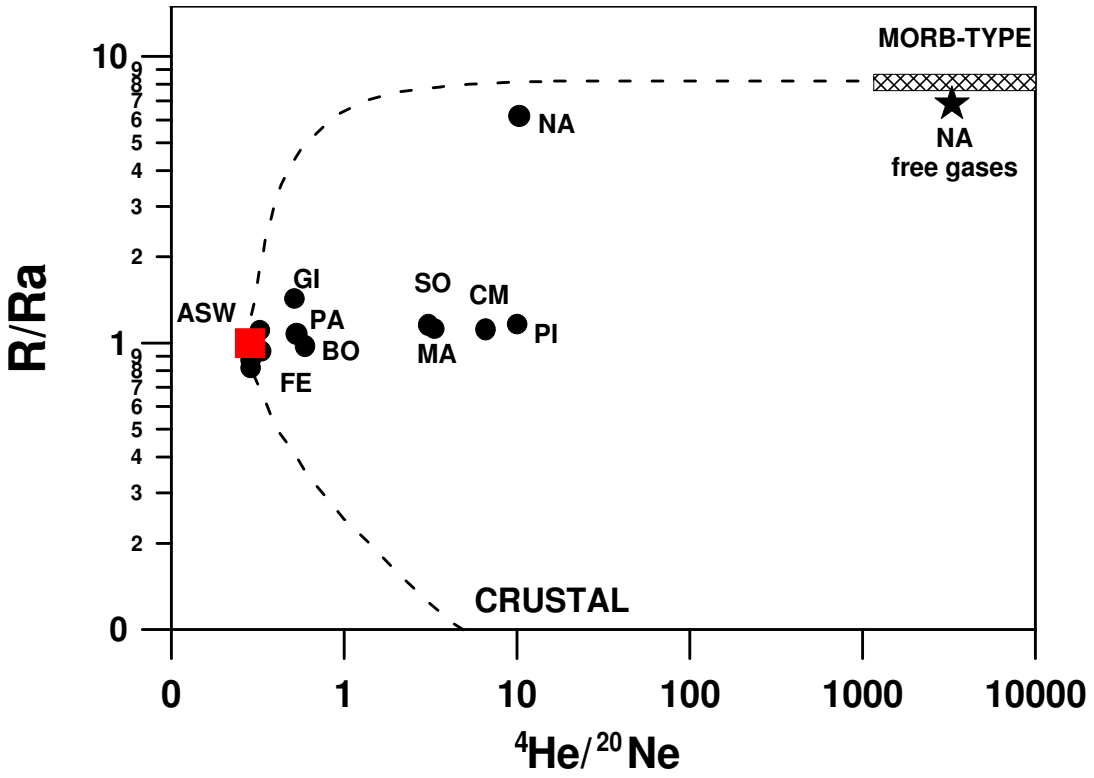

Figure 59: *He isotope ratio vs 4He/20Ne ratio. Mixing lines connecting the point representative of Air Saturated Water (ASW) and MORB-type and ASW-Crustal are also reported.*

At NA well air component can be assumed negligible, being lower than 3%. He content dissolved in this sample is mainly upper mantle-derived (up to 80%) with a slight crustal contribute. Such a high He isotope ratio is similar to that collected from the Mofeta dei Palici gas manifestation, located very close to NA well.

If, in the other samples having $^4He/^{20}Ne$ ratios greater than the ASW, the air contribution is excluded, the remaining components indicate a quite homogeneous partitioning between

crustal (85-88%) and mantle (12-15%) sources except for GI sample, where the ^{3}He-excess can be interpreted as a result of addition of about 25% of mantle-derived Helium.

Finally four water samples (OT, FE, SE and GU) showed $^{3}He/^{4}He$ ratios typical for atmosphere-equilibrated samples. Despite a remarkable CO_2 deep contribute, FE spring belongs to this group. This suggests at least two hypotheses: the first one implies that the gas phase interacting with the aquifer feeding FE spring is chemically different from that rising at Mofeta dei Palici area. In particular, even if the carbon isotope composition seems to be similar ($\delta^{13}C_{CO2}$ =-1‰) it doesn't contain mantle derived helium. The second hypothesis, could derive from the fact that FE sampling site is a little pool where dissolved He can easily re-equilibrated with air.

11. CONCLUSIONS

The present thesis reports a hydrogeological and geochemical study of groundwaters flowing through the aquifers hosted within the Hyblean plateau.Particular attention has been focused on the isotopic characterization of the rainwater and the relationship with local groundwaters.

Data collected during a 2-years period from a raingauges-thermometric network consisting of 6 stations located at different altitudes have revealed that temperature is the main factor controlling the isotopic composition of rainwater. In fact, isotope composition of precipitation is depleted in heavy isotopes during cold seasons, while more positive values have been recorded during summer.

The altitude effect on the 18-oxygen values on Southern and Eastern flanks gives rise to vertical gradients equal to $0.19\delta^{18}O/100m$ and $0.24\delta^{18}O/100m$, respectively. Coupling chemical and isotopic analyses of rainwater it has been possible to identify that the prevalent directions of the wet air masses are from south-west and south-east.

This results in a slightly continental effect identified at SC station located on the Northern flank about 100 Km inland with respect to the South coast. The slope (6.14) of the relationship between δD and $\delta^{18}O$ in rainwater suggests that evaporative processes during rainfall events have a great influence mainly at stations located along the coast (MRG and SR).

Spatial distribution of 18-oxygen in groundwaters highlights that the most heavy-isotope depleted samples are located in the higher portion of the Hyblean Mountains, while more positive values are recorded in the marginal area. In SU sample located along the coast, heavy-isotope enrichment is related to aerosol seawater contamination.

Almost constant isotope composition in some groundwaters has revealed the existence of deep aquifers having long residence time and fed by huge catchment areas. Wider range in δ-values refers to shallower aquifers that reflect, even if to a lesser extent, seasonal changes in the rainwater isotopic composition.

The comparison between local infiltrating water and Hyblean groundwaters has highlighted the occurrence of evaporative processes in the soil during infiltration. In fact, the $\delta D/\delta^{18}O$ relationship is described by a linear fit line having a slope of 4.56. Such low slope values are typical for areas having arid or semi-arid climatic conditions.

Climatic diagrams considering the mean monthly temperature and rainfall values has highlighted that at coastal stations, arid climatic condition are reached for periods longer than 6 months.

Secondary processes involving rainwater during infiltration in the soil, make difficult the use of stable isotopes as a tracer to identify the areas and the mechanisms of recharge of groundwater in the Hyblean aquifers.

In agreement with the local hydrogeological setting and the location of sampling sites, Hyblean groundwaters have been arranged in two main groups: sedimentary aquifers (SE aquifers) and mainly volcanic aquifers (VO aquifers).

On the base of the major elements content, groundwaters circulating in sedimentary aquifers have been distinguished in four groups: calcium-magnesium-bicarbonate waters (Group A), sulphate waters (Group B), nitrate-waters (Group C) and finally sodium-chloride waters (Group D). These last three groups (B, C, and D) are representatives of only small aquifers located on the marginal parts of the basin. Groundwaters belonging to the group A are hosted within the Oligo-Miocene limestone.

The hydrogeological model proposed for these groundwaters suggests the existence of a shallower aquifer (A1) characterized by lower temperature (T_{mean}=16°C) and lower Mg-contents, overlying on a deeper aquifer (A2) having higher temperature (T_{mean}=22°C) and higher Mg contents.

This is consistent with the Hyblean carbonate succession that include at depth of about 100-150 m the presence of a marls layer which separate two different aquifers. The shallower one is hosted within the Irminio member belonging to the Ragusa Formation, while the deeper one is hosted within the Amerillo Formation and the Leonardo member of the Ragusa Formation.

Higher Mg content in A2 groundwaters seems to be due to the leaching of Mg-silicates interbedded within the Amerillo Formation and the underlying geological complexes, while interaction processes with Mg-rich carbonate rocks seem to be excluded. Intermediate terms between A1 and A2 end-members confirms the hydraulic connection between the shallow aquifer and the deeper one in correspondence only of both karst and tectonic structures

Some groundwaters (CM, SO, MA and PI samples) hosted within the deep aquifers show higher Na and Cl content together with low Eh values, intense smell of hydrogen sulphide, higher amount of dissolved CH_4.

They are located along the tectonic structure connecting the M. Ragusa and the Scicli-M.Lauro fault system. It is reasonable to think that deep fluids, probably connected to the hydrocarbon reservoirs, could rise along these structural discontinuities.

Saturation state reveals that all the samples hosted within SE aquifer are saturated with respect to calcite while only the most evolved samples are saturated with respect to dolomite.

Furthermore, they have attained the equilibrium with oxidised Fe (III)-bearing minerals such as Goethite and Hematite. While, in some samples (CM, SO, MA and PI samples), where reducing conditions prevail, saturation state is achieved with respect to iron-sulphide minerals.

Almost all SE groundwaters are saturated with respect to barite. This mineral phase exerts a control on Ba contents in these groundwaters. While both Sr and Mn contents are in equilibrium with Sr- and Mn-$CaCO_3$ solid mixtures respectively.

Groundwaters hosted within the volcanic aquifer (VO aquifer) during their flow path modify some physico-chemical parameters as a consequence of the proceeding of water-rock interaction.

It appears evident that, at initial stage of the flow path, VO groundwaters are enriched in earth alkaline elements released both from carbonate and silicate rocks. During the late stage of the evolution, water-basalt process prevails and then both pH value and alkali content increase, while Ca and Mg are depleted.

This can be mainly related to two geochemical processes:

- the formation of Ca- and Mg-bearing secondary minerals, both carbonate (calcite and dolomite) and silicate (Ca- and Mg-Smectite, Talc, Sepiolite);
- the occurrence of ion-exchange reactions.

The NA sample receiving a marked input of deep CO_2 is isolated from this general context. In this case, as a consequence of lower pH values, mineral solubilities will increase and then groundwaters characterized by higher salinity will form.

All VO groundwaters are undersaturated with respect to primary ferro-magnesian basaltic minerals, while they are in the range of saturation with respect to plagioclase and Al- and Fe- oxides and hydroxides.

In the North-eastern part of the Hyblean region, very close to the onshore portion of the Hyblean Malta escarpment, a sulphurous aquifer has been also identified. Groundwaters flowing in this aquifer are characterized by negative Eh values and trace of H_2S.

Chemical and isotope analyses of dissolved gases mainly CO_2, CH_4 and He, both in SE and VO groundwaters have allowed the individuation of the main degassing areas. They are located in proximity of the main tectonic discontinuities.

In particular highest pCO_2 values have been recorded at the "Mofeta dei Palici" area, a natural gas manifestation (CO_2-dominant) located in correspondence of the thrust belt of the Gela Nappe.

Moreover, on the western margin at FE sample relevant amount of rising CO_2 is converted in HCO_3 ions. In both cases, isotopic composition measurements of total dissolved inorganic carbon indicate a deeply-derived CO_2, having an isotopic composition close to that discharged at "Mofeta dei Palici" (-1δ ‰ vs V-PDB).

Furthermore, groundwaters located along the Scicli-M. Lauro fault system belonging to the A2.1 aquifer are CH_4-rich and they show intense smell of H_2S.

Both in all these groundwaters and in groundwaters samples located along the Scordia-Lentini Graben on northern flanks and along the Hyblean Malta escarpment dissolved He has been also recognized

He isotope ratios dissolved in the Hyblean groundwaters indicate three sample-types:

- a MORB-type helium enriched with a 20% of a crustal component, having R/Ra close to 6.2;
- a mixed crustal (85%)-MORB (15%)-type, with R/Ra ranging from 1.1 to 1.42;
- air-equilibrated He, having both concentration and isotope ratio very close to the atmosphere.

On the base of the origin and the pattern of the fluids it is reasonable to think that the most suitable geochemical parameters for earthquake prediction should be water temperature, pH, Eh, Electrical conductivity, as well as He, pCO_2 and H_2S.

Furthermore, based on the obtained results and the geochemical model of groundwaters circulation in the Hyblean region, some sites of great interest have been chosen to project a geochemical network for the continuous monitoring of the local seismic activity.

All the selected sites show geochemical features attesting the input of deep-source fluids. They are:

- CM, SO, MA and PI wells, along the Scicli-M. Lauro fault system;
- GI and GU wells close to the onshore prolongation of the Hyblean Malta escarpment;
- NA well, near the "Mofeta dei Palici" area;
- PA and BO along the Southern margin of the Scordia-Lentini graben;
- FE spring, located on the western margin.

A common features to all these sites is that they are located mainly along the most important local active tectonic structures being the fault systems the preferential way of uprising of deep fluids.

AKNOWLEDGEMENTS

First of all, I wish to thank my tutor Prof. Mariano Valenza. His continuous encouragement helped me in the interpretation of data, stimulating me in search of a comprehensive geochemical approach. I am also indebted with him for his patience during the draft of this work.

I am grateful to Prof. Mario Nuccio, coordinator of the *Dottorato di Ricerca in Geochimica* for his precious suggestions throughout the last three years, and the entire *Dipartimento CFTA*.

I'm very grateful to Dr. Rocco Favara, director of the *Istituto Nazionale di Geofisica e Vulcanologia*-S*ection of Palermo* for his unceasing scientific and human support. Moreover, he gave me the possibility to have full access to all INGV laboratories where many of the analyses reported in this work have been performed.

I also take the opportunity to thank all the staff, both researchers and technicians of the *Istituto Nazionale di Geofisica e Vulcanologia*-S*ection of Palermo,* which supported me during field works and laboratory analyses. Special thanks to Dr G. Capasso and Dr. S. Inguaggiato for many fruitful scientific discussions and for their comments about the manuscript and to S. Francofonte for his assistance during several surveys at Hyblean Mountains.

I cannot forget the friendly hospitality of Dr. E. Faber (Institute of Geosciences, BGR, Hannover, Germany) during my stay there. He helped me carrying out chemical and isotope analyses of dissolved hydrocarbons.

I wish to remember Dr. Rosario Ruggeri, Dr. Rosario Zaccaria and the entire staff of the *Centro Ibleo di Ricerche Speleo-Idrogeologiche* (Ragusa) indispensible for field activities.

I thank also Prof. P. Censi and his staff for their help during analyses of trace elements.

Prof. Antonio Longinelli and Prof. Luigi Marini, reviewers of this manuscript, improved this thesis with their useful and precious comments.

Finally, I would like to dedicate a particular remark to the unforgettable human and scientific experience I shared with Mauro Martelli, Bianca Parisi, Daniela Salvagio Manta and Daniela Varrica, my friends first and then collegues.

12. REFERENCES

Adam J., Reuther C.D., Grasso M. & Torelli L. (2000) – *Active fault kinematics and crustal stresses along the Ionian margin of south-eastern Sicily*. Tectonophysic 326, 217-239.

AGIP (1994)-*Acque dolci sotterranee. Inventario dei dati raccolti dall'AGIP durante la ricerca di idrocarburi in italia (dal 1971 al 1990).* AGIP S.p.A. Ed. S. Donato Milanese. 515 pp.

Aiuppa A., Allard P., D'Alessandro W., Michel A., Parello F., Treuil M. & Valenza M. (2000)- *Mobility and fluxes of major, minor and trace metals during basalt weathering and groundwater transport at Mt. Etna volcano (Sicily)*. Geochim. Cosmochim. Acta 64, 1827-1841.

Al T., Martin C. & Blowes D. (2000)-*Carbonate-mineral/water interactions in sulfide mine tailings.* Geochim. Cosmochim. Acta 64, 3933-3948.

Appelo C.A.J. & Postma D. (1993)- *Geochemistry, Groundwater and Pollution.* Balkema, Rotterdam.

Aureli A. (1989) - *Indagine geochimica comparata a modelli idrogeologici sugli acquiferi del settore Nord-Orientale Ibleo (Sicilia).* Tesi inedita di Dottorato di Ricerca, Palermo.

Aureli, A., (1993a)- *Carta della vulnerabilità delle falde idriche. Settore nord-occidentale ibleo (Sicilia S.E.).*

Aureli, A., (1993b)- *Carta della vulnerabilità delle falde idriche. Settore sud-occidentale ibleo (Sicilia S.E.).*

Aureli, A., (1993c)- *Carta della vulnerabilità delle falde idriche. Settore sud-orientale ibleo (Sicilia S.E.).*

Aureli, A., Adorni. G., Chiavetta, A.F., Fazio, F., Fazzina, S. and Messineo, G. (1993)- *Carta della vulnerabilità delle falde idriche. Settore nord-orientale ibleo (Sicilia S.E.)*

Battaglia M., Cristofolini R., Di Girolamo P. & Stanzione D. (1976)- *Rare earth elements and other trace elements distribution and the origin of the iblean magma.* Volcanol. Geotherm. Res., 1, 331-346.

Beccaluva L., Siena F., Coltorti F., Di Grande A., Lo Giudice A., Macciotta G., Tassinari R. & Vaccaro C. (1998) - *Nephelinitic to Tholeiitic Magma Generation in a Transtensional Tectonic Settino: an Integrated Model for the Iblean Volcanism, Sicily*. Journal of petrology 39, 1547-1576.

Bianchi F., Carbone S., Grasso M., Invernizzi G., Lentini F., Longaretti G., Merlini S. & Mostardini F. (1987) - *Sicilia Orientale: profilo geologico Nebrodi-Iblei*. Mem. Soc. Geol. It. 38, 429-458.

Brand, U. (1981) *Mineralogy and chemistry of the Lower Pennsylvanian Kendick fauna, eastern Kentucky, 1. Trace elements.* Chem Geol., 32: 1-16

Bruno J., Duro L., de Pablo J., Casa I., Ajora c., Delgado J., Gimeno M.J., Linklater C., Perez del Villar L. & Gomez P. (1998) -*Estimation of the concentrations of trace metals in natural systems: The application of codissolution and coprecipitation approaches to El Berrocal and Pocos de Caldas*. Chem. Geol. 151, 277-291.

Carbone S., Grasso M. & Lentini F. (1987) - *Lineamenti geologici del plateau Ibleo (Sicilia S.E.) presentazione delle carte geologiche della Sicilia Sud-Orientale.* Mem. Soc. Geol. It. 38, 127-135.

Chiodini G., Frondini F., Cardellini C., Parello F. & Peruzzi L. (2000)- *Rate of diffuse carbon dioxide Earth degassing estimated from carbon balance of regional aquifers: The case of central Apennine, Italy*. Mem. Journal of Geophysical Research 105, 8423-8434.

Craig H. (1961)- *Isotopic variation in meteoric waters*. Science 133, 1702-1703.

Dall'Aglio M., Quattrocchi F. & Tersigli S. (1995)- *Geochemical evolution of groundwater of the Iblean Foreland (Southeastern Sicily) after the December 13, 1990 earthquake (M = 5.4).* Annali di Geofisica, XXXVIII.

De Rosa R., Mazzuoli R. & Trua R. (1992)- *A petrogenetic model for the coexistence of alkali basalts and tholeiites in the Plio-Pleistocene volcanism of Iblean plateau (Suth-East Sicily, Italy)*. Acta Vulcanologica, 2, 199-207.

Deines P., Langmuir D. & Harmon R.S. (1974)-*Stable carbon isotope ratios and the existence of a gas phase in the evolution of carbonate ground waters*. Geochim. Cosmochim. Acta, 38, 1147-1164.

Favara R., Grassa F., Inguaggiato S. & D'Amore F. (1998)- *Geochemical and hydrogeological characterization of thermal springs in Western Sicily, Italy.* Journal of Volcanology and Geotermal Research, 84, 125-141.

Favara, R., Grassa, F., Inguaggiato, S. and Valenza, M. (2001)- *Hydrogeochemistry and stable isotopes of thermal springs: earthquake-related chenges along Belice fault (Western Sicily).* Appl. Geochem. 16, 1-17.

Favara R., Grassa F., Inguaggiato S., Pecoraino G., Capasso G. *A simple method to determine the $\delta^{13}C$ of total dissolved inorganic carbon*. Geofisica. International. (submitted)

Gat JR. & Carmi H. (1970)- *Evolution of the isotopic composition of atmospheric waters in the Mediterranean Sea area.* Geophys Res 75, 3039-3040.

Ghisetti F. & Vezzani L. (1980)- *The structural features of the Iblean Plateau and of the Mount Iudica (South Eastern Sicily). A microtectonic contribution to the deformational history of the Calabrian.* Arc. Boll. Soc. Geol. It. 99, 57-102.

Ghisetti F. & Vezzani L. (1981)- *Contribution of structural analysis to undestanding the geodynamic evolution of the Calabrian arc (Southern Italy).* J. Struct. Geol., 3, 371-381.

Gislason S. R. & Arnorsson S. (1993)- *Dissolution of primary minerals in natural waters: Saturation state and kinetics*. Chem. 105, 117-135.

Gislason S., Arnòrsson S. & Armannsson H. (1996)- *Chemical weathering of basalt in southwest Iceland: effects of runoff, age of rocks and vegetative/glacial cover.* American Journal of Science 296, 897-907.

Gislason S.R. & Eugster H. P. (1987a)- *Meteoric water-basalt interactions. I: A laboratory study*. Geochim. Cosmochim. Acta 51, 2827-2840.

Gislason S.R. & Eugster H. P. (1987b)- *Meteoric water-basalt interactions. II: A field study in N.E. Iceland*. Geochim. Cosmochim. Acta 51, 2841-2855.

Gonfiantini R. (1986)- *Enviromental isotopes in lake studies. Handbook of Enviromental Isotopes Goechemistry*. 2,113-168.

Grasso M. (1993)- *Pleistocene structures along the lonian side of the Hyblean Plateau (SE Sicily): implications for the tectonic evolution of the Malta Escarpment.* In: Max, M.D., Colantoni P., *Geological Development of the Sicilian Tunisian Platform*. UNESCO Reports in Marine Science 58, 49-54.

Grasso M., Martyn Pedley H., Maniscalco R & Ruggieri R. (2000)- *Geological context and explanatory notes of the "Carta Geologica del settore centro-meridionale dell'Altopiano Ibleo"*. Mem. Soc. Geol. It. 55, 45-52.

Hargreaves, G.H. (1994)- *Defining and using reference evapo-transpiration.* Irrigat Drain Eng 120, 77-91.

Hauser S., Dongarrà G., Favara R. & Longinelli A. (1980)- *Composizione isotopica delle pioggie in Sicilia. Riferimenti di base per studi idrogeologici e relazione con altre aree mediterranee.* Rend. Soc.Ital. Min.e Petr. 36, 671-680.

Helgeson H. C., (1969)- *Thermodynamics of hydrothermal systems at elevated temperature and pressure*. Amer J. Sci 267, 729-804.

Helgeson H. C., Delany J. M., Nesbitt H. W. & Bird D. K. (1978)- *Summary and critique of the thermodynamic properties of rock-forming minerals*. Amer J. Sci 278A, 1-229.

Husseini M.I., Jovanovich D.B., Randal M.J. & Freund L.B. (1975)- *The fracture energy of earth-quakes.* Geophys. J. Roy. Astr. Soc., 43, 367-385.

Johnson J. W., Oelkers E. H. & Helgeson H. C. (1992)- *A software package for calculating the standards molal properties of minerals, gases, aqueous species, and reaction from 1 to 1000°C.* Computer Geosci. 18, 899-947.

Jouzel J.(1986)- *Isotopes in cloud physics : multiphase and multistage condensation processes. Handbook of Enviromental Isotopes Goechemistry*. 2, 61-112.

Lentini F., Grasso M. & Carbone S. (1987) - *Introduzione alla geologia della Sicilia e guida all'escursione*. In "convegno Soc. Geol. It.", Naxos-Pergusa, Aprile 1987.

Leontiadis, L., Vergis, S. and Christodoulou, Th. (1996)- *Isotope hydrology study of areas in Eastern Macedonia and Thrace, northern Greece*. Journal of Hydrology, 182 1-17.

Longaretti G. & Rocchi S. (1990) - *Il magmatismo dell'avampaese ibleo (Sicilia orientale) tra il trias e il quaternario: dati stratigrafici e metrologici di sottosuolo.* Mem. Soc. Geol. It. 45, 911-925.

Mantovani E., Albarello D., Tamburelli C. & Babbucci D. (1996)- *Evolution of the tyrrhenian basin and surrounding regions as a result of the Africa-Eurasia convergence.* Geodynamics 35-72.

Milliman, J.D. (1974)- *Marine Carbonates*. Springer Berlin, 375 pp.

Monaco C. & Tortorici L. (2000)- *Active faulting in the Calabrian arc and eastern Sicily*. Journal of Geodynamics 29, 407-424.

Mook, W. G., Bommerson, J.C., Staverman ,W. H., (1974). *Carbon Isotope fractionation between dissolved bicarbonate and gaseous carbon dioxide*. Earth Planet. Sci. Lett. 22 (2), 169-176.

Parkhurst D. L. (1995)- *A computer program for speciation, reaction path, advective transport, and inverse geochemical calculations.* USGS Water-Resources Investigations Report 95, 4227.

Patanè G. & Imposa S. (1987) - *Tentativo di applicazione di un modello reologico per l'Avampaese Ibleo ed aree limitrofe.* Mem. Soc. geol. It. 38, 341-359.

Pingitore N. E. (1986)- *Models of coprecipitation of Ba^{2+} and Sr^{2+} with calcite. In Geochemical Processes at Mineral Surfaces.* ACS Symp. Ser. 323, 574-586.

Rikitake, T. (1976)- Earthquake Prediction. Elsevier. 135 pp.

Rimstidt D., Balog A. & Webb J. (1998)- *Distribution of trace elements between carbonate minerals and aqueous solutions.* Geochim. Cosmochim. Acta, 62, 1851-1863.

Romano R. & Villari L. (1973) - *Caratteri petrologici e magmatologici del vulcanismo ibleo.* Rend. Soc. It. Miner. Petrol., 29, 453-484.

Ruggieri R. (1990) – *Zonazione idrogeologica e grado di carsificazione della serie carbonatica oligo-miocenica affiorante nel comprensorio urbano di Ragusa.* Atti del 1° Convegno Regionale di Speleologia della Sicilia, pp. 201-226.

Ruggieri R. (1997) – *Problematiche di protezione della risorsa idrica in rocce fessurate e carsificate: la fiumara di Modica e la sorgente Salto di Lepre (Rg), un caso emblematico di inquinamento negli Iblei.* Atti del 2° Congresso Regionale dell'Ordine dei Geologi di Sicilia, pp. 91-102. Erice 2-4 ottobre, 1997.

Sano, Y., Tominaga, T., Nakamura, Y. and Wakita, H. (1982) *$^{3}He/^{4}He$ ratios of methane-rich natural gases in Japan.* Geochem. J., 16, 237-245.

Santoro M. (1970)- *Sull'applicabilità della formula del Turc per il calcolo della evapotraspirazione effettiva in Sicilia.* Atti I Convegno Int Acque Sotterranee, Palermo, Italy.

Servizio Idrografico del Genio Civile, (Hydrographic Service of Civil Engineers, from 1966 to 1990)- *Annali idrologici.* Parte II. Regione Siciliane Ed. Palermo.

Stumm W. & Morgan J. J. (1996)- *Aquatic chemistry: Chemical equlibria and rates in natural waters.* Wiley-Interscience publication.

Tesoriero A. & Pankow J.(1996)- *Solid solution partitioning of Sr^2, Ba^2, and Cd^{2+} to calcite*. Geochim. Cosmochim. Acta 60, 1053-1063.

Thiessen A.H., (1911)- *Precipitation average for large areas*. Monthly Weather Rev 3, 5-25.

Thornthwaite C.W. (1948)- *An approach towards a rational classification of climate*. Geogr. Rev. Americ. Geoph. Soc.55, 94.

Turc L. (1955)- *Le bilan D'eau des sols. Relation entre les precipitations, l'evaporation et l'ecoulement*. Ann Agron 5, 125-144.

Valenza, M. and Nuccio, P.M. (1993)- *Geochemical precursors of earthquakes. Some experience in Italy.* In: isotopic and geochemical precursors of earthquakes and volcanic eruptions. IAEA. TEDOC 726, 44-47.

Wakita, H. (1977)- *Geochemistry as a tool for earthquake prediction.* J. Phys. Earth 25, 175-183.

Wakita, H. (1982)- *Changes in groundwater level and chemical composition*. In: Asadad, T. (Ed), Earthquake prediction techinques university of Tokyo Press, Tokyo, 171-216, Chap.8.

Wigley T.M.L., Plummer L.N. & Pearson F.J. (1978)- *Mass transfer and carbon isotope evolution in natural water systems*. Geochim. Cosmochim. Acta, 42, 1117-1139.

Wilhelm E., Battino R. And Wilcock R.J. (1977)- Low-pressure solubility of gases in liquid water. *Chemical Reviews* 77, 219-262.

Xu C. Y., Schwartz . W. & Traina S. J. (1997)- *Treatment of acid-mine water with calcite and quartz*. Env. Eng. Sc. 14, 141-152.

Zimmerman U., Ehhalt D. & Munnich K.O. (1967)- *Soil water movement and evapo-transpitation: change in the isotopic composition of the water.* In: Isotopes in Hydrology. IAEA, Vienna, 567-585.

APPENDIX

SAMPLING AND ANALYTICAL METHODS

At the beginning of 1999, six rain-gauges were installed in the area of the Hyblean Plateau. These rain-gauges were homemade by using a PET tube (height=100 cm) and a PVC funnel (diameter=30 cm). The rainwater samples were monthly samples and after the collection the rain-gauges were refilled with 300 cc of vaseline oil in order to avoid evaporation processes after the rain events. Using this procedure, the collected rainwater samples are suitable for isotopic analyses. Within each station, together with the rain-gauge, a thermometer and a hygrometer connected to a data logger were installed.

Between 1999 and 2000, more then one hundred water samples were collected from cold and slightly hot wells and springs widespread located within the whole studied area.

Water temperature, electrical conductivity, pH, and Eh have been measured directly in the field. Samples for laboratory analyses have been collected and stored in polyethylene containers. HCO_3 content has been determined by titration with HCl 0.1 N, using orangemethyl as indicator. Chemical analyses of major constituents have been performed in the INGV-Palermo laboratories, by ion-chromatography (Dionex 2000i) on filtered (0.45μm) and acidified (100μl HNO_3 Suprapure) samples (Na, K, Mg and Ca) and untreated samples (F, Cl, Br, NO_3, SO_4).

Dissolved silica has been determined by colorimetry technique, using a spectrophotometer Shimadzu UV 1601 at INGV-Palermo laboratories. Chemical reactants and analytical procedure were contained in a Spectroquant determination kit (Merck).

Specific water samples for trace elements determination, were filtered, acidified and stored in Nalgene bottles (50cc). Analytical determinations were carried out by using of a Finnigan Element 2 ICP-MS. The external standard calibration and Rh as internal standard has been also used. Analytical accuracy reproducibility, tested on reference materials is better than 10%.

Isotope determinations (D/H and $^{18}O/^{16}O$) on water samples were performed by equilibration technique (Epstein and Mayeda, 1952 for oxygen) and water reduction (hydrogen production by using granular Zn, Kendall and Koplen 1982). Measurements were carried out using a Finnigan Delta Plus mass spectrometer and AP 2003 automatic preparation system coupled with an IRMS both at INGV-Palermo laboratory. Analytical precision for each measure is better than 0.2‰ for $\delta^{18}O$ and 1‰ for δD.

Chemical composition of dissolved gases (He, H_2, O_2, N_2, CO, CH_4 and CO_2) were performed by using a re-equilibration headspace technique (Capasso and Inguaggiato, 1998). Concentration and partial pressure for each of the gas species were calculated as

suggested by Capasso and Inguaggiato (1998) and by Capasso et al. (2000). Extracted gases were analysed using a GC Perkin-Elmer 8500, having a Carbosieve II column and double detector (HWD and FID).

Isotope composition of total dissolved inorganic carbon was determined by using a simple extraction technique (Favara et al., in press). This procedure is based on the physico-chemical stripping and purification in a vacuum line of yielded CO_2 through the acidification of water samples collected in a sealed glass bottle, by adding about 5 cc of H_3PO_4 85%. Carbon isotope ratios (±0.2 δ‰) were measured at INGV-Palermo laboratories by using of a Finnigan Delta Plus IRMS.

Determination of dissolved He isotope ratio is based on a gas-water re-equilibration method by using a headspace technique (Inguaggiato and Rizzo, 2001). The extracted gas was purified in a vacuum line through a liquid nitrogen trap at-196°C (for carbon dioxide and water), two Al-Zr Getter pumps (for hydrogen, methane and nitrogen) and another cryogenic charcoal trap at –233°C (for neon). ^{4}He and ^{20}Ne concentrations were calculated scaling the He and Ne partial pressures of samples to air-standard measured with a QMS (VG Quartz). The high-vacuum purification line is connected to double collector mass spectrometer (VG 5400-TFT) equipped with three detectors (two Faraday caps and a Daly photomultiplier). Analytical reproducibility and accuracy on helium isotope ratio are better than 5% and 3% respectively.

The collected rock samples were powdered in an agate mill and analysed by X-Ray fluorescence (XRF) at CFTA department of University of Palermo. Major elements were determined by a full matrix correction procedure and their accuracy was controlled with certified materials (PCC1 and G2). Loss on Ignition (LOI) was determined by a gravimetric method.

The isotopic analyses on carbonate were performed both at CFTA department (University of Palermo) and at INGV-Palermo laboratories. The samples were cooked for 30 minutes at temperature of 350°C in a vacuum line, with the aim to separate the organic fraction. Afterwards, 10-15 mg of powdered sample reacts, in an evacuated tube, with 100% H_3PO_4. The produced carbon dioxide is then purified using standard techniques (Mc Rea, 1950). Carbon isotope measurement (±0.2 δ‰), were carried out on a Finnigan Delta Plus IRMS.

TABLE 1: ***AVERAGE PRECIPITATION (P), EVAPOTRANSPIRATION (ETR) AND EFFECTIVE PRECIPITATION (I+R), ESTIMATED FOR EACH OF THE FIVE HYDROGEOLOGICAL BASINS REPORTED IN FIGURE 3. ST REFERS TO RAINGAUGE STATION.***

Acate River	**P (mm)**	**Extension Km^2**	**Average Etr (mm)**	**I+R (mm)**
ST1	532	286.3	325	
ST2	452	688.1	308	
ST3	600	20.8	333	
ST4	690	292.6	354	
ST7	585	25.9	369	
total	**527.4**	**1313.8**	**323.5**	**203.9**
Irminio River	**P (mm)**	**Extension Km^2**	**Average Etr (mm)**	**I+R (mm)**
ST2	452	264.9	308	
ST3	600	146.1	333	
ST4	690	86.4	354	
ST8	582	5.2	328	
ST9	443	48.7	289	
total	**528.9**	**551.3**	**320.3**	**208.6**
Tellaro River	**P (mm)**	**Extension Km^2**	**Average Etr (mm)**	**I+R (mm)**
ST2	452	0.6	308	
ST3	600	108.4	333	
ST5	450	33.8	315	
ST8	582	396.5	328	
ST9	443	389.5	289	
total	**520.9**	**928.8**	**311.7**	**209.2**
Anapo River	**P (mm)**	**Extension Km^2**	**Average Etr (mm)**	**I+R (mm)**
ST4	690	190.0	354	
ST5	450	511.9	315	
ST6	581	236.3	362	
ST8	582	100.0	328	
total	**536.5**	**1038.1**	**334.1**	**202.4**
Lentini River	**P (mm)**	**Extension Km^2**	**Average Etr (mm)**	**I+R (mm)**
ST4	690	89.6	354	
ST6	581	357.9	362	
ST7	585	105.2	369	
total	**599.4**	**552.8**	**362.0**	**237.4**
Hyblean Mountains	**P (mm)**	**Extension Km^2**	**Average Etr (mm)**	**I+R (mm)**
	537.4	**4384.6**	**328.0**	**209.4**

Table 2: *Estimation of infiltrating water volume for each hydrogeological basin. P.I.C. = Potential infiltration coefficient (see text).*

		P.I.C.		Infiltrating volume (m^3)	
ACATE River	**Extension (Km^2)**	**min**	**max**	**min**	**max**
Alluvial deposits	69.6	0.50	0.70	7.10E+06	9.93E+06
Calcarenite	792.7	0.60	0.80	9.70E+07	1.29E+08
Evaporite	72.5	0.60	0.80	8.87E+06	1.18E+07
Volcanic Rock	32.9	0.50	0.75	3.35E+06	5.03E+06
Limestone	326.7	0.60	0.90	4.00E+07	6.00E+07
Impermeable	19.4	-	-	-	-
total	1313.8			1.56E+08	2.16E+08
IRMINIO River	**Extension (Km^2)**	**min**	**max**	**min**	**max**
Alluvial deposits	38.4	0.50	0.70	4.01E+06	5.61E+06
Limestone	512.8	0.60	0.90	6.42E+07	9.63E+07
total	551.2			6.82E+07	1.02E+08
TELLARO River	**Extension (Km^2)**	**min**	**max**	**min**	**max**
Limestone and volcanic	55.6	0.60	0.85	6.98E+06	9.89E+06
Volcanic	9.2	0.50	0.75	9.62E+05	1.44E+06
Limestone	519.8	0.60	0.90	6.52E+07	9.79E+07
Calcarenites	41.6	0.60	0.80	5.22E+06	6.96E+06
Alluvial deposits	96.5	0.50	0.70	1.01E+07	1.41E+07
Impermeable	206.1	-	-	-	-
total	928.8			8.85E+07	1.30E+08
ANAPO River	**Extension (Km^2)**	**min**	**max**	**min**	**max**
Volcanic Rock	115.4	0.50	0.75	1.17E+07	1.75E+07
Limestone	511.2	0.60	0.90	6.21E+07	9.31E+07
Calcarenites	64.5	0.60	0.80	7.83E+06	1.04E+07
Alluvial deposits	87.0	0.50	0.70	8.80E+06	1.23E+07
Impermeable	260.0	-	-	-	-
total	1038.1			9.04E+07	1.33E+08
LENTINI River	**Extension (Km^2)**	**min**	**max**	**min**	**max**
Volcanic Rock	353.3	0.50	0.75	4.19E+07	6.29E+07
Calcarenites	154.5	0.60	0.80	2.20E+07	2.93E+07
Alluvial deposits	43.5	0.50	0.70	5.24E+06	7.34E+06
total	551.3			6.92E+07	9.96E+07
Total Infiltrating Volume		**m^3/year**		**4.73E+08**	**6.81E+08**
		m^3/km^2		**1.08E+05**	**1.55E+05**
		m^3/sec		**15**	**22**

TABLE 3: ***MONTHLY δD AND $\delta^{18}O$ VALUES OF RAINWATER. MONTHLY AMOUNT AND MEAN WEIGHTED VALUES FOR EACH STATION ARE ALSO LISTED. ISOTOPE VALUES ARE EXPRESSED IN δ PER MIL UNITS VS V-SMOW. THE AMOUNT OF RAINWATER IS REPORTED IN MM. ML = M. LAURO (986 M A.S.L.). SC = SCORDIA (158 M A.S.L.). SO = SORTINO (445 M A.S.L.). MRG = MARINA DI RAGUSA (5 M A.S.L.). RG = RAGUSA (535 M A.S.L.). SR = SIRACUSA (15 M A.S.L.).***

Station	Date	Amount	δ D	$\delta^{18}O$
ML	feb-99	61.9	-38	-7.4
	mar-99	27.6	-32	-6.5
	apr-99	11.3	-30	-6.0
	may-99	7.4	-5	-3.0
	jul-99	36.0	-40	-7.3
	aug-99	68.3	-20	-4.7
	sep-99	88.8	-36	-7.1
	oct-99	71.5	-33	-6.8
	nov-99	283.1	-33	-7.0
	dec-99	106.9	-32	-6.7
	jan-00	176.2	-72	-11.8
	feb-00	28.9	-40	-7.6
	apr-00	70.6	-34	-6.9
	may-00	68.4	-26	-6.1
	jun-00	5.1	-6	-2.1
	sep-00	129.1	-32	-6.8
	oct-00	74.6	-33	-6.8
	nov-00	72.8	-42	-7.8
	dec-00	170.7	-49	-9.3
	jan-01	87.2	-48	-9.1
	feb-01	38.2	-33	-7.4
		Mean Weighted		
		δ D		-41
		$\delta^{18}O$		-7.8

Station	Date	Amount	δ D	$\delta^{18}O$
SC	feb-99	37.8	-40	-6.9
	mar-99	12.7	-8	-2.6
	apr-99	6.7	-13	-2.6
	jul-99	49.2	-23	-4.9
	aug-99	46.7	-15	-3.6
	sep-99	38.6	-28	-5.8
	oct-99	81.0	-28	-5.5
	nov-99	270.3	-20	-5.2
	dec-99	103.3	-37	-7.0
	jan-00	177.6	-68	-11.0
	feb-00	27.5	-29	-5.7
	apr-00	46.1	-10	-3.5
	may-00	18.1	-4	-0.6
	sep-00	60.0	-25	-4.7
	oct-00	39.1	-24	-5.0
	nov-00	25.5	-30	-5.7
	dec-00	96.8	-29	-6.5
	jan-01	60.3	-39	-7.4
	feb-01	29.7	-27	-5.3
		Mean Weighted		
		δ D		-32
		$\delta^{18}O$		-6.4

Station	Date	Amount	δ D	$\delta^{18}O$
SO	feb-99	54.5	-35	-7.2
	mar-99	15.2	-19	-4.7
	apr-99	4.1	-2	-2.2
	jun-99	3.5	-6	-2.8
	jul-99	11.3	-12	-4.0
	aug-99	77.8	-14	-4.5
	sep-99	50.2	-32	-6.7
	oct-99	26.2	-27	-6.1
	nov-99	379.3	-20	-5.8
	dec-99	148.6	-23	-6.0
	jan-00	278.8	-56	-10.2
	feb-00	29.4	-39	-7.5
	apr-00	53.5	-22	-4.7
	may-00	65.7	-19	-4.3
	sep-00	142.5	-24	-5.0
	oct-00	34.0	-27	-5.1
	nov-00	36.8	-30	-6.4
	dec-00	178.6	-39	-7.7
	jan-01	38.2	-37	-7.4
	feb-01	45.3	-34	-6.6
		Mean Weighted		
		δ D		-31
		$\delta^{18}O$		-6.6

Station	Date	Amount	δ D	$\delta^{18}O$
MRG	feb-99	61.6	-40	-7.2
	mar-99	22.8	-20	-4.0
	apr-99	7.4	-20	-3.7
	aug-99	17.7	-28	-5.1
	sep-99	35.7	-24	-4.8
	oct-99	92.7	-31	-6.4
	nov-99	166.3	-19	-5.2
	dec-99	69.4	-27	-5.7
	jan-00	76.4	-48	-8.4
	feb-00	24.1	-24	-4.6
	apr-00	69.4	-15	-4.3
	sep-00	35.5	-15	-4.2
	oct-00	58.0	-25	-5.4
	nov-00	53.5	-34	-6.5
	dec-00	115.5	-41	-7.6
	jan-01	69.9	-39	-7.4
	feb-01	31.8	-36	-7.0
		Mean Weighted		
		δ D		-28
		$\delta^{18}O$		-5.9

TABLE 3 – ***CONTINUE.***

Station	Date	Amount	δ D	$\delta^{18}O$
RG	feb-99	69.8	-25	-5.8
	mar-99	32.4	-22	-5.4
	apr-99	6.7	-13	-3.5
	jul-99	48.8	-17	-4.7
	aug-99	23.4	-15	-4.2
	sep-99	56.6	-40	-7.6
	oct-99	70.4	-29	-6.1
	nov-99	240.6	-20	-5.7
	dec-99	158.5	-44	-8.5
	jan-00	96.2	-50	-9.0
	feb-00	22.6	-30	-6.1
	apr-00	58.0	-32	-6.3
	may-00	25.5	-11	-3.4
	jun-00	20.9	-21	-3.9
	sep-00	113.4	-38	-7.3
	oct-00	48.4	-24	-5.5
	nov-00	82.1	-30	-6.6
	dec-00	138.7	-44	-8.4
	jan-01	89.2	-48	-8.6
	feb-01	59.4	-39	-7.4
		Mean Weighted		
		δ D		-33
		$\delta^{18}O$		-6.9
Station	**Date**	**Amount**	**δ D**	**$\delta^{18}O$**
SR	feb-99	44.6	-36	-6.7
	mar-99	20.5	-25	-5.1
	apr-99	3	7	0.5
	jul-99	14.9	-21	-4.6
	aug-99	80.7	-19	-4.3
	sep-99	23.4	-30	-5.4
	oct-99	60.9	-24	-5.2
	nov-99	251.9	-17	-4.6
	dec-99	118.9	-25	-5.5
	jan-00	109.0	-48	-8.6
	feb-00	19.1	-32	-5.8
	apr-00	59.7	-16	-3.9
	may-00	15.0	1	-1.2
	sep-00	70.3	-19	-5.1
	oct-00	26.3	-17	-4.4
	nov-00	20.4	-31	-5.6
	dec-00	67.9	-31	-6.2
	jan-01	34.0	-34	-7.4
	feb-01	27.6	-29	-6.0
		Mean Weighted		
		δ D		-25
		$\delta^{18}O$		-5.4

TABLE 7: ***CALCULATED SATURATION INDEX (SI = LOG (IAP/K_{SP})) FOR SEVERAL PURE MINERALOGICAL PHASES IN HYBLEAN GROUNDWATERS. SATURATION STATE IS ACHIEVED WHEN SI = 0, WHILE UNDERSATURATION AND SUPERSATURATION CORRESPOND TO SI<0 AND SI > 0 RESPECTIVELY.***

		BA	CM	CO	GN	LU	MA	OT
	Formula	**jul-00**	**jul-00**	**jul-00**	**jul-00**	**jul-00**	**jul-00**	**jul-00**
$Al(OH)_3(a)$		-1.6	-1.9	-1.9		-1.9	-2.0	-2.3
Albite	$NaAlSi_3O_8$	-1.9	-0.7	-3.7		-1.2	-0.6	-1.1
Alunite	$KAl_3(SO_4)_2(OH)_6$	-2.7	-3.3	-7.2		-4.9	-4.0	-6.1
Anhydrite	$CaSO_4$	-2.1	-20.6	-2.8	-1.7	-2.2	-14.8	-2.3
Anorthite	$CaAl_2Si_2O_8$	-3.7	-3.7	-4.6		-3.0	-3.4	-3.6
Aragonite	$CaCO_3$	-0.3	-0.5	-0.3	-0.2	0.2	-0.3	0.0
Barite	$BaSO_4$	0.0	-17.4	-1.2	0.2	0.0	-11.6	-0.1
Calcite	$CaCO_3$	-0.1	-0.3	-0.2	-0.1	0.2	-0.1	0.1
Chalcocite	Cu_2S	-16.9	7.9	-19.4		-22.7	7.1	17.3
Chalcopyrite	$CuFeS_2$		9.8	-57.7		-62.1	10.2	12.1
Ca-Montmorillonite	$Ca_{0,165}Al_{2,33}Si_{3,6}O_{10}(OH)_8$	2.4	2.9	0.3		3.0	2.8	2.5
Celestite	$SrSO_4$	-2.5	-20.0	-3.2	-2.0	-2.2	-14.3	-2.2
Chalcedony	SiO_2	0.0	0.3	-0.4	0.0	0.3	0.3	0.4
Chlorite(14A)	$Mg_5Al_2Si_3O_{10}(OH)_8$	-10.1	-6.1	-10.7		-4.8	-4.1	-4.1
Chrysotile	$Mg_3Si_2O_5(OH)_4$	-8.8	-6.1	-9.0	-7.8	-5.3	-4.9	-4.5
Dolomite	$CaMg(CO_3)_2$	-0.9	-0.3	-1.1	-0.5	0.1	0.0	0.2
$Fe(OH)_3(a)$			-10.2	-2.2	-1.7	-0.9	-8.9	-5.9
Fluorite	CaF_2	-1.8	-0.7	-2.1	-1.6	-1.2	-0.7	-1.1
Gibbsite	$Al(OH)_3$	1.1	0.8	0.8		0.9	0.8	0.5
Gypsum	$CaSO_4 \cdot 2H_2O$	-1.9	-20.3	-2.6	-1.4	-1.9	-14.5	-2.1
Goethite	FeOOH		-5.8	3.6	4.0	4.8	-4.9	-0.2
Hausmannite	Mn_3O_4	-30.0	-42.0	-25.0	-27.0	-23.9	-39.3	-35.2
Hematite	Fe_2O_3		-9.6	9.2	10.0	11.5	-7.7	1.7
Illite	$K_{0,6}Mg_{0,25}Al_{2,3}Si_{3,5}O_{10}(OH)_2$	1.3	2.1	-1.7		2.0	2.1	1.5
Jarosite-K	$KFe_3(SO_4)_2(OH)_6$		-38.1	-18.5	-12.8	-12.8	-35.0	-27.7
Kaolinite	$Al_2Si_2O_5(OH)_4$	3.9	3.9	2.5		0.2	3.8	3.4
K-feldspar	$KAlSi_3O_8$	-0.5	0.5	-3.4		0.2	0.6	0.1
K-mica	$KAlSi_3O_{10}(OH)_2$	7.3	7.7	3.8		7.5	7.7	6.6
Manganite	MnOOH	-11.7	-18.6	-10.2	-10.8	-9.4	-17.3	-15.0
Melanterite	$FeSO_4 * 7H_2O$		-8.5	-9.1	-7.0	-7.8	-8.3	-7.9
Orpiment	As_2S_3	-106.7	12.8	-121.0	-109.3	-129.3	11.8	-5.9
Pyrite	FeS_2		4.9	-62.7	-56.0	-66.3	6.4	2.7
Pyrochroite	$Mn(OH)_2$	-9.8	-9.5	-8.6	-9.0	-8.3	-9.0	-8.9
Pyrolusite	MnO_2	-20.5	-33.7	-18.3	-19.3	-17.5	-31.9	-27.8
Quartz	SiO_2	0.4	0.8	0.0	0.4	0.8	0.7	0.8
Realgar	AsS	-47.9	-0.2	-53.5	-49.0	-56.8	-1.4	-9.8
Rhodochrosite	$MnCO_3$	-3.3	-2.7	-2.4	-2.5	-2.1	-2.5	-2.6
Sepiolite	$Mg_2Si_3O_{7,5}OH * 3H_2O$	-5.9	-3.7	-6.7	-5.2	-3.0	-2.9	-2.4
Sepiolite(d)	$Mg_2Si_3O_{7,5}OH * 3H_2O$	-8.6	-6.6	-9.5	-8.0	-5.7	-5.7	-5.1
Siderite	$FeCO_3$		-3.4	-2.0	-0.9	-1.1	-3.4	-1.0
$SiO_2(a)$		-0.9	-0.5	-1.3	-0.9	-0.6	-0.5	-0.5
Smithsonite	$ZnCO_3$	-4.9	-3.6	-2.7	-3.2	-3.6	-3.1	-3.3
Sphalerite	ZnS	-32.7	-0.3	-33.7	-31.3	-37.2	0.2	2.4
Strontianite	$SrCO_3$	-1.9	-1.3	-2.0	-1.9	-1.3	-1.2	-1.3
Talc	$Mg_3Si_4O10(OH)_2$	-5.2	-1.7	-6.2	-4.1	-1.0	-0.6	-0.1
Uraninite	UO_2	-3.5	0.5	-4.1	-3.7	-4.6	0.4	-0.9
Witherite	$BaCO_3$	-3.6	-2.7	-4.1	-3.8	-3.3	-2.6	-3.2

TABLE 7: ***CONTINUE***

		P8	P9	PB	PI	PO	SE	SO
	Formula	**jul-00**	**jul-00**	**jul-00**	**jul-00**	**jul-00**	**jul-00**	**jul-00**
$Al(OH)_3$(a)		-2.4	-1.2	-2.3	-2.6	-1.5	-1.7	-2.5
Albite	$NaAlSi_3O_8$	-2.3	-1.6	-2.6	-1.4	-1.9	-1.4	-2.2
Alunite	$KAl_3(SO_4)_2(OH)_6$	-5.0	-0.7	-1.8	-5.6	-0.8	-4.7	-4.4
Anhydrite	$CaSO_4$	-1.9	-1.6	-0.4	-11.2	-1.9	-2.7	-20.0
Anorthite	$CaAl_2Si_2O_8$	-4.9	-2.9	-4.9	-5.1	-3.9	-3.1	-5.6
Aragonite	$CaCO_3$	-0.1	-0.2	-0.1	-0.6	-0.5	-0.3	-0.5
Barite	$BaSO_4$	0.1	0.2	0.4	-8.4	0.0	0.0	-17.2
Calcite	$CaCO_3$	0.0	-0.1	0.1	-0.5	-0.3	-0.2	-0.4
Chalcocite	Cu_2S	-29.1	-19.4	-14.8	7.0	-21.4	9.6	8.7
Chalcopyrite	$CuFeS_2$	-72.0	-54.5	-45.6	10.5	-58.9	-1.1	10.8
Ca-Montmorillonite	$Ca_{0,165}Al_{2,33}Si_{3,6}O_{10}(OH)_8$	1.2	3.4	0.9	1.5	2.9	2.9	0.8
Celestite	$SrSO_4$	-2.3	-2.1	-1.0	-10.9	-2.3	-2.3	-19.6
Chalcedony	SiO_2	0.1	0.0	0.0	0.4	0.1	0.2	0.1
Chlorite(14A)	$Mg_5Al_2Si_3O_{10}(OH)_8$	-10.5	-9.8	-13.4	-8.7	-13.0	-4.3	-10.9
Chrysotile	$Mg_3Si_2O_5(OH)_4$	-8.1	-9.3	-10.1	-6.9	-10.7	-5.4	-8.3
Dolomite	$CaMg(CO_3)_2$	-0.5	-0.8	-0.9	-0.7	-1.3	-0.1	-0.8
$Fe(OH)_3$(a)		-1.8	-2.6	-3.6	-9.3	-2.5	-4.6	-10.0
Fluorite	CaF_2	-1.3	-1.4	-0.1	-1.0	-1.4	-1.3	-0.7
Gibbsite	$Al(OH)_3$	0.4	1.6	0.4	0.1	1.2	1.0	0.3
Gypsum	$CaSO_4 \cdot 2H_2O$	-1.7	-1.3	-0.2	-11.0	-1.7	-2.4	-19.7
Goethite	FeOOH	3.8	3.1	2.2	-4.4	3.2	1.3	-5.5
Hausmannite	Mn_3O_4	-27.6	-28.6	-30.8	-41.2	-28.1	-33.3	-42.7
Hematite	Fe_2O_3	9.6	8.1	6.4	-6.8	8.4	4.6	-9.1
Illite	$K_{0,6}Mg_{0,25}Al_{2,3}Si_{3,5}O_{10}(OH)_2$	-0.1	1.8	-0.7	0.5	1.6	1.8	-0.1
Jarosite-K	$KFe_3(SO_4)_2(OH)_6$	-14.2	-15.8	-16.0	-35.8	-14.5	-23.3	-37.9
Kaolinite	$Al_2Si_2O_5(OH)_4$	2.7	4.8	2.6	2.7	4.3	4.0	2.5
K-feldspar	$KAlSi_3O_8$	-1.1	-0.8	-1.8	-0.2	-0.3	-0.3	-0.8
K-mica	$KAlSi_3O_{10}(OH)_2$	5.2	7.9	4.7	5.6	7.7	7.3	5.3
Manganite	MnOOH	-10.5	-11.3	-12.4	-17.8	-11.0	-14.5	-18.3
Melanterite	$FeSO_4 * 7H_2O$	-8.5	-7.7	-7.0	-8.8	-7.7	-7.4	-8.2
Orpiment	As_2S_3	-142.7	-114.5	-95.3	10.4	-118.7	-25.4	13.2
Pyrite	FeS_2	-74.4	-58.3	-49.7	7.2	-62.5	-9.4	5.7
Pyrochroite	$Mn(OH)_2$	-9.9	-9.7	-10.3	-10.0	-9.7	-9.2	-9.5
Pyrolusite	MnO_2	-18.0	-19.6	-20.9	-31.8	-19.0	-25.7	-34.1
Quartz	SiO_2	0.6	0.4	0.5	0.8	0.5	0.6	0.6
Realgar	AsS	-62.1	-51.4	-43.8	-2.6	-52.7	-16.8	-0.3
Rhodochrosite	$MnCO_3$	-3.3	-2.8	-3.2	-3.1	-2.6	-2.6	-2.6
Sepiolite	$Mg_2Si_3O_{7,5}OH * 3H_2O$	-5.2	-6.2	-6.8	-4.1	-7.1	-3.5	-5.3
Sepiolite(d)	$Mg_2Si_3O_{7,5}OH * 3H_2O$	-7.9	-9.0	-9.7	-6.9	-9.8	-6.4	-8.1
Siderite	$FeCO_3$	-2.5	-1.7	-2.0	-13.2	-1.7	-0.4	-3.1
SiO_2(a)		-0.7	-0.9	-0.8	-0.5	-0.8	-0.7	-0.7
Smithsonite	$ZnCO_3$	-3.7	-4.6	-3.9	-3.6	-4.0	-3.6	-4.1
Sphalerite	ZnS	-41.7	-33.7	-28.2	0.0	-35.8	-5.2	-0.4
Strontianite	$SrCO_3$	-1.8	-2.1	-2.0	-1.6	-2.2	-1.2	-1.5
Talc	$Mg_3Si_4O10(OH)_2$	-4.3	-5.7	-6.4	-2.4	-7.0	-1.4	-4.4
Uraninite	UO_2	-6.1	-4.0	-2.7	0.4	-4.7	1.1	0.6
Witherite	$BaCO_3$	-3.6	-3.9	-4.7	-3.2	-4.1	-3.1	-3.2

TABLE 8: ***CALCULATED SATURATION INDEX (SI = LOG (IAP/K_{SP})) FOR SEVERAL PURE MINERALOGICAL PHASES IN HYBLEAN GROUNDWATERS. SATURATION STATE IS ACHIEVED WHEN SI = 0, WHILE UNDERSATURATION AND SUPERSATURATION CORRESPOND TO SI<0 AND SI > 0 RESPECTIVELY. OLIVINE, CLINOPYROXENE AND PLAGIOCLASE HAVE BEEN CONSIDERED AS SOLID SOLUTIONS.***

		AGR	BO	CAR	CAR1	ER	FAV	FE	FR3
	Formula	**mar-00**	**jul-00**	**mar-00**	**mar-00**	**jul-00**	**mar-00**	**jul-00**	**jun-01**
$Al(OH)_3(a)$		-2.0	-3.4	-2.5	-2.0	-3.4	-1.3	0.2	-2.1
Albite	$NaAlSi_3O_8$	-0.9	-0.2	-1.7	-1.0	-1.4	-0.9	2.1	-0.8
Alunite	$KAl_3(SO_4)_2(OH)_6$	-6.1	-14.2	-11.6	-7.5	-11.1	-2.7	1.5	-5.4
Anhydrite	$CaSO_4$	-2.6	-3.3	-3.1	-3.1	-2.8	-2.3	-3.1	-2.0
Anorthite	$CaAl_2Si_2O_8$	-3.0	-3.3	-2.7	-2.7	-4.8	-2.4	0.5	-2.8
Aragonite	$CaCO_3$	0.0	0.4	0.6	0.0	0.1	-0.4	0.2	-0.1
Barite	$BaSO_4$	-0.7	-0.9	-1.4	-1.6	-1.6	-0.5	0.3	-1.5
Calcite	$CaCO_3$	0.1	0.6	0.7	0.1	0.2	-0.2	0.3	0.1
Chalcocite	Cu_2S	-38.7	-33.3	-48.4	-49.4	-14.4	-7.7	-1.1	-31.9
Chalcopyrite	$CuFeS_2$	-8.2	-81.3	-105.7	-106.4	-46.8	-36.7	-13.4	-77.5
Ca-Montmorillonite	$Ca_{0,165}Al_{2,33}Si_{3,6}O_{10}(OH)_8$	2.7	-0.6	1.3	3.3	-0.1	4.3	6.6	2.8
Celestite	$SrSO_4$	-2.3	-3.0	-3.5	-3.1	-2.2	-3.3	-2.7	-2.2
Chalcedony	SiO_2	0.3	0.2	0.2	0.4	0.5	0.2	0.0	0.4
Chlorite(14A)	$Mg_5Al_2Si_3O_{10}(OH)_8$	-1.7	8.5	0.7	-2.6	-0.4	-6.2	3.1	-2.2
Chrysotile	$Mg_3Si_2O_5(OH)_4$	-3.3	4.3	-1.3	-3.9	-0.9	-6.8	-3.1	-3.5
Clinopyroxene	$Mg_{0,404}Fe_{0,166}Ca_{0,43}SiO_3$	-4.5	-2.5	-3.8	-4.6	-3.9	-5.1	-4.4	-4.3
Dolomite	$CaMg(CO_3)_2$	0.5	1.6	0.9	0.1	0.8	-0.8	1.4	0.0
$Fe(OH)_3(a)$		0.3	1.1	0.9	0.5	-1.7	-2.9	-3.6	-0.1
Fluorite	CaF_2	-2.1	-2.3	-2.5	-1.9	-2.0	-2.2	-0.6	-4.5
Gibbsite	$Al(OH)_3$	0.7	-0.7	0.2	0.8	-0.8	1.5	2.9	0.6
Gypsum	$CaSO_4 \cdot 2H_2O$	-2.4	-3.1	-2.8	-2.8	-2.6	-2.0	-2.9	-1.7
Goethite	FeOOH	6.0	7.1	6.8	6.2	4.3	2.6	2.2	5.7
Hausmannite	Mn_3O_4	-22.1	-12.9	-16.6	-20.7	-21.6	-29.2	-26.8	-22.9
Hematite	Fe_2O_3	14.0	16.2	15.5	14.4	10.6	7.2	6.4	13.3
Illite	$K_{0,6}Mg_{0,25}Al_{2,3}Si_{3,5}O_{10}(OH)_2$	2.0	0.3	0.6	2.2	-0.2	3.0	7.0	2.2
Jarosite-K	$KFe_3(SO_4)_2(OH)_6$	-9.8	-10.3	-11.4	-10.7	-15.4	-19.2	-20.1	-9.8
Kaolinite	$Al_2Si_2O_5(OH)_4$	3.7	0.6	2.4	4.0	1.0	5.3	7.4	3.7
K-feldspar	$KAlSi_3O_8$	0.3	0.8	-0.5	0.3	0.2	0.2	3.3	0.8
K-mica	$KAlSi_3O_{10}(OH)_2$	7.4	5.0	5.4	7.4	4.3	8.9	14.6	7.7
Manganite	MnOOH	-8.4	-6.3	-6.6	-7.7	-9.8	-11.4	-11.8	-9.0
Melanterite	$FeSO_4 * 7H_2O$	-8.7	-10.2	-10.9	-10.1	-8.6	-8.0	-7.8	-8.1
Olivine	$Mg_{0,855}Fe_{0,145}SiO_4$	-7.7	-3.6	-7.0	-8.4	-6.7	-9.4	-6.8	-7.9
Orpiment	As_2S_3	-175.4	-172.8	-209.0	-205.1	-105.4	-77.4	-37.7	-158.1
Pyrite	FeS_2	-89.3	-84.6	-105.5	-105.5	-52.3	-43.4	-18.4	-80.1
Plagioclase	$Na_{0,39}Ca_{0,59}K_{0,02}Si_3O_8$	-0.2	0.9	-0.2	-0.1	-1.0	-0.2	3.4	-0.1
Pyrochroite	$Mn(OH)_2$	-8.8	-5.9	-7.8	-9.1	-7.3	-8.7	-7.1	-8.7
Pyrolusite	MnO_2	-14.8	-12.2	-11.6	-12.9	-17.8	-21.7	-23.0	-15.8
Quartz	SiO_2	0.1	0.6	0.6	0.9	0.9	0.7	0.4	0.8
Realgar	AsS	-74.9	-73.8	-88.0	-86.4	-47.4	-35.9	-21.0	-68.2
Rhodochrosite	$MnCO_3$	-2.7	-1.4	-2.5	-3.0	-1.5	-2.6	-0.5	-2.9
Sepiolite	$Mg_2Si_3O_{7,5}OH * 3H_2O$	-1.8	2.9	-0.7	-1.9	-0.2	-4.0	-2.1	-1.8
Siderite	$FeCO_3$	-1.5	-1.8	-2.6	-2.4	-1.0	-1.5	0.1	-1.6
$SiO_2(a)$		-0.6	-0.6	-0.7	-0.4	-0.4	-0.6	-0.9	-0.5
Smithsonite	$ZnCO_3$	-1.9	-3.6	-2.6	-2.5	-3.3	-3.4	-3.7	-2.6
Sphalerite	ZnS	-48.3	-46.0	-57.0	-57.5	-28.6	-23.7	-10.7	-43.6
Strontianite	$SrCO_3$	-1.0	-0.6	-1.2	-1.4	-0.6	-2.1	-0.8	-1.6
Talc	$Mg_3Si_4O10(OH)_2$	0.9	8.5	2.8	0.6	3.7	-2.8	0.6	0.9
Uraninite	UO_2	-8.3	-8.6	-10.0	-9.9	-4.2	-1.4	-0.9	-6.9
Witherite	$BaCO_3$	-3.6	-2.6	-3.2	-4.0	-4.1	-4.1	-1.8	-5.1

TABLE 8: ***CONTINUE***

		FR5	FRB	FRE	FRP	GI	GM	LI
	Formula	**jun-01**	**jun-01**	**jun-01**	**jun-01**	**jul-00**	**jul-00**	**jul-00**
$Al(OH)_3(a)$		-2.1	-3.3	-2.3	-3.2	-2.7	-3.1	-2.9
Albite	$NaAlSi_3O_8$	-0.7	-0.4	-0.2	-0.2	-1.2	-1.6	-2.2
Alunite	$KAl_3(SO_4)_2(OH)_6$	-7.4	-12.4	-7.8	-13.2	-8.5	-10.7	-7.6
Anhydrite	$CaSO_4$	-2.5	-3.1	-2.8	-3.3	-2.9	-3.4	-2.3
Anorthite	$CaAl_2Si_2O_8$	-2.5	-3.9	-2.7	-3.6	-4.3	-5.0	-5.2
Aragonite	$CaCO_3$	0.3	0.1	0.0	0.0	-0.1	-0.2	-0.2
Barite	$BaSO_4$	-1.0	-0.9	-1.7	-1.0	-0.5	-1.5	0.1
Calcite	$CaCO_3$	0.4	0.2	0.2	0.1	0.1	0.0	0.0
Chalcocite	Cu_2S	-42.2	-19.8	-18.2	-21.7	5.8	4.2	-15.9
Chalcopyrite	$CuFeS_2$	-94.3	-56.4	-3.6	-60.0	-7.1	-11.6	-50.0
Ca-Montmorillonite	$Ca_{0,165}Al_{2,33}Si_{3,6}O_{10}(OH)_8$	3.0	-0.2	2.5	-0.3	0.4	-0.5	0.7
Celestite	$SrSO_4$	-2.7	-2.2	-2.0	-3.1	-2.4	-2.5	-1.3
Chalcedony	SiO_2	0.4	0.3	0.4	0.2	0.1	0.1	0.3
Chlorite(14A)	$Mg_5Al_2Si_3O_{10}(OH)_8$	-0.9	3.7	2.0	2.6	-0.5	0.6	-6.4
Chrysotile	$Mg_3Si_2O_5(OH)_4$	-2.7	1.3	-0.8	0.5	-1.9	-0.7	-5.0
Clinopyroxene	$Mg_{0,404}Fe_{0,166}Ca_{0,43}SiO_3$	-4.2	-3.2	-3.9	-3.1	-4.1	-4.0	-5.5
Dolomite	$CaMg(CO_3)_2$	0.7	0.7	0.8	0.0	0.6	0.7	0.1
$Fe(OH)_3(a)$		0.5	0.1	-0.9	0.4	-3.5	-3.4	-3.5
Fluorite	CaF_2	-2.5	-2.2	-2.1	-3.0	-1.8	-2.1	-1.3
Gibbsite	$Al(OH)_3$	0.6	-0.6	0.3	-0.5	0.0	-0.4	-0.2
Gypsum	$CaSO_4 \cdot 2H_2O$	-2.3	-2.9	-2.6	-3.1	-2.6	-3.1	-2.1
Goethite	FeOOH	6.2	6.1	5.0	6.4	2.3	2.5	2.3
Hausmannite	Mn_3O_4	-20.7	-19.8	-20.2	-15.7	-29.8	-27.6	-27.4
Hematite	Fe_2O_3	14.5	14.2	12.0	14.9	6.7	6.8	6.5
Illite	$K_{0,6}Mg_{0,25}Al_{2,3}Si_{3,5}O_{10}(OH)_2$	2.1	0.2	2.4	-0.1	0.4	-0.3	-0.3
Jarosite-K	$KFe_3(SO_4)_2(OH)_6$	-10.0	-11.7	-13.2	-11.8	-21.1	-21.9	-19.7
Kaolinite	$Al_2Si_2O_5(OH)_4$	3.7	1.0	3.2	0.9	-0.3	1.1	2.0
K-feldspar	$KAlSi_3O_8$	0.5	0.6	1.3	0.2	0.0	-0.3	-0.8
K-mica	$KAlSi_3O_{10}(OH)_2$	7.2	4.9	7.6	4.8	5.6	4.6	4.5
Manganite	MnOOH	-8.1	-9.1	-9.1	-7.7	-13.1	-12.2	-11.2
Melanterite	$FeSO_4 * 7H_2O$	-9.2	-8.7	-8.4	-9.0	-7.8	-8.6	-9.2
Olivine	$Mg_{0,855}Fe_{0,145}SiO_4$	-7.6	-5.2	-6.5	-5.5	-6.6	-6.0	-10.0
Orpiment	As_2S_3	-186.0	-125.7	-117.2	-135.2	-35.2	-42.9	-104.0
Pyrite	FeS_2	-94.8	-61.6	-58.6	-65.1	-15.0	-19.6	-54.7
Plagioclase	$Na_{0,39}Ca_{0,59}K_{0,02}Si_3O_8$	0.2	0.5	0.7	1.0	-0.7	-1.2	-2.0
Pyrochroite	$Mn(OH)_2$	-8.7	-7.2	-7.2	-6.0	-8.1	-7.4	-9.0
Pyrolusite	MnO_2	-13.8	-16.4	-16.8	-14.8	-24.3	-23.2	-19.8
Quartz	SiO_2	0.9	0.7	0.9	0.6	0.5	0.5	0.8
Realgar	AsS	-79.0	-55.2	-51.9	-59.1	-20.3	-23.1	-46.9
Rhodochrosite	$MnCO_3$	-2.7	-2.2	-1.3	-1.4	-2.3	-1.9	-2.6
Sepiolite	$Mg_2Si_3O_{7,5}OH * 3H_2O$	-1.2	1.0	0.0	0.3	-1.3	-0.5	-2.9
Siderite	$FeCO_3$	-1.8	-0.7	-0.8	-1.0	-0.4	-0.7	-2.5
$SiO_2(a)$		-0.4	-0.5	-0.4	-0.7	-0.8	-0.8	-0.5
Smithsonite	$ZnCO_3$	-2.7	-2.1	-2.0	-2.9	-3.7	-3.0	-3.8
Sphalerite	ZnS	-52.0	-32.3	-30.9	-34.6	-8.0	-9.6	-30.2
Strontianite	$SrCO_3$	-1.2	-0.3	-0.5	-1.2	-0.9	-0.6	-0.6
Talc	$Mg_3Si_4O10(OH)_2$	1.9	5.6	3.8	4.6	2.0	3.1	-0.7
Uraninite	UO_2	-9.0	-5.5	-5.1	-6.8	0.1	-1.1	-4.0
Witherite	$BaCO_3$	-3.7	-3.1	-4.3	-3.1	-3.1	-3.8	-3.2

TABLE 8: ***CONTINUE***

		NA	PA	PSO	SA	SS	ST2	SU
	Formula	**mar-00**	**jul-00**	**mar-00**	**mar-00**	**mar-00**	**mar-00**	**jul-00**
$Al(OH)_3(a)$		-2.0	-3.2	-2.5	-2.4	-3.1	-1.9	-1.7
Albite	$NaAlSi_3O_8$	0.8	-0.2	-2.3	-1.0	0.1	-1.3	-0.3
Alunite	$KAl_3(SO_4)_2(OH)_6$	0.1	-12.7	-9.2	-6.5	-12.7	-6.1	-1.2
Anhydrite	$CaSO_4$	-1.7	-3.0	-3.4	-2.6	-2.4	-2.6	-1.3
Anorthite	$CaAl_2Si_2O_8$	-4.2	-3.5	-3.4	-3.9	-2.4	-2.9	-3.2
Aragonite	$CaCO_3$	-0.6	0.2	0.5	-0.5	0.8	-0.1	-0.1
Barite	$BaSO_4$	0.1	-1.1	-0.9	-0.3	-1.8	-0.1	0.2
Calcite	$CaCO_3$	-0.5	0.3	0.7	-0.3	0.9	0.1	0.1
Chalcocite	Cu_2S	10.3	-26.6	-31.1	-27.6	-49.2	-25.6	-29.0
Chalcopyrite	$CuFeS_2$	7.9	-69.5	-75.5	-71.2	-106.9	-67.2	-65.1
Ca-Montmorillonite	$Ca_{0,165}Al_{2,33}Si_{3,6}O_{10}(OH)_8$	4.5	-0.2	1.0	1.5	0.8	3.2	2.0
Celestite	$SrSO_4$	-1.5	-3.2	-3.0	-1.9	-2.3	-2.7	-1.5
Chalcedony	SiO_2	0.9	0.2	0.2	0.2	0.3	0.3	-0.1
Chlorite(14A)	$Mg_5Al_2Si_3O_{10}(OH)_8$	-11.5	2.1	-4.0	-3.6	9.1	-5.7	-0.2
Chrysotile	$Mg_3Si_2O_5(OH)_4$	-9.2	0.3	-4.2	-4.2	4.4	-5.8	-2.9
Clinopyroxene	$Mg_{0,404}Fe_{0,166}Ca_{0,43}SiO_3$	-5.9	-3.2	-4.7	-4.8	-3.6	-4.7	-4.5
Dolomite	$CaMg(CO_3)_2$	-0.6	0.2	0.7	-0.4	2.1	-0.4	0.8
$Fe(OH)_3(a)$		-6.0	0.2	-0.5	-0.9	0.8	-0.1	-1.3
Fluorite	CaF_2	-1.5	-3.7	-2.3	-1.7	-2.0	-2.3	0.2
Gibbsite	$Al(OH)_3$	0.7	-0.5	0.2	0.3	-0.4	0.9	1.0
Gypsum	$CaSO_4 \cdot 2H_2O$	-1.5	-2.8	-2.2	-2.4	-2.2	-2.3	-1.1
Goethite	FeOOH	-0.2	6.2	5.5	5.1	6.7	5.5	4.4
Hausmannite	Mn_3O_4	-35.7	-14.9	-23.0	-22.5	-13.6	-22.8	-22.3
Hematite	Fe_2O_3	1.6	14.4	13.0	12.2	15.4	12.9	10.8
Illite	$K_{0,6}Mg_{0,25}Al_{2,3}Si_{3,5}O_{10}(OH)_2$	3.1	0.1	-0.2	0.9	1.2	1.9	2.2
Jarosite-K	$KFe_3(SO_4)_2(OH)_6$	-22.3	-12.1	-12.7	-11.6	-11.0	-12.1	-10.7
Kaolinite	$Al_2Si_2O_5(OH)_4$	4.9	1.0	2.3	2.7	1.6	4.2	3.5
K-feldspar	$KAlSi_3O_8$	1.4	0.5	-1.2	-0.1	0.9	-0.1	0.8
K-mica	$KAlSi_3O_{10}(OH)_2$	8.5	5.1	4.7	6.1	5.7	7.3	8.4
Manganite	MnOOH	-15.3	-7.2	-9.7	-9.6	-5.6	-8.7	-9.0
Melanterite	$FeSO_4 * 7H_2O$	-5.6	-9.7	-9.0	-8.5	-11.4	-7.9	-7.6
Olivine	$Mg_{0,855}Fe_{0,145}SiO_4$	-11.1	-5.8	-9.0	-8.5	-6.2	-8.8	-6.9
Orpiment	As_2S_3	-3.6	-151.9	-153.8	-145.9	-212.4	-138.8	-128.6
Pyrite	FeS_2	2.2	-73.8	-78.1	-74.6	-106.7	-71.2	-65.9
Plagioclase	$Na_{0,39}Ca_{0,59}K_{0,02}Si_3O_8$	-0.2	0.8	-0.9	-0.2	0.9	-0.6	-0.1
Pyrochroite	$Mn(OH)_2$	-9.5	-6.0	-9.0	-8.8	-6.8	-7.9	-7.9
Pyrolusite	MnO_2	-27.3	-13.8	-15.9	-15.9	-10.6	-16.9	-16.9
Quartz	SiO_2	1.3	0.6	0.6	0.7	0.8	0.8	0.3
Realgar	AsS	-8.8	-65.8	-66.3	-63.1	-89.5	-60.4	-56.6
Rhodochrosite	$MnCO_3$	-1.5	-1.4	-2.8	-2.6	-2.3	-2.0	-1.9
Sepiolite	$Mg_2Si_3O_{7,5}OH * 3H_2O$	-4.8	0.2	-2.9	-2.7	3.4	-3.2	-2.2
Siderite	$FeCO_3$	0.2	-1.8	-1.4	-1.6	-3.5	-0.8	-1.7
$SiO_2(a)$		0.0	-0.6	-0.7	-0.6	-0.5	-0.6	-1.0
Smithsonite	$ZnCO_3$	-3.2	-3.8	-2.7	-3.6	-4.0	-2.9	-4.4
Sphalerite	ZnS	0.4	-40.2	-42.7	-41.6	-58.2	-39.3	-37.4
Strontianite	$SrCO_3$	-1.8	-1.3	-1.4	-1.2	-0.4	-1.5	-1.6
Talc	$Mg_3Si_4O10(OH)_2$	-3.8	4.4	-0.2	0.1	8.8	-1.6	0.5
Uraninite	UO_2	0.7	-7.3	-6.7	-6.5	-10.4	-5.5	-5.7
Witherite	$BaCO_3$	-4.2	-3.2	-3.4	-3.5	-4.0	-3.1	-4.1

TABLE 9: ***AQUEOUS SPECIATION CALCULATIONS PERFORMED BY USING PHREEQC PROGRAM (PARKHURST, 1995). THE MAIN STABLE AQUEOUS SPECIES ARE REPORTED BOTH IN OXIDISED AND REDUCED HYBLEAN GROUNDWATERS. IN PARENTHESIS ARE ALSO REPORTED, THE RELATIVE PERCENTAGE OF EACH SPECIES WITH RESPECT TO THE TOTAL AMOUNT.***

Element	OXIDISED WATERS	REDUCED WATERS
Al	$Al(OH)_4^-$	$Al(OH)_4^-$ (90%) AlF_2^+(10%)
As	$HAsO_4^{2-}$ (85) $H_2AsO_4^-$ (15%)	$HAsO_3$
Ba	Ba^{2+} (85%) $BaSO_4$ (15%)	Ba^{2+} (95%) $BaSO_4$ (5%)
Ca	Ca^{2+}	Ca^{2+}
Cr	$Cr(OH)_3$ (65%) $Cr(OH)_2^+$ (35%)	$Cr(OH)_3$ (50%) $Cr(OH)_2^+$ (50%)
Cu	$Cu(OH)_2$ (55%) Cu^+ (45%) Cu^{2+} (5%)	Cu^+ (90%) $Cu(OH)_2$ (10%)
Fe	Fe^{+2} (65%) $FeHCO_3^+$ (20%) $Fe(OH)_3$ (15%)	Fe^{+2} (65%) $FeHCO_3^+$ (30%) $FeCO_3$ (5%)
K	K^+	K^+
Mg	Mg^{2+}	Mg^{2+}
Mn	Mn^{2+} (55%) $MnCO_3$ (30%) $MnHCO_3^+$ (15%)	Mn^{2+} (60%) $MnHCO_3^+$ (25%) $MnCO_3$ (15%)
Na	Na^+	Na^+
Ni	$NiCO_3$ (80%) $Ni(CO_3)_2^{2-}$ (15%) Ni^{2+} (5%)	$NiCO_3$ (95%) Ni^{2+} (5%)
Rb	Rb^+	Rb^+
Si	H_4SiO_4	H_4SiO_4
Sr	Sr^{2+}	Sr^{2+}
U	$UO_2(CO_3)_2^{2-}$ (60%) $UO_2(CO_3)_3^{4-}$ (40%)	$U(OH)_5^-$ (90%) $UO_2(CO_3)_3^{4-}$ (10%)
V	$H_2VO_4^-$ (65%) HVO_4^{2-} (35%)	$V(OH)_3$ (95%)
Zn	Zn^{2+} (40%) $ZnCO_3$ (25%) $Zn(CO_3)_2^{2-}$ (20%) $ZnHCO_3^+$ (15%)	Zn^{2+} (45%) $ZnCO_3$ (25%) $ZnHCO_3^+$ (25%) $Zn(CO_3)_2^{2-}$ (5%)

TABLE 10: ***DISSOLUTION REACTIONS FOR PRIMARY BASALTIC MINERALS (GISLASON AND ARNORSSON, 1993, MODIFIED). SOLID SOLUTION COMPOSITIONS ARE FROM DE***

OLIVINE (Fo0.855, Fa0.145)

$Mg_{1.71}Fe_{0..29}SiO4 + 4H^{+} <> 1.71\ Mg^{2+} + 0.29\ Fe^{2+} + H_4SiO_4$

ΔG^0_{ss}= -36645 Kcal/mol Log K_{ss}= 26.95

CLINOPYROXENE (En0.404, Fs0.166, Wo0.40)

$Mg_{0.404}Fe_{0.166}Ca_{0.40}SiO_3 + 2H^{+} + H_2O <> 0.404\ Mg^{2+} + 0.166\ Fe^{+2} + 0.4\ Ca^{+2} + H_4SiO_4$

ΔG^0_{ss}= -16605 Kcal/mol Log K_{ss}= 12.17

PLAGIOCLASE (An0.6, Ab0.4)

$(Ca, Al)_{0.6}(Na, Si)_{0.4}AlSi_2O_8 + 8\ H_2O <> 0.4\ Na^{+} + 0.6\ Ca^{+2} + 1.6Al(OH)_4^{-} + 2.4\ H_4SiO_4$

ΔG^0_{ss}= 25603 Kcal/mol Log K_{ss}= -18.77

ROSA ET AL. (1992).

TABLE 11: ***CONCENTRATIONS OF MINOR AND TRACE ELEMENTS IN SOME HYBLEAN GROUNDWATERS. *VALUES EXPRESSED IN μG/L. ** VALUES ARE EXPRESSED IN ηG/L. N.M. NOT MEASURED.***

Sample	AGR	BA	BO	CAR	CAR-1	CM	CO	ER	FAV
date	mar-00	aug-00	aug-00	mar-00	mar-00	aug-00	aug-00	aug-00	aug-00
Al*	9.1	5.9	31.4	14.2	8.9	7.4	6.1	1.1	16.5
As*	0.69	1.03	1.49	0.23	0.90	0.26	0.24	0.17	0.20
Ba*	22.9	81.6	8.3	20.5	11.1	545.3	19.7	3.3	18.3
Fe*	9.0	n.m.	58.0	9.7	3.8	8.7	6.5	11.3	20.6
Mn*	0.3	0.3	1.3	0.2	0.2	0.9	1.5	3.2	1.1
Mo*	32.3	2.4	18.1	0.9	1.3	0.5	1.1	8.8	0.7
Rb*	1.5	2.0	2.9	0.9	1.1	5.6	0.8	8.2	1.3
Sr*	994	469	77	223	597	1812	311	1257	262
U*	1.66	1.75	0.42	0.79	2.38	0.15	1.02	0.12	1.33
V*	1.24	1.16	0.25	0.80	1.94	0.04	0.32	0.11	2.77
Zn*	54.03	0.54	2.84	7.31	15.47	2.09	15.01	1.44	3.77
Co**	21	63	38	25	11	12	24	13	17
Cr**	111	68	374	156	259	364	210	118	262
Cu**	399	551	1608	569	423	279	1088	325	1242
Ni**	3477	90	145	5362	2230	63	138	139	52
La**	68	n.m.	433	24	8	486	n.m.	48	88
Ce**	50	n.m.	480	39	19	612	194	92	164
Pr**	5	1	57	4	2	98	25	11	20
Nd**	18	11	211	30	29	285	93	57	233
Eu**	15	36	25	15	9	210	22	14	411
Gd**	4	1	44	8	9	2	56	4	19
Tb**	2	n.m.	4	3	2	2	4	1	2
Dy**	10	15	18	10	14	19	10	2	9
Ho**	3	2	3	3	4	1	5	3	5
Er**	3	2	14	3	1	2	15	3	9
Lu**	14	1	9	6	9	1	4	n.m.	2

TABLE 11: ***CONTINUE***

Sample	FE	FR3	FR5	FRB	FRE	FRP	GI	GN	GU
date	aug-00	mar-00	mar-00	mar-00	mar-00	mar-00	aug-00	aug-00	aug-00
Al*	1743.6	8.7	9.6	11.5	13.9	34.9	5.2	n.m.	3.4
As*	5.37	0.56	0.98	4.60	0.72	1.13	0.27	0.40	0.26
Ba*	780.7	1.8	14.9	7.4	2.5	3.8	33.4	65.8	5.2
Fe*	251.2	8.8	6.0	10.0	19.1	13.5	54.9	137.8	17.6
Mn*	39.4	0.2	0.2	0.3	4.2	1.5	0.5	2.1	0.9
Mo*	1.1	1.8	1.3	15.9	8.6	28.9	6.8	0.9	1.6
Rb*	36.7	2.2	1.3	4.0	6.8	3.7	6.6	1.1	4.0
Sr*	1026	395	556	448	1725	35	657	726	936
U*	0.89	0.68	1.38	0.26	0.10	0.05	0.57	2.26	0.05
V*	1.43	7.73	3.84	0.09	0.09	0.08	0.03	0.48	0.03
Zn*	1.08	12.61	6.60	43.45	32.01	12.60	0.64	8.26	3.11
Co**	770	13	14	11	12	11	20	53	25
Cr**	175	309	216	70	55	48	144	277	150
Cu**	1184	535	454	350	330	375	788	n.m.	512
Ni**	118	1739	7	5957	6423	2612	108	135	158
La**	74	37	25	77	59	54	51	n.m.	79
Ce**	122	20	18	46	98	95	37	466	130
Pr**	17	2	2	5	2	1	6	51	18
Nd**	84	3	4	21	37	49	35	180	90
Eu**	12	0	7	5	1	3	27	34	22
Gd**	20	3	1	9	1	14	n.m.	22	22
Tb**	1	2	2	2	2	2	1	7	2
Dy**	12	10	10	20	10	14	16	57	12
Ho**	6	3	3	3	7	7	3	0	6
Er**	5	1	2	2	2	5	6	10	2
Lu**	1	10	9	8	12	5	2	2	n.m.

TABLE 11: ***CONTINUE***

Sample	**LI**	**LU**	**MA**	**NA**	**OT**	**P8**	**P9**	**PA**	**PB**
date	aug-00	aug-00	aug-00	mar-00	aug-00	aug-00	aug-00	aug-00	aug-00
Al*	0.6	6.6	6.7	58.6	3.3	1.1	17.4	6.6	9.4
As*	0.28	0.93	0.09	0.69	0.01	0.43	0.01	0.33	0.12
Ba*	108.4	69.7	536.9	70.2	85.8	73.7	61.0	3.3	38.2
Fe*	1.5	35.4	11.9	5378.5	37.1	5.9	24.3	5.6	29.3
Mn*	0.8	2.1	1.0	65.6	0.6	0.2	1.0	1.5	1.0
Mo*	6.6	8.4	0.8	7.9	3.6	2.3	0.4	25.7	11.9
Rb*	2.4	1.6	4.7	10.6	1.7	0.8	0.6	3.7	2.1
Sr*	6043	833	1655	2447	929	555	510	30	1646
U*	0.35	4.17	0.22	0.06	0.01	2.42	2.41	0.17	6.03
V*	0.03	0.53	0.08	0.38	0.02	0.85	0.34	0.10	0.29
Zn*	0.92	1.66	5.63	23.45	2.79	1.83	0.43	1.16	3.96
Co**	27	55	15	42	10	42	214	23	67
Cr**	37	160	267	106	72	282	240	93	147
Cu**	187	710	462	717	647	306	343	694	711
Ni**	107	401	58	2416	42	86	85	282	627
La**	n.m.	275	360	77	16	n.m.	470	30	293
Ce**	n.m.	58	248	107	25	n.m.	680	30	365
Pr**	1	10	34	3	4	1	74	3	41
Nd**	8	32	123	101	48	11	257	25	164
Eu**	46	33	224	46	43	40	18	7	30
Gd**	25	7	16	1	11	27	18	18	9
Tb**	1	2	1	5	n.m.	n.m.	5	1	3
Dy**	14	12	14	21	12	15	31	13	3
Ho**	2	6	7	14	1	2	15	2	1
Er**	n.m.	4	12	9	2	5	17	1	10
Lu**	1	1	2	9	1	1	4	n.m.	2

TABLE 11: ***CONTINUE***

Sample	PI	PO	PSO	SA	SE	SO	SS	ST2	SU
date	aug-00	aug-00	mar-00	aug-00	aug-00	aug-00	mar-00	mar-00	aug-00
Al*	1.3	11.8	5.2	6.1	11.8	2.6	22.5	7.3	17.2
As*	0.03	0.52	0.60	1.70	0.15	0.17	1.09	2.32	2.01
Ba*	243.0	64.6	32.3	38.2	174.0	259.8	0.8	103.7	44.4
Fe*	5.9	43.5	9.2	6.9	213.3	16.4	12.1	61.3	20.9
Mn*	0.4	2.8	0.2	0.4	0.8	1.5	0.2	2.4	9.3
Mo*	0.5	1.7	1.0	15.4	3.9	0.2	9.9	4.9	1.0
Rb*	3.9	4.0	n.m.	3.4	1.7	5.6	2.1	1.5	30.2
Sr*	1016	542	361	962	1441	1639	344	545	1497
U*	0.11	2.26	1.79	0.79	0.10	0.13	1.24	1.05	1.16
V*	0.04	1.32	0.89	0.50	0.04	0.06	7.21	0.40	0.84
Zn*	2.73	2.17	6.52	0.89	1.77	1.16	0.58	7.42	0.57
Co**	11	232	13	18	19	11	13	42	29
Cr**	130	482	108	103	102	58	195	55	1030
Cu**	378	1070	365	1611	678	315	338	776	647
Ni**	52	267	2329	220	121	82	3699	2622	74
La**	4	169	8	42	31	19	3	59	59
Ce**	36	133	11	25	65	34	50	41	85
Pr**	2	16	1	4	6	6	5	5	10
Nd**	18	73	1	12	24	26	28	58	35
Eu**	143	38	21	16	48	115	n.m.	70	21
Gd**	19	11	21	3	1	2	8	13	5
Tb**	n.m.	1	2	1	n.m.	n.m.	13	2	n.m.
Dy**	4	n.m.	10	13	18	11	17	10	11
Ho**	16	1	3	7	1	6	13	3	6
Er**	2	8	2	2	3	2	2	2	3
Lu**	1	2	10	1	1	n.m.	16	10	n.m.

TABLE 12: ***CONCENTRATION OF DISSOLVED GASES IN HYBLEAN GROUNDWATERS. VALUES ARE EXPRESSED AS PARTIAL PRESSURE (ATM) CALCULATED COMPUTED AT SAMPLING TEMPERATURES BASED ON THE K_H REPORTED BY WILHELM ET AL. (1977).***

Sample	date	pHe	pH_2	pO_2	pN_2	pCO	pCH_4	pCO_2
DI	apr-99	n.d.	1.2E-05	0.020	0.25	<0.1E-6	<0.05E-6	1.3E-02
GU	aug-00	n.d.	2.7E-05	<0.001	0.68	<0.1E-6	1.2E-03	1.8E-03
OR	apr-99	n.d.	2.8E-05	0.088	0.87	<0.1E-6	1.4E-06	1.5E-02
GU	jul-01	6.2E-06	4.5E-05	<0.001	1.28	<0.1E-6	7.5E-03	2.1E-03
MI	apr-99	n.d.	6.0E-05	0.077	0.69	2.4E-06	1.4E-05	1.0E-02
TR	apr-99	n.d.	6.4E-05	0.073	0.38	3.9E-05	2.1E-04	1.8E-02
PA	aug-00	n.d.	6.8E-05	0.246	1.32	<0.1E-6	8.4E-06	3.0E-03
PD	apr-99	n.d.	6.8E-05	0.246	1.32	<0.1E-6	8.4E-06	3.0E-03
SE3	may-99	n.d.	6.9E-05	0.020	0.52	1.8E-05	7.2E-04	1.4E-02
SE2	may-99	n.d.	8.2E-05	0.112	0.94	5.5E-05	6.6E-04	1.1E-02
DN	may-99	n.d.	8.2E-05	0.037	0.58	<0.1E-6	1.2E-04	1.9E-02
F4	may-99	n.d.	8.3E-05	0.148	0.84	5.2E-05	6.3E-04	5.3E-03
LI2	apr-99	n.d.	9.5E-05	0.122	1.35	<0.1E-6	<0.05E-6	1.1E-02
PC	apr-99	n.d.	9.9E-05	0.066	0.35	<0.1E-6	<0.05E-6	3.5E-02
SF	apr-99	n.d.	1.0E-04	0.072	0.39	<0.1E-6	1.8E-04	9.9E-03
P9	aug-00	n.d.	1.1E-04	0.040	0.45	<0.1E-6	3.1E-05	2.8E-02
LA	may-99	n.d.	1.7E-04	0.044	0.62	2.2E-05	4.9E-04	1.8E-02
ST	may-99	n.d.	1.8E-04	0.013	0.71	1.5E-05	7.2E-04	4.9E-03
CA	may-99	n.d.	2.2E-04	0.015	0.64	<0.1E-6	9.9E-01	1.7E-02
BB	may-99	n.d.	2.4E-04	0.041	0.45	4.1E-05	8.0E-04	2.7E-02
BM	may-99	n.d.	2.5E-04	0.045	0.58	2.3E-05	7.3E-04	5.9E-03
ER	aug-00	n.d.	2.6E-04	0.075	1.15	<0.1E-6	1.6E-04	3.2E-03
AP	apr-99	n.d.	<1.0E-6	0.136	1.01	1.3E-05	9.0E-04	2.0E-02
AR	apr-99	n.d.	<1.0E-6	0.091	1.06	2.7E-06	1.7E-05	9.6E-03
AV	may-99	n.d.	<1.0E-6	0.215	1.01	9.7E-05	3.4E-03	1.1E-02
SP5	may-99	n.d.	<1.0E-6	0.042	0.74	<0.1E-6	6.8E-04	1.2E-02

TABLE 12**: *CONTINUE***

Sample	date	pHe	pH_2	pO_2	pN_2	pCO	pCH_4	pCO_2
BA	aug-00	n.d.	<1.0E-6	0.121	0.97	<0.1E-6	<0.05E-6	1.3E-02
MA	aug-00	2.4E-04	<1.0E-6	0.003	0.88	<0.1E-6	1.3E+00	2.2E-02
MS	may-99	n.d.	<1.0E-6	0.113	0.95	<0.1E-6	<0.05E-6	1.5E-02
NA	mar-00	2.0E-03	<1.0E-6	0.011	1.35	<0.1E-6	1.1E-02	3.4E+00
OT	aug-00	n.d.	<1.0E-6	<0.001	0.71	<0.1E-6	2.3E-03	1.6E-02
OT	jul-01	7.6E-06	<1.0E-6	0.042	0.85	<0.1E-6	1.3E-04	1.4E-02
P2	apr-99	n.d.	<1.0E-6	0.026	0.91	<0.1E-6	2.7E-02	1.9E-02
P5	aug-00	n.d.	<1.0E-6	0.119	0.86	<0.1E-6	1.8E-05	2.5E-02
P8	may-99	n.d.	<1.0E-6	0.046	0.53	<0.1E-6	1.9E-05	2.1E-02
PA	jul-01	8.1E-06	<1.0E-6	0.058	0.90	<0.1E-6	1.5E-04	3.1E-03
PB	aug-00	n.d.	<1.0E-6	0.152	1.04	<0.1E-6	<0.05E-6	3.2E-02
PB2	may-99	n.d.	<1.0E-6	0.009	1.38	<0.1E-6	4.2E-05	3.1E-02
PI	aug-00	6.4E-05	<1.0E-6	0.001	0.54	<0.1E-6	5.7E-01	1.5E-02
PI	jul-01	4.2E-04	<1.0E-6	<0.001	1.04	<0.1E-6	1.6E+00	2.0E-02
PL	may-99	n.d.	<1.0E-6	0.005	0.45	<0.1E-6	1.0E-03	1.2E-02
PO	may-99	n.d.	<1.0E-6	0.070	0.92	<0.1E-6	<0.05E-6	3.3E-02
SA	may-99	n.d.	<1.0E-6	0.125	1.70	<0.1E-6	2.0E-05	9.5E-03
SC	apr-99	n.d.	<1.0E-6	0.045	1.13	<0.1E-6	<0.05E-6	2.4E-02
SCT	may-99	n.d.	<1.0E-6	0.058	0.76	4.9E-05	2.4E-04	2.2E-02
SE	aug-00	n.d.	<1.0E-6	0.200	0.88	<0.1E-6	7.3E-05	1.0E-02
SE	jul-01	4.2E-06	<1.0E-6	0.008	0.95	<0.1E-6	9.7E-05	1.3E-02
SG	may-99	n.d.	<1.0E-6	0.019	0.92	1.8E-05	5.6E-04	2.8E-02
SG2	may-99	n.d.	<1.0E-6	0.168	1.26	<0.1E-6	<0.05E-6	1.3E-02
SO	jul-01	7.2E-05	<1.0E-6	<0.001	0.89	<0.1E-6	5.4E-01	1.6E-02
SO	aug-00	1.6E-04	<1.0E-6	<0.001	1.28	1.8E-05	7.0E-01	2.0E-02
SU	aug-00	n.d.	<1.0E-6	0.013	1.21	<0.1E-6	3.4E-04	2.2E-03

TABLE 12**: *CONTINUE***

Sample	date	pHe	pH_2	pO_2	pN_2	pCO	pCH_4	pCO_2
BO	aug-00	n.d.	<1.0E-6	0.126	0.99	1.1E-05	4.9E-05	8.8E-04
BO	jul-01	1.0E-05	<1.0E-6	0.053	1.18	<0.1E-6	6.8E-05	7.3E-03
BR	may-99	n.d.	<1.0E-6	0.063	0.51	<0.1E-6	2.3E-04	2.5E-03
BSP	aug-00	n.d.	<1.0E-6	0.004	0.54	<0.1E-6	1.5E-01	3.7E-03
CD	may-99	n.d.	<1.0E-6	0.042	0.79	<0.1E-6	2.5E-04	8.5E-03
CI	apr-99	n.d.	<1.0E-6	0.097	0.93	<0.1E-6	6.3E-05	1.1E-02
CM	aug-00	8.1E-05	<1.0E-6	0.001	0.56	<0.1E-6	8.8E-01	2.2E-02
CM	jul-01	2.4E-04	<1.0E-6	<0.001	0.76	<0.1E-6	1.6E+00	2.7E-02
CN	may-99	n.d.	<1.0E-6	0.011	1.32	<0.1E-6	<0.05E-6	6.3E-03
CN1	mar-00	n.d.	<1.0E-6	0.062	1.28	1.5E-05	<0.05E-6	4.5E-03
CN2	mar-00	n.d.	<1.0E-6	0.083	0.68	<0.1E-6	<0.05E-6	3.4E-03
CO	aug-00	n.d.	<1.0E-6	0.013	1.28	<0.1E-6	<0.05E-6	9.5E-03
DB	may-99	n.d.	<1.0E-6	0.158	1.01	4.7E-05	6.4E-04	2.1E-03
DE	dec-99	n.d.	<1.0E-6	0.078	0.66	<0.1E-6	1.8E-05	7.1E-02
DM	may-99	n.d.	<1.0E-6	0.022	0.31	<0.1E-6	5.7E-04	2.4E-02
DP	may-99	n.d.	<1.0E-6	0.059	0.42	<0.1E-6	3.5E-06	5.7E-03
FAV	mar-00	n.d.	<1.0E-6	0.060	0.91	<0.1E-6	<0.05E-6	8.0E-03
FE	jul-01	3.6E-06	<1.0E-6	0.001	0.56	<0.1E-6	4.7E-01	1.4E-02
GE	aug-00	n.d.	<1.0E-6	0.016	0.63	<0.1E-6	1.1E-05	1.3E-02
GI	jul-01	6.4E-06	<1.0E-6	0.002	0.91	<0.1E-6	3.1E-03	5.5E-03
GN	aug-00	n.d.	<1.0E-6	0.111	0.78	<0.1E-6	<0.05E-6	2.0E-02
IN1	may-99	n.d.	<1.0E-6	0.108	1.00	6.8E-05	7.6E-04	8.2E-03
IN4	may-99	n.d.	<1.0E-6	0.009	0.21	<0.1E-6	1.7E-04	6.3E-03
LI	aug-00	n.d.	<1.0E-6	0.001	1.08	<0.1E-6	2.8E-05	1.8E-02
LO	may-99	n.d.	<1.0E-6	0.104	1.15	6.0E-05	7.8E-04	1.2E-02
LU	aug-00	n.d.	<1.0E-6	0.103	0.83	<0.1E-6	3.5E-05	1.2E-02
MA	jul-01	5.9E-05	<1.0E-6	<0.001	0.53	<0.1E-6	1.0E+00	1.8E-02

TABLE 13: ***CARBON AND HYDROGEN ISOTOPE COMPOSITION OF DISSOLVED METHANE IN CH_4-RICH HYBLEAN GROUNDWATERS. VALUES ARE EXPRESSED IN δ PER MIL VS V-PDB AND VS V-SMOW FOR CARBON AND HYDROGEN RESPECTIVELY.***

Sample	date	δD_{CH4}	$\delta^{13}C_{CH4}$
CM	feb-01	-150.4	-52
FE	feb-01	-205.1	-68
MA	apr-01	-123.7	-50
PI	apr-01	-158.2	-55
SO	apr-01	-200.7	-75
SP	apr-01	-153.9	-54

TABLE 14: ***CARBON ISOTOPIC COMPOSITION OF TDIC (TOTAL DISSOLVED INORGANIC CARBON). VALUES ARE REPORTED IN δ PER MIL VS V-PDB.***

Sample	$\delta^{13}C_{TDIC}$	Sample	$\delta^{13}C_{TDIC}$	Sample	$\delta^{13}C_{TDIC}$	Sample	$\delta^{13}C_{TDIC}$
BO	-5.8	S2	-3.8	IN1	-8.5	AP	-9.9
PA	-10.6	LI2	-8.9	IN4	-10.0	DM	-15.4
GU	-4.6	P8	-14.8	MA	-5.4	BG	-13.0
GI	-3.8	PB	-12.7	DP	-8.0	BL	-8.2
BA	-15.1	PO	-12.7	SE	-5.0	DN	-15.8
DB	-17.7	GE	-14.4	CM	-6.7	SL	-13.3
ER	-3.8	CI	-11.3	SF	-16.4	CA	-4.4
FE	-1.4	OT	-9.6	LI	-11.7	SC	-12.2
SP5	-13.7	BB	-14.3	AR	-10.5	PCN	-8.7
GN	-11.6	P9	-14.0	S3	-4.9	SCT	-13.9
PD	-11.2	DI	-11.9	SU	-8.0	PS	-13.4
SG2	-14.3	LA	-7.4	BM	-21.0	SO	-12.8
CO	-10.7	OR	-14.7	MI	-15.5	PC	-13.3
SA	-5.1	SG1	-15.5	LU	-11.3	DE	-12.3
PI	-9.2	CN1	-11.5	CN2	-9.7	NA	-1.1

TABLE 15: ***CARBON AND OXYGEN ISOTOPE COMPOSITION OF SELECTED CARBONATE ROCKS FROM HYBLEAN PLATEAU. VALUES ARE REPORTED IN δPER MIL VS V-PDB AND VS V-SMOW FOR CARBON AND OXYGEN RESPECTIVELY .***

Sample	$\delta^{13}C_{CaCO3}$	$\delta^{18}O_{CaCO3}$
B1	-3.1	-1.6
B2	0.0	0.1
OCM1	0.2	0.2
MCM1	3.0	0.6
OS1	-0.9	-0.6
A1	0.0	0.0
PP6	-3.3	-2.3
MC1	-1.8	-0.5
AVB2	-0.8	-0.7
MCM1	0.0	1.0

TABLE 16: CONCENTRATION (IN CC/G STP) AND ISOTOPE RATIO OF DISSOLVED HELIUM IN SELECTED HYBLEAN GROUNDWATERS. $^3HE/^4HE$ RATIOS IN SAMPLES (R_S) HAVE BEEN COMPARED TO THE SAME RATIO IN THE ATMOSPHERE (R_A=1.39 *10^{-6}). HE/NE RATIOS HAVE BEEN ALSO REPORTED. ON THE BASE OF THE OBTAINED HE/NE RATIOS, RELATIVE PERCENTAGES OF ATMOSPHERIC (ATM), CRUSTAL (CR) AND MAGMATIC (MAG) COMPONENTS HAVE BEEN COMPUTED (SEE TEXT).

Sample	date	pHe (atm)	He	R_s/R_a	He/Ne	%Atm	%Cr	%Mag
NA	jul-01	4.14E-04	2.2E-06	6.19	10.39	2.7	19.4	77.9
PI	jul-01	4.22E-04	7.6E-06	1.16	10.14	2.8	83.0	14.2
CM	jul-01	2.35E-04	7.7E-07	1.11	6.66	4.3	82.4	13.4
MA	jul-01	5.93E-05	4.3E-07	1.11	3.34	8.5	78.6	12.9
SO	jul-01	7.18E-05	4.4E-07	1.15	3.10	9.2	77.6	13.3
BO	jul-01	1.01E-05	9.9E-08	0.97	0.60	47.6	46.2	6.2
PA	jul-01	8.12E-06	8.0E-08	1.07	0.54	53.0	40.2	6.8
GI	jul-01	6.35E-06	6.9E-08	1.42	0.52	54.7	34.3	11.0
FE	jul-01	3.61E-06	2.4E-08	0.93	0.34	85.0	14.0	1.0
OT	jul-01	7.63E-06	1.1E-07	1.10	0.33	86.7	10.4	2.9
SE	jul-01	4.20E-06	4.5E-08	0.81	0.29	96.2	3.8	0.0
GU	jul-01	6.17E-06	6.1E-08	0.87	0.29	97.0	3.0	0.0